ABSTRACT

Title of Dissertation / Thesis: **STUDY OF OCULAR TRANSPORT OF DRUGS RELEASED FROM A SUSTAINED RELEASE DEVICE**

Hyuncheol Kim, Ph.D., 2004

Dissertation / Thesis Directed By: **Associate Professor Nam Sun Wang, Department of Chemical Engineering**

Delivering ocular therapeutics to a target site with minimal side effects requires detailed information about the distribution and elimination pathways. This knowledge can guide the development of new drug delivery devices. In this study, we investigated the movement of two drug surrogates, H-110, which is lipophilic, and Gd-DTPA, which is hydrophilic, released from polymer-based implants using a fluorescein technique and magnetic resonance imaging (MRI). We also studied the pharmacokinetics of intravitreally injected triamcinolone acetonide, a low water soluble drug used for treating sight-threatening diseases such as diabetic retinopathy and choroidal neovascularization associated with age-related macular degeneration (AMD).

At 24 hour post implantation, H-110 released from an intravitreal implant

was detected in the subretinal space. However, following a subconjunctival implant, very little H-110 fluorescence was detected in the subretinal region. H-110 most likely reached the subretinal space from an intravitreal implant by diffusion through the vitreous and retina. However, most of the H-110 released from a subconjunctival implant is thought to dissipate through the choroidal blood flow.

Concentration profiles of Gd-DTPA, which was released from an intravitreal implant in a New Zealand white rabbit, approached pseudo-steady state within 7 to 8 hours and showed gradients at the rabbit's vitreous-retina border suggesting that diffusion was occurring into the retinal-choroidal-scleral membrane. Parametric analysis with a finite element mathematical model of the rabbit eye yielded for Gd-DTPA a diffusion coefficient of 2.8×10^{-6} cm^2/sec in the vitreous and a permeability of 1.0×10^{-5} cm/sec in the composite retina-choroid-sclera membrane. Gd-DTPA concentration decreased away from the implant. Such regional concentration variations throughout the vitreous may have clinical significance when the ubiquitous eye diseases are treated using a single positional implant. Subconjunctival implants *in vivo* delivered a mean total of 2.7 μg of Gd-DTPA over 8 hours into the vitreous representing only 0.12% of the total amount of compound released from the implant *in vitro*. No Gd-DTPA was detected in the posterior segment of the eye. *Ex vivo*, the Gd-DTPA concentration in the vitreous was 30 fold higher suggesting the elimination of significant *in vivo* barriers to the movement of drugs from the subconjunctival space into the vitreous.

We developed a new preservative-free formulation for intravitreal injections

of triamcinolone acetonide for the treatment of diabetic macular edema, and choroidal neovascularization associated with AMD in human clinical trials at the National Institutes of Health. A pharmacokinetic study in rabbits was done to estimate elimination rate of two injection amounts of triamcinolone acetonide, 4 mg and 16 mg, from the vitreous. From our pharmacokinetic model, we found the half-lives for 4 mg and 16 mg injection in the vitreous to be 18.6 days and 37.6 days, respectively. We subsequently estimated the half-lives of 1 mg and 8 mg triamcinolone acetonide injection in order to predict therapeutic exposure in human.

There are three components in this thesis: the study of lipophilic H-110 transport with fluorescence, the study of hydrophilic transport of Gd-DTPA with MRI, and the pharmacokinetic analysis of triamcinolone acetonide. They have each contributed to further insights into our fundamental understanding of drug movement in the eye and the implication on optimal therapeutic delivery.

STUDY OF OCULAR TRANSPORT OF DRUGS RELEASED FROM A SUSTAINTED RELEASE DEVICE

By

Hyuncheol Kim

Thesis or Dissertation submitted to the Faculty of the Graduate School of the
University of Maryland, College Park, in partial fulfillment
of the requirements for the degree of
Doctor of Philosophy
2004

Advisory Committee:

Professor Nam Sun Wang, Chair
Professor William E. Bentley
Professor Sheryl H. Ehrman
Dr. Robert J. Lutz
Professor Yang Tao, Dean's Representative

DEDICATION

I would like to dedicate this Ph.D dissertation to my family.

ACKNOWLEDGEMENTS

I would like to thank Dr. Nam Sun Wang for his advice and support as an academic advisor. Over the past four years, his guidance and encouragement has been critical in my biochemical engineering research.

I consider myself fortunate to have had the opportunity to research drug delivery systems with Dr. Robert J. Lutz at the National Institutes of Health (NIH). I am sincerely grateful for the timely advice, ideas, guidance, support, and patience that he has provided.

I would like to thank Dr. Michael Robinson. He has helped me studying and understanding medical area, specially, ophthalmology. Studying and combining engineering area and medical area might be impossible without Dr. Robert J. Lutz and Dr. Michael Robinson's support.

I gratefully appreciate Dr. Martin Lizak's assistance and advice about magnetic resonance imaging. In the MRI experiments, his help was very important for organizing the animal experiments.

I am grateful to Dr. Ginger Tansey, Dr. Judit Baffi, Mark Szarowicz and Chris Hillman for assistance with the animal experiments. I would like to thank to Dr. Robert Dedrick, Dr. Peter Bungay, Dr. Paul Morrison, and Dr. Malisa Samtinoranont at the division of bioengineering and physical science program at NIH who helped create a collaborative and rich environment to conduct biochemical engineering research.

TABLE OF CONTENTS

LIST OF TABLES

LIST OF FIGURES

CHAPTER 1. Introduction

1.1 Background and Motivation

1.1.1. Structure of the eye

The structure of the eye can be depicted with three different layers: external layer (cornea and sclera), intermediate layer (iris-ciliary body and choroid), and internal layer (retina) [1]. The eye is filled with two kinds of fluids: aqueous humor between the cornea and the iris and vitreous humor between the lens and retina (Figure 1-1).

The cornea is an optically transparent tissue that allows light to reach the retina. This tissue is non-vascular, and nutrients and oxygen are supplied by diffusion from lachrimal fluid and aqueous humor as well as from blood vessels located at the junction between the cornea and the sclera. The tissue is approximately 0.5 mm thick in the central region and 0.7 mm at the peripheral region. The cornea is composed of five layers of tissues: epithelium, Bowman's membrane, stroma, Decement's membrane, and endothelium [2]. The epithelium has tight junctions and is a hydrophobic layer, which makes it a dominant important barrier to drug delivery. The Bowman's membrane separates the epithelium and the stroma. The stroma comprises 90% of the corneal thickness. This region is hydrophilic because 85% of the stroma is water. The Decement's membrane lies between the stroma and the endothelium. The endothelium contacts the aqueous humor and is responsible for

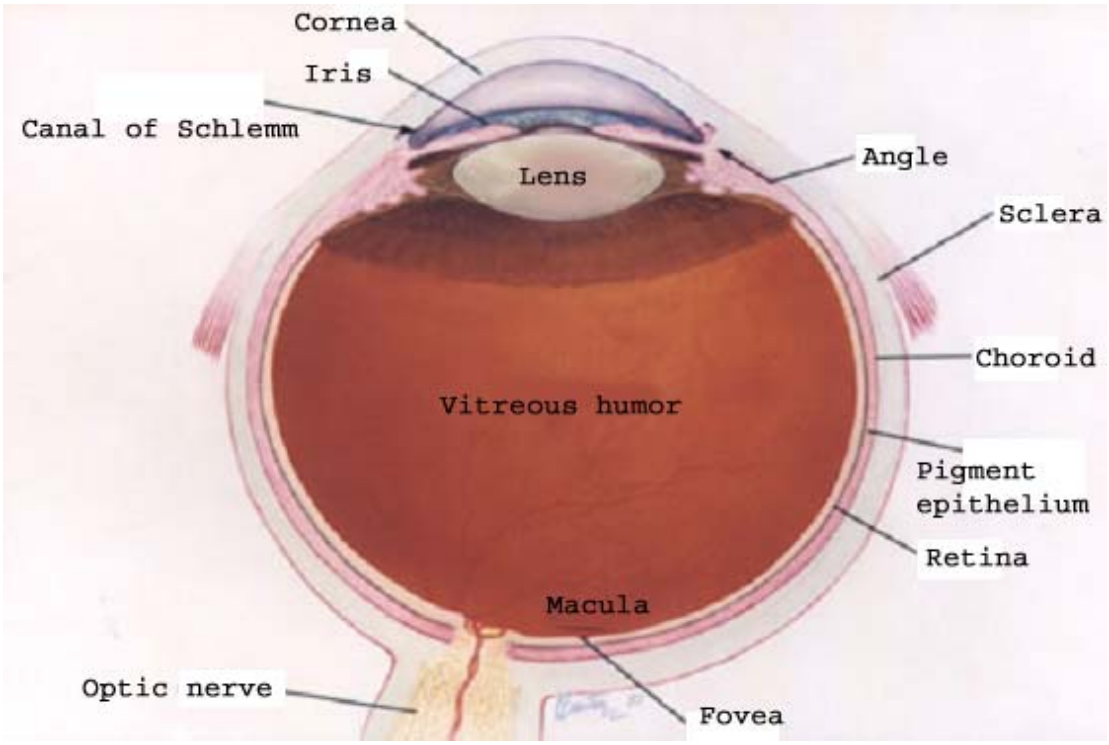

Figure 1-1. The anatomy of the eye (Copied from

http://www.nei.nih.gov/photo/eyean/index.asp')

controlling corneal hydration. To deliver therapeutic agents into the eye through the cornea using topical eye drops, drug carriers must possess both hydrophilic and lipophilic properties and be sufficiently small to pass through tight junctions.

The sclera forms about five-sixth area of the outer envelope of the eye [3]. The sclera is a fibrous tissue extending from the cornea to the optic nerve. It is usually referred to as the "white of the eye" and is a protective layer. About 70 % of the sclera is water, and the remaining components are mainly fibrillar collagen (predominately collagen type I) and proteoglycans containing glycosaminoglycan side chain [3].

The iris is the colored part of the eye and controls light entering eye. The iris divides the anterior humor chamber from the posterior humor chamber. The ciliary body produces the aqueous humor at rate of 2.2×10^{-3} ml/min [4]. 1-2% of aqueous humor production flows in the posterior direction into the vitreous [5] and the remaining flows in the anterior direction and drains through the Schlemm's canal.

The choroid is vascular and pigmented tissue between the retina and the sclera. The retinal pigment epithelium (RPE) is located between the choroid and the retina and the superchoroidal space is between the choroid and the sclera. The choroid is composed of layers of blood vessels that nourish the subretinal region.

The retina is a multi-layered membrane occupying the internal space of the posterior portion of the eye wall (Figure 1-2). One side of the retina contains the rod and cones and is adjacent to the retinal pigment epithelium (RPE) and the choroid; the other side of the retina faces the vitreous. Photoreceptor cells are located in the subretinal region near to the choroid. The macula is the center part of retina

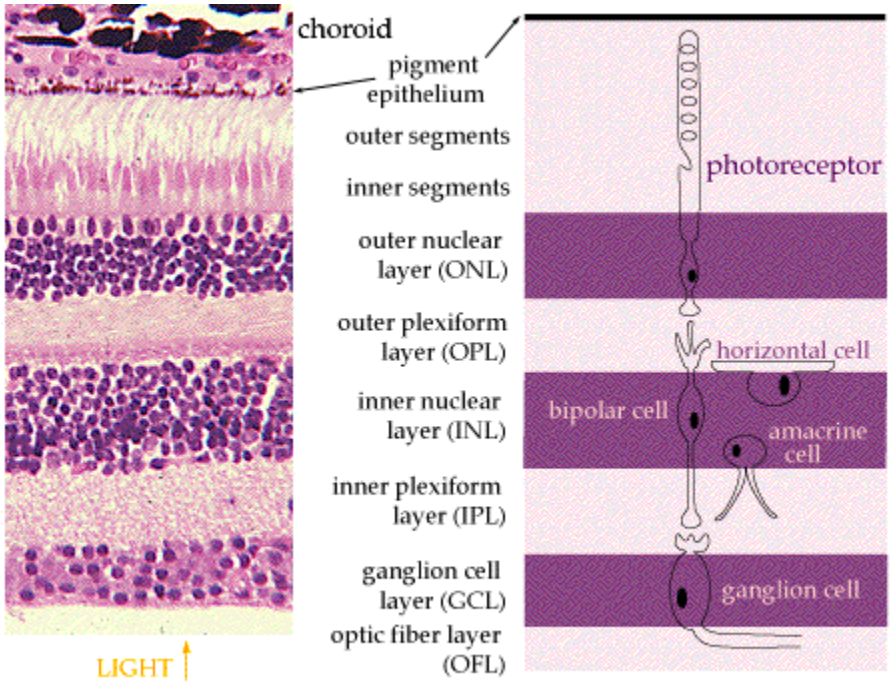

1-2. Detailed cross section view of the retina [1]

that serves fine central vision and color perception. The fovea is a depression at the center of macula.

The vitreous is a transparent substance that fills the center of the eye between the lens and the retina. It is composed of hyaluronic acid and collegn [6] in 98% water. Aqueous humor is the water fluid that fills the space between the cornea and the iris. It is continually produced by the ciliary body at a rate of 2.2×10^{-3} ml/min [4]. This fluid nourishes the cornea and the lens.

1.1.2. Ocular diseases

Millions of people suffer from various ocular diseases, many of which lead to irreversible blindness. Table 1-1 shows statistics about the number of people suffering from ocular diseases [7]. The number is increasing as the worldwide population continues to age. Among ocular diseases, the posterior segment ocular diseases, AMD, diabetic retinopathy, and glaucoma, are the main causes of irreversible blindness in developed countries. Studies have been aimed at developing treatments of these diseases [8-12]. However, only few therapeutic agents for the posterior segment ocular diseases have been commercialized [13]. Table 1-2 shows pharmacological agents for retinal diseases in ongoing clinical trials.

Choroidal neovascularization (CNV) is associated with AMD. Several treatments are available to treat CNV including photodynamic therapy, radiotherapy, and transpupillary thermotherapy [14]. The initial successful results that patients may experience with these treatments are frequently lost with recurrent CNV. As a result,

pharmacologic approaches are being developed using anti-angiogenic agents to treat CNV. However, adequate drug delivery systems to treat CNV are lacking.

Table 1-1. Ocular diseases and number of patients

Disease	Number of patients
Cataract	6 – 19% of patients over 43 years of age
Age-related macular degeneration	11 – 28% of patients over 65 years of age
Glaucoma	1 – 4% of patients over 45 years of age
Diabetic retinopathy	71 – 90% diabetics over 10 years of age
Dry eye (US)	50 – 60 million (~ 10 – 15% of US population)
Ocular allergy	~ 25% of US population
Retinitis pigmentosa	1 in 3000 – 5000 people

Table 1-2. Pharmacological agents for retinal diseases.

Drug class	Drug	Disease injection
Photodynamic therapy	Visudyne	AMD CNV[11]
PKC-β inhibitor	Ruboxistaurin, Mesylate (LY333531)	DME, DR[50, 51]
Anti-VEGF	Pegatanib sodium (EYE001)	AMD CNV[52]
	RhuFab	
Angiostatic cortisense	Anecortave acetate (AL-3789)	AMD CNV[53]
Glucocorticoid	Fluocinolone acetonide	DME, uveitis [54]
	Triamcinolone acetonide	DME, AMD CNV [18]

Note: AMD CNV: age-related macular degeneration – associated choroidal Neovascularization; DME: diabetic macular edema; DR: diabetic retinopathy; PME: persistent macular oedema; RhuFab: recombinant human antibody fragment; VEGF: vascular endothelial growth factor

1.1.3. Ocular drug delivery

Ocular therapeutic agents can be delivered to a target site by several

types of drug delivery methods (Figure 1-3). Methods of ocular drug delivery in Figure 1-3 are roughly categorized into three methods: topical administration, injection, and sustained-release implant.

Systemic administration of therapeutic agents has been used for the treatment of ocular diseases. However, only 1 – 2% of plasma drug concentration reaches the vitreous cavity [1]. To achieve a therapeutic drug level in the eye, frequent systemic administration with high drug doses are required which may induce systemic side effects.

Ocular drug delivery by topical administration such as eye drops accounts for nearly 90% of ocular therapeutic formulations [15]. It has been reported that less than 5% of a topically applied drug permeates the cornea because of physical properties of the cornea, and tear washout [16]. Few topically applied drugs can reach the posterior segment of the eye because of the long diffusion distance and the rapid clearance by aqueous humor flow.

Directly injecting drugs into the vitreous [17-19] or placing an intravitreal sustained release device (Figure 2 (G) and (F)) [20-22] have shown favorable results at delivering therapeutic agents to the posterior segment of the eye in clinical trials. However, some complications such as vitreous hemorrhage, retinal detachment, and endophthalmitis have been reported [23, 24].

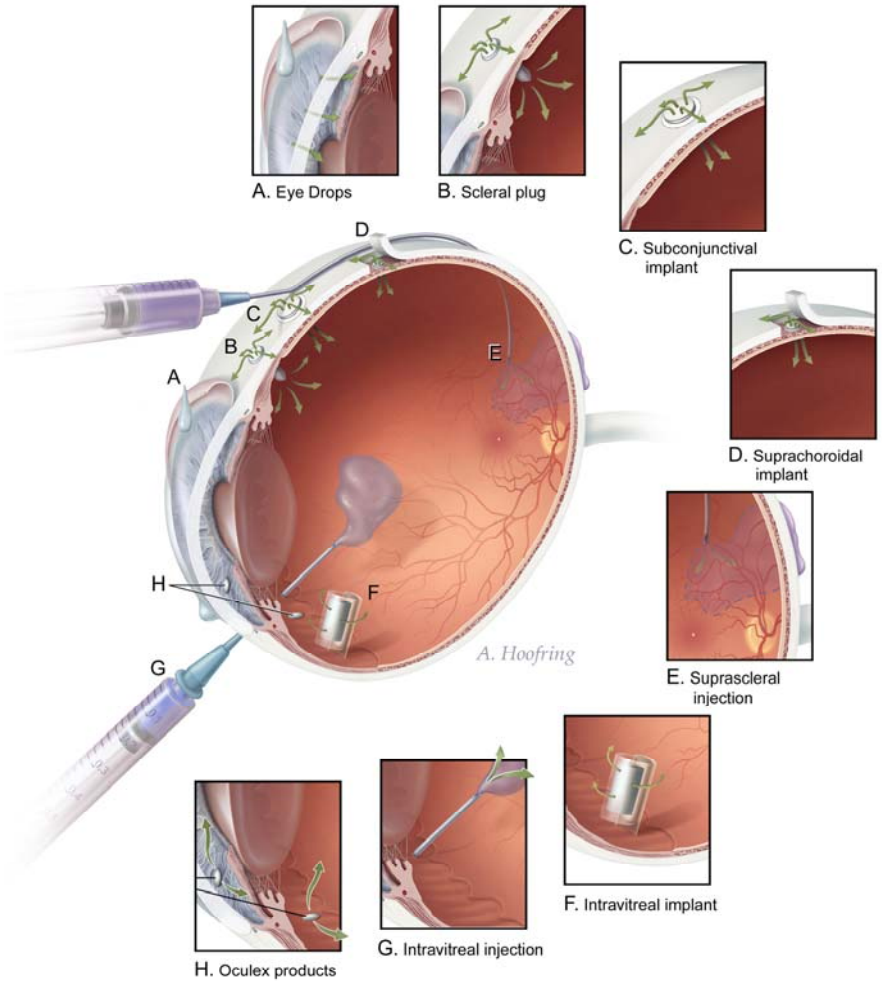

Figure 1-3. Ocular drug delivery methods

Since an intravitreal injection and intravitreal implants can produce complications, and since many of the posterior segment ocular diseases are chronic and require delivery of ocular agents for extended time periods, many researchers have investigated the use of transscleral drug release devices. In *in vitro* studies, it has been found that drugs with a molecular weight up to 150 kDa can diffuse through the sclera [3, 25, 26]. In *in vivo* studies, subconjunctivally applied drugs were detected in the retina and in the vitreous [27-30]. Table 1-3 lists several implant devices that have been studied as alternative sustained delivery methods. However, at this time, only a few intravitreal vitreous ocular implants have been commercialized, but no transscleral implants.

Table 1-3. Summary of Sustained release ocular implants.

Implant	Material	Model drug	Property	Ref.
Subconjunctival implant	POE	5-fluorouracil	bioerodible	[55]
	PVA	cytochalasin E	biocompatible	[56]
	PLGA	ganciclovir	biodegradable	[57]
Scleral implant	PLGA	fluconazole	biodegradable	[12]
	PLGA	Betamethasone phosphate	biodegradable	[58]
	hyaluronan		Biocompatibility & biodegradable	[59]
Subconjunctival injection	PLA	Budesonide	biodegradable	[60]
Periocular injection	PLGA	PKC412	biodegradable	[51]
Intravitral & subconjunctival implant	PLGA	5-fluorouridine, triamcinolone, plasminogen activator	biodegradable	[61]

Note: POE: poly(ortho ester); PVA: poly(vinyl alcohol); PLGA: poly (lactic-glycolic acid); poly(lactic acid)

1.1.4. MRI in the ocular research

MRI, magnetic resonance imaging, can produce images of internal regions of the body based on the principles of nuclear magnetic resonance. When an experimental object is placed in a strong electromagnetic field, hydrogen atoms in the object align themselves parallel with the magnetic field, either in the same direction or opposite to the direction of the field depending on magnetic charge. At pre-determined slice through the object, a short radio frequency signal (RF) is sent through the experimental object, perpendicular to the main magnetic field. The hydrogen atoms, which have the same frequency as the RF, become excited and resonate with the excitation wave. When the RF is turned off, the hydrogen atoms return to their original energy state. The excited energy is released in the form of radio waves, which are detected by antenna coils in the MRI machine. The time it takes for the excited hydrogen atoms to return to their original energy level depends on the number of atoms and characteristic physical properties of the various tissue types. This time is measured and analyzed by a computer. These measurements are used to construct images of tissues of the experimental object. MRI has been used widely in investigations of the eye such as determining anatomy and pathology [31-33], following movement of the aqueous humor [34-36], detecting blood retinal barrier breakdown [37] or preretinal neovascularization in diabetic retinopathy [38], and detecting the effect of vascular endothelial growth factor (VEGF) [39].

The concentration distribution and clearance of a MRI contrast agent, Gd-DTPA delivered to the rabbit eye by subconjunctival and intraocular (injections and implants) administration, are evaluated in this thesis by MRI.

1.1.5. Pharmacokinetics

Pharmacokinetics, which describes the quantitative relationship between administered dose and tissue concentration over time, is an important tool in drug development. Worakul et al. [40] reviewed various ocular pharmacokinetic models for drug delivery systems to the front of the eye, but not to the posterior segment of the eye. Currently, the two available clinical methods to deliver ocular therapeutic agents to the deep eye structures are direct injections into the vitreous and intravitreal placement of sustained release implants. To optimize drug concentration at the target sites, pharmacokinetic studies are useful. Several studies have investigated the elimination of applied drugs in the vitreous with compartmental models [41, 42]. Both the vitreous and the aqueous humor were represented by homogenous compartments and the elimination rate constant and the half-lives were determined. One of assumptions of lumped compartmental analysis is that model drug distributes homogeneously throughout each compartment [43]. Therefore, a limitation of the compartmental pharmacokinetics is that the spatial distribution of an applied drug within the region of interest such as the vitreous is not obtained. We used pharmacokinetic compartment models to analyze our Gd-DTPA data and triamcinolone acetonide data. To overcome the limitation of the compartmental pharmacokinetics, several studies have been done to determine the disposition of ocular drug injected or released from an intravitreal implant in the vitreous using finite element mathematical models of the eye [4, 44-49].

We have developed such a finite element model and compared our

experimental MRI data for Gd-DTPA to the simulations in order to estimate several transport parameter values such as retinal permeability. In addition, we simulated the distribution of model drug in the vitreous and the posterior segment of the eye.

1.2 Research objectives

Our general research objectives were to develop new drug delivery methods and optimize the delivery of therapeutic agents to a specific target site, in this case, the posterior segment of the eye. To achieve this goal, it is necessary to understand the movement and the elimination of therapeutic agents injected or released from a sustained release implant. To this end, the following studies have been done:

(1) Investigate the distribution of fluorescein conjugated lipophilic material released from either a subconjunctival implant or an intravitreal implant in the Brown-Norway rat eye in Chapter 2.

(2) Study the 3-D dynamic movement of drug surrogate, Gd-DTPA released from either a subconjunctival implant or an intravitreal implant in the rabbit eye with a MRI technique in Chapter 3.

(3) Develope a finite element mathematical eye model to analyze the MRI experimental data quantitatively by comparing the data to simulations in Chapter 4 and 5.

(4) Study the pharmacokinetics of intravitreal administration of a triamcinolone acetonide preservative-free (TAC-PF) formulation in the

rabbit eye to determine obtain a model of drug residence time that could be extrapolated to human trials in Chapter 6.

To accomplish these goals, it was necessary to develop a sustained release implant device for both intravitreal and subconjunctival placement. We developed implants of polyvinyl alcohol (PVA) or hydroxypropyl methyl cellulose (HPMC) to provide a simple and convenient device to deliver H-110 and Gd-DTPA.

CHAPTER 2. Movement of H-110 in the eye

2.1 Objectives

The movement of a small size and lipophilic agent released from sustained release implants will be determined in the rat eye with fluorescence technology.

2.2 Introduction

Previous studies have been performed to aid in the understanding of the movement of drugs injected intravitreally or subconjunctivally in the eye [62-64]. Also, simulations have been done to predict the distribution of ocular drugs in the eye [4, 44]. However, most of these previous studies have related to the movement of hydrophilic fluorescein or fluorescein-conjugates.

A limited number of studies [56, 65, 66] have been done that delivered lipophilic anti-angiogenic therapeutics to the subretinal region and the retina pigment epithelium (RPE) with sustained release technology. These studies are relevant since one of factors affecting the movement of administered drugs is solubility and many anti-angiogenic agents are lipophilic.

In this study, we determined the distribution of a small size and lipophilic agent, 5-hexadecanoylaminofluorescein (H-110), released from a polyvinyl alcohol (PVA) based implant or a hydroxypropyl methyl cellulose (HPMC) based implant in rat eye.

2.3 Materials and methods

2.3.1 Materials

5-hexadecanoylaminofluorescein was purchased from Molecular Probes (Eugene, OR, USA). Polyvinyl alcohol (AIRVOL® 125, 99.48 mol % hydrolysis) was purchased from Air Products and Chemicals (Allentown, PA, USA). Hydroxypropyl methyl cellulose (HPMC) was purchased from Sigma (St. Louis, MO, USA).

2.3.2 Implants fabrication

Two types of sustained release matrix implants were fabricated by mixing the model compound, H-110 (MW = 586) with either polyvinyl alcohol (PVA) (implant A) or hydroxypropyl methyl cellulose (HPMC) (implant B). Both implants A and B were 1.5 mm flat discs, making them suitable for insertion into the vitreous and the subconjunctival space of a rat eye. Both implants were prepared using the following procedure: a 15% polyvinyl alcohol (PVA) (w/v) solution was prepared by placing 0.75 g of PVA in 5 ml of molecular biology grade water (Eppendorf Scientific, Inc., Westbury, NY, USA) in a closed vial, and placed in a waterbath at 100 ºC for 3 hours. A 30% H-110 matrix suspension was produced by adding 0.321 g of H-110 to the PVA solution. The drug suspension was stirred until uniform and poured onto a glass plate to form a thin film and dried at room temperature in the dark. The film was punched with a biopsy punch (Acu·Punch® 1.5 mm, Acuderm, USA) to make 1.5 mm diameter disks.

Comparable 30% H-110 implants were made in a similar fashion using 15%

HPMC instead of PVA. Sham implants (implants without H-110), of 15% PVA or 15% HPMC, were also made.

2.3.3 *In vitro* study

In vitro release rate experiments were performed on the 15% PVA / 30% H-110 for 7 days and the 15% HPMC / 30% H-110 for 5 hours. Implants were placed in 20 ml of phosphate buffered saline (PBS) (pH 7.4) and stirred slowly with a magnetic stirrer. The solution was assayed at designated time intervals and completely replaced with fresh PBS at each sampling time to maintain sink condition. H-110 assays were performed using a spectrofluorometer (QuantaMaster, Photon Technology International, Lawrenceville, NJ) at excitation wavelength 497 nm and emission wavelength 519 nm. The release rates were determined from the amount of H-110 released over time and recorded as μg per day.

2.3.4 Animal experiment

All animal care conformed with the ARVO Statement for the Use of Animals in Ophthalmic and Vision Research and was approved by the Animal Care and Use Committee at the National Eye Institute. Before surgeries, the rats were anesthetized by intraperitoneal injection of a mixture of ketamine (100 mg/kg) and xylazine (9 mg/kg). The implants were surgically placed in the subconjunctival space or the vitreous cavity of Brown Norway rats. The HPMC based implants or the PVA based implants were placed in the subconjunctival space and the animals were sacrificed at 1, 2, 3, and 4.5 hours post implantation or at 3, 5, and 7 days post

implantation, respectively. Only HPMC based implants were placed in the vitreous cavities and the animals were sacrificed at 1, 2, 3, and 24 hours post implantation.

2.4 Results

2.4.1 *In vitro* release rates

Fifteen% PVA / 30% H-110 implants (n=4) released H-110 over 7 days following an initial bursts (Figure 2-1 (A)). On the other hand, 15% HPMC / 30% H-110 implants (n=4) released most of its contents of H-110 within the first 1 hour sample time. HPMC is a very water-soluble material and disintegrates quit rapidly in water (Figure 2-1 (B)). A HPMC-based implant shows a time release profile similar to a large bolus injection.

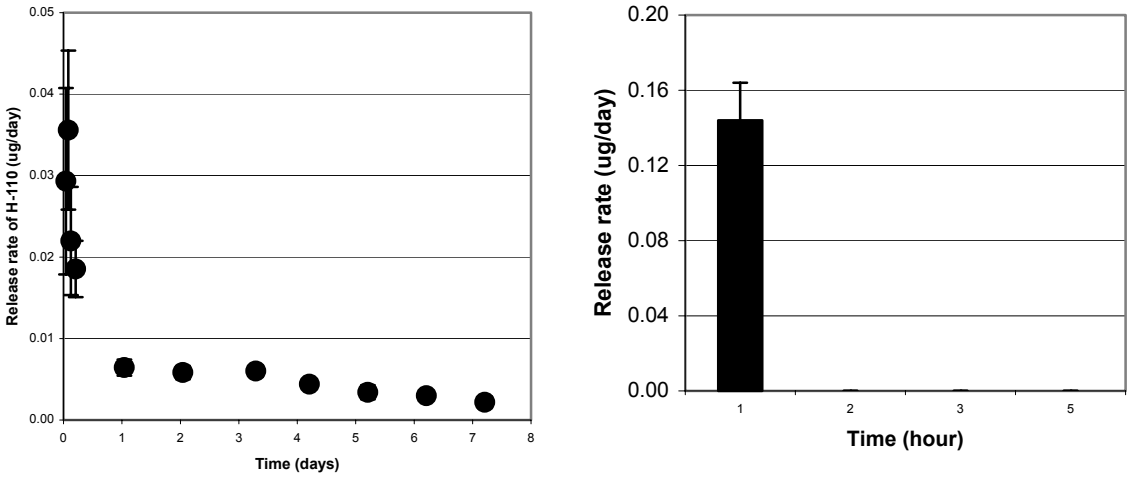

(A) (B)

Figure 2-1. *In vitro* release rate of H-110 from (A) 15% PVA / 30% H-110 implant (n=4) and (B) 15% HPMC / 30% H-110 implants (n=4).

2.4.2 Distribution of H-110 released from subconjunctival implants

Figure 2-2 are frozen section tissue slices showing the position of implants in the subconjunctival space for: (A) the PVA based subconjunctival implant in the posterior segment of the eye and (B) the HPMC based subconjunctival implant. Since the HPMC based implant dissolved quickly, its outline is not as readily visible as the PVA based implant. Figure 2-3 (A) shows the fluorescence intensity in a tissue slice 3 days after the subconjunctival implantation of a PVA implant. H-110 is seen to be distributed in the subconjunctival space and the sclera which can be compared to the sham implant in Figure 2-3 (B). In Figure 2-3 (A), the black rectangle designates the position of the implant in the subconjunctival space. A small amount of H-110 was found in the subretinal region; but is much less than that found in the sclera. Figure 2-4 and 2-5 show serial frozen sections of eye tissue at different magnification. We can see that a small amount of H-110 released from an HPMC-based subconjunctival implant reaches the subretinal from a PVA-based subconjunctival implant (Figure 2-4). This may result from the more rapid release of H-110 from the HPMC implant compared to the PVA implant. These findings suggest that there might be a formidable barrier such as the choroid, between the retina and the sclera.

Figure 2-6 presents an interesting finding that the HPMC-based subconjunctival implant distributes around the circumference of the sclera as quickly as 4.5 hours post implantation. This distribution of H-110 is faster than would be expected from only pure diffusion. Additional mechanisms of H-110 movement may

be in play, such as uveal-scleral flow [64] and enhance the distribution. Investigation of the possible mechanism was beyond the range of this study.

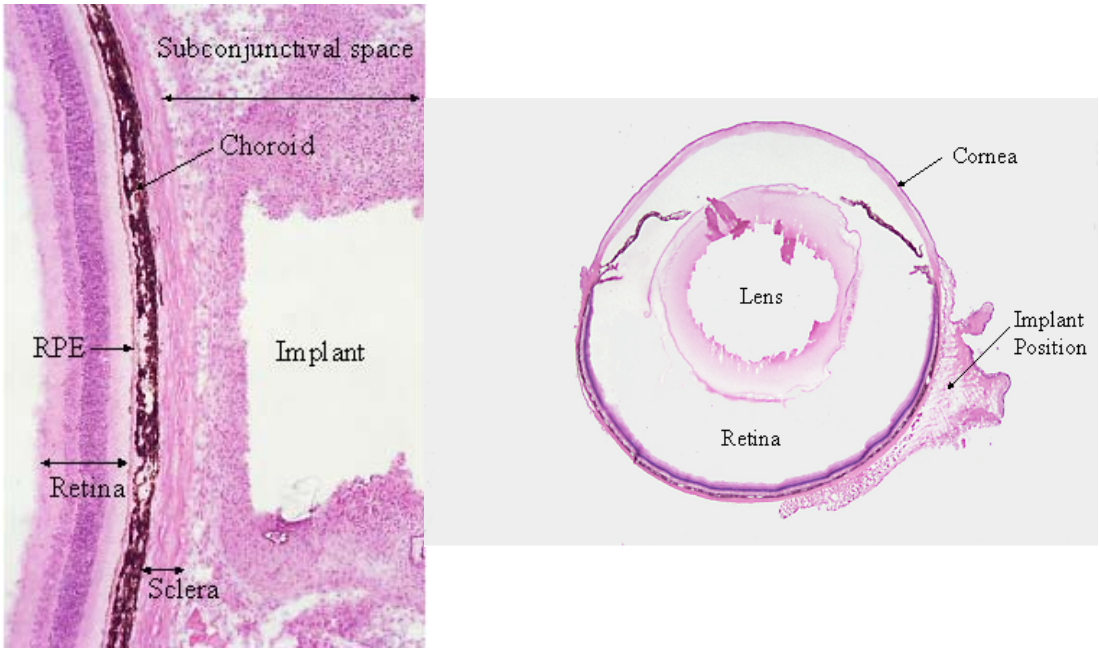

(A) (B)

Figure 2-2. (A) The position of the PVA-based subconjunctival implant at the posterior segment of the eye; (B) the position of the HPMC-based subconjunctival implant.

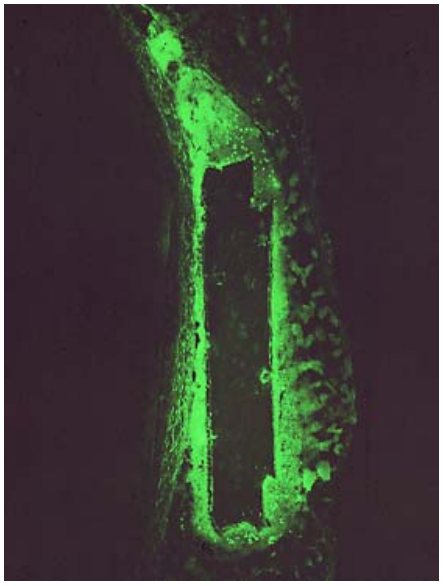

(A)

(B)

Figure 2-3. Florescence intensity distribution of H-110 in tissue slice 3 days post implantation in the sclera, the choroids, and retina regions; (A) a 15% PVA / 30% H-110 subconjunctival implant (×5 magnification); (B) control of (A).

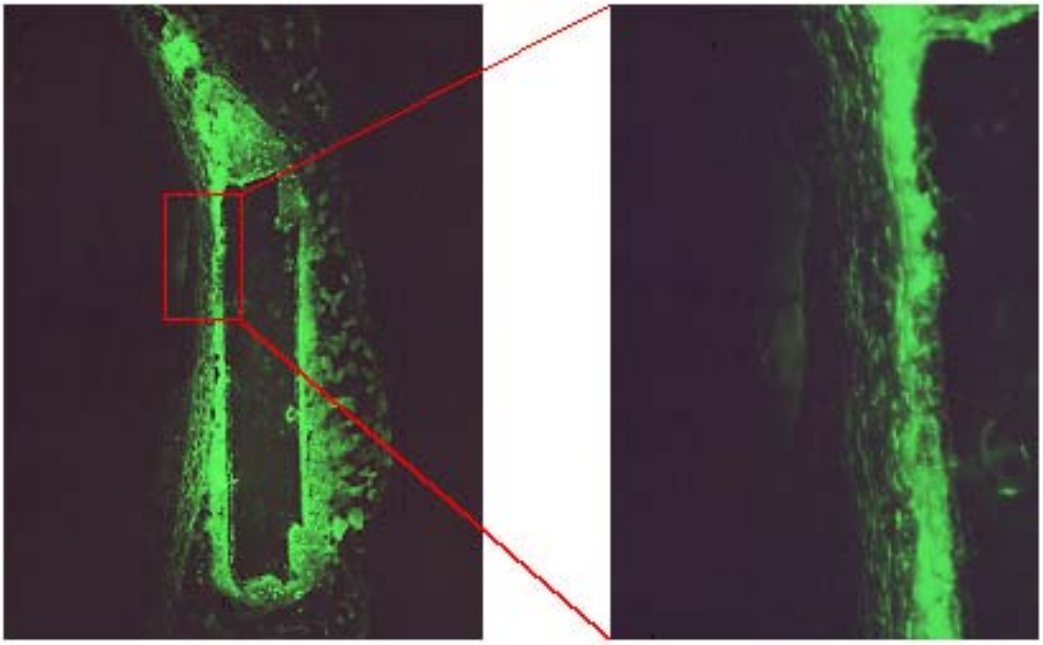

Figure 2-4. Distribution of H-110 released from a 15% PVA / 30% H-110 subconjunctival implant 3 days post implantation. The right image (×20 magnification) focuses on the red rectangular region in the left image (×5 magnification).

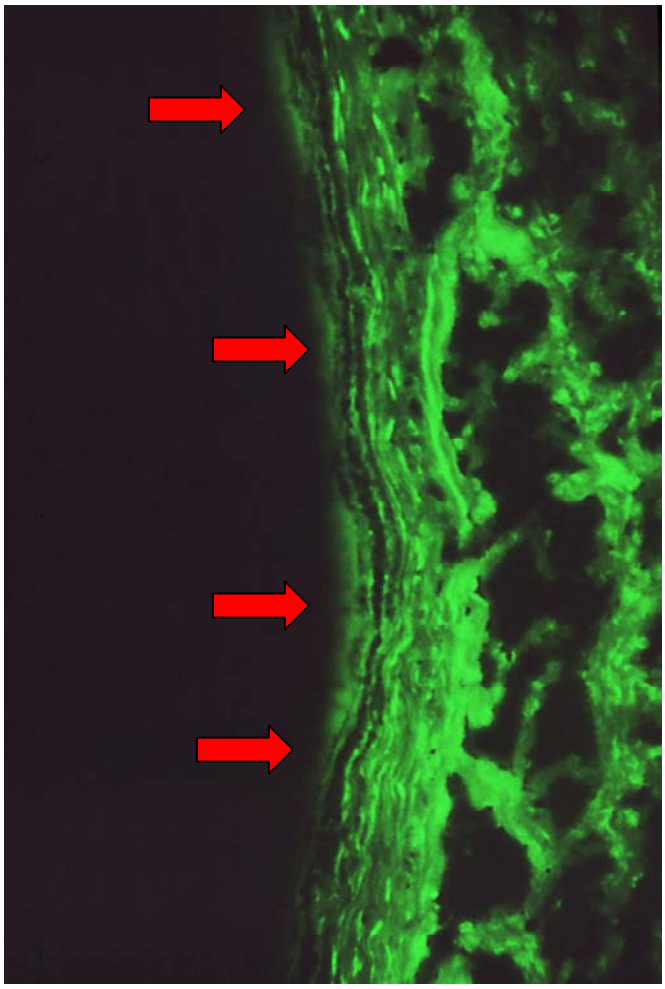

Figure 2-5. Distribution of H-110 released from a 15% HPMC / 30% H-110 implant 3 hours post implantation (×20 magnification). The red arrows indicate H-110 in the subretinal region.

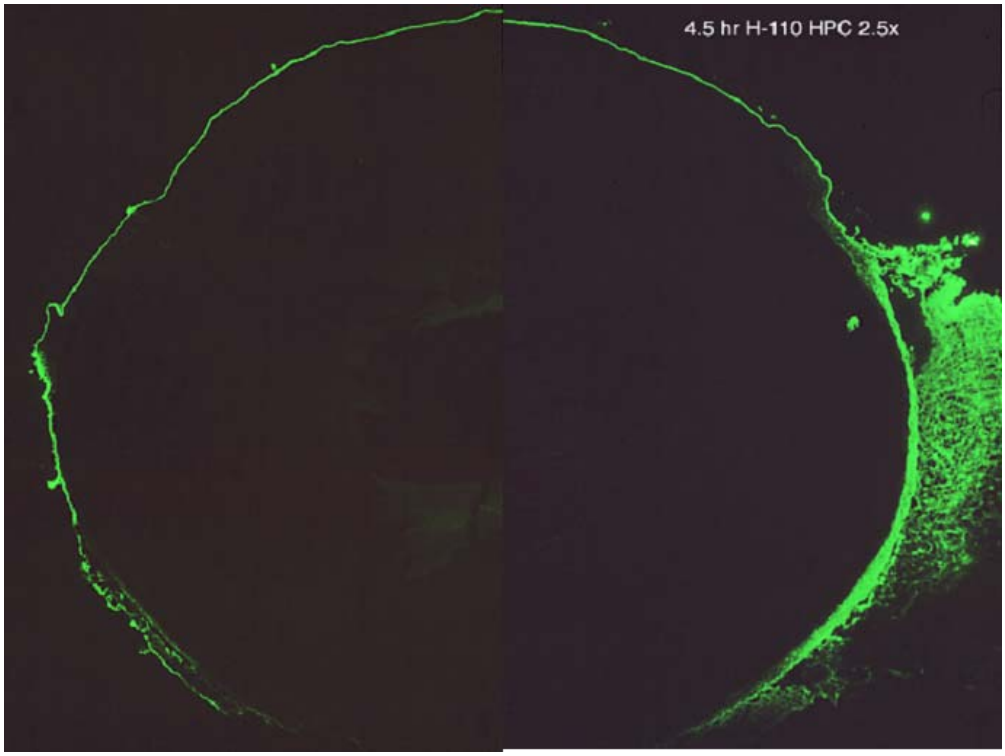

Figure 2-6. Distribution of H-110 released from a 15% PVA / 30% H-110 implant in the eye 4.5 hours post implantation (×2.5 magnification).

2.4.3 Distribution of H-110 released from intravitreal implants

Delivering therapeutic agents from the vitreous is an alternative delivery route to the subretinal region in the posterior segment of the eye. To date, only the intravitreal implants among several sustained release implants have been commercialized [13]. We used an HPMC based implant to release H-110 into the vitreous cavity. Figure 2-7, 2-8, and 2-9 show the distribution of H-110 released from the intravitreal implant in the posterior segment of the eye, specially, in the retina. With time, we could see the penetration of released H-110 into the retina. H-110 diffused by the inner segments layer and by the outer plexiform layer in the retina 1 hour and 3 hours post implantation (Figure 2-7 and 2-8), respectively. After 1 day, H-110 was found in the subretinal region (Figure 2-9).

Compared to the subconjunctival experimental data, delivery of lipophilic agents from the vitreous to the subretinal region was found to be more efficient than delivery from the subconjunctival space to the subretinal region.

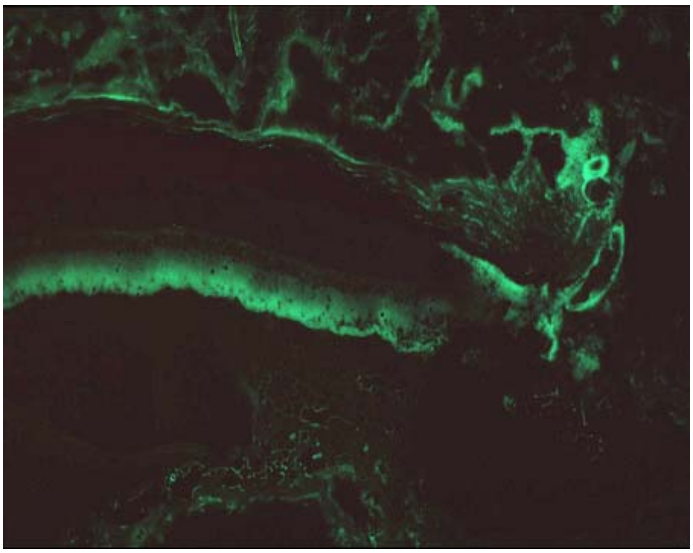

(A)

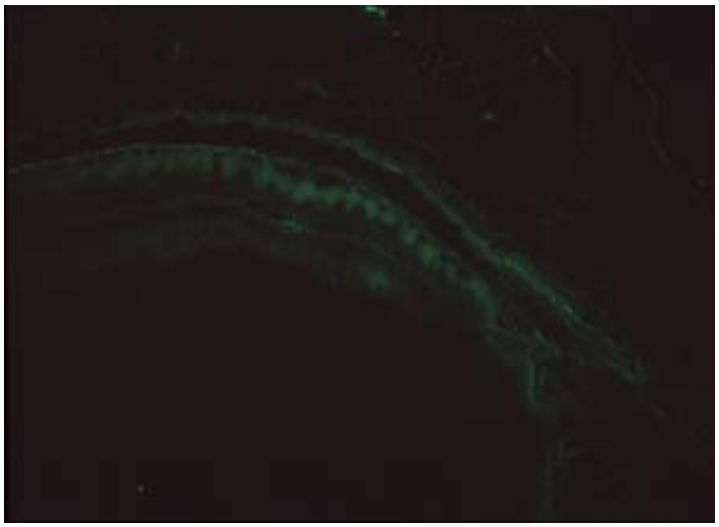

(B)

Figure 2-7. (A) Distribution of H-110 released from a 15% HPMC / 30% H-110 intravitreal implant 1hour post implantation (×10 magnification). (B) The control showing auto fluorescein (×10 magnification).

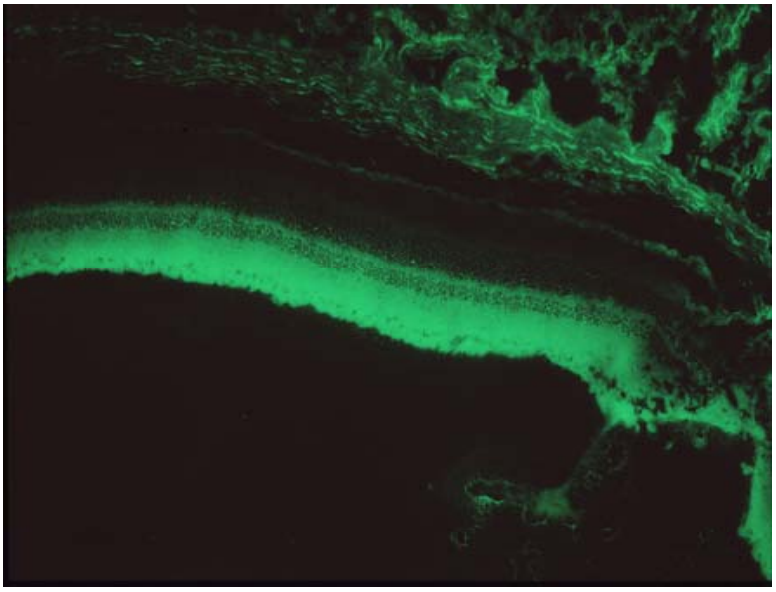

(A)

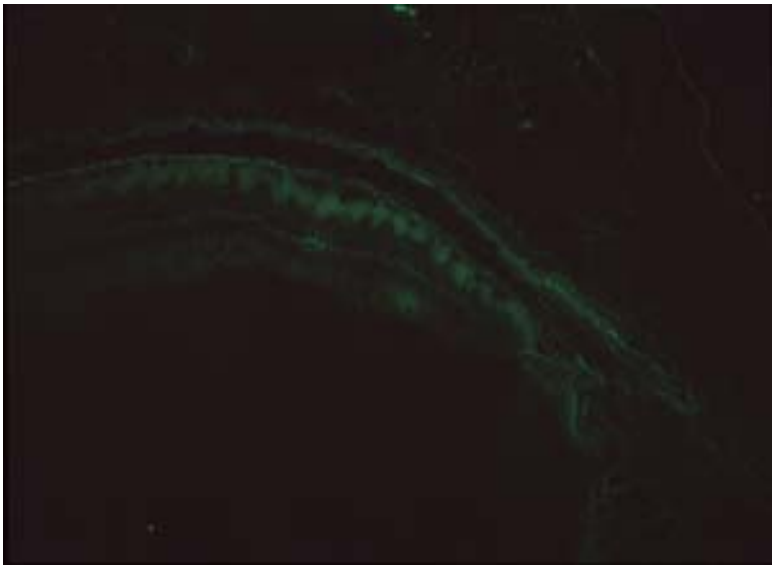

(B)

Figure 2-8. (A) Distribution of H-110 released from a 15% HPMC / 30% H-110 intravitreal implant 3 hours post implantation (×10 magnification). (B) The control showing auto fluorescence (×10 magnification).

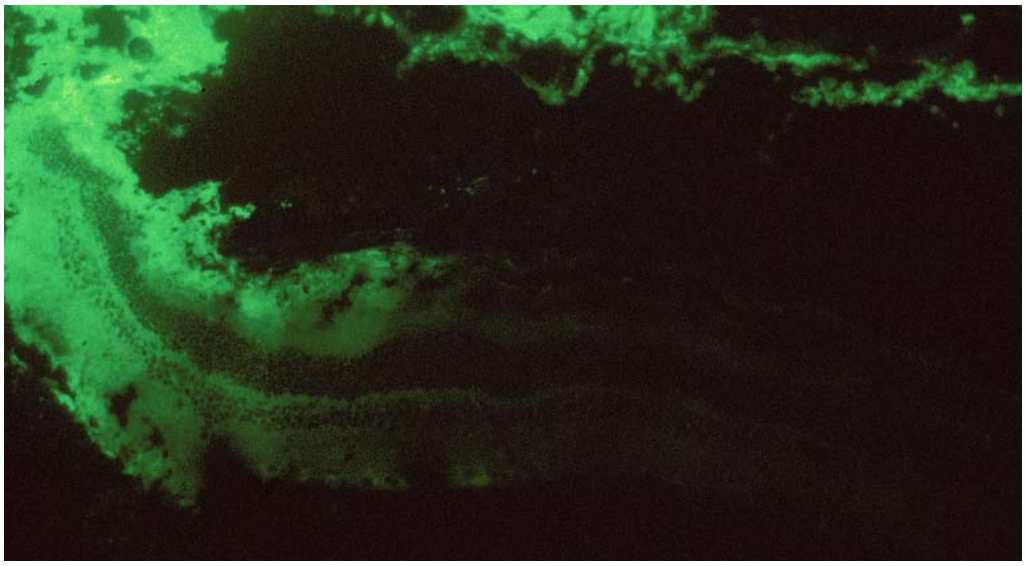

Figure 2-9. Distribution of H-110 released from a 15% HPMC / 30% H-110 intravitreal implant 1day post implantation (×10 magnification).

2.5 Discussion

Recent studies have suggested that lipophilic therapeutic agents are useful for treating a variety of subretinal disorders such as AMD in experimental animal models [28, 54, 60, 65]. According to clinical reports, corticosteriods such as budesonide and triamcinolone acetonide, which are lipophilic agents, have shown reasonable results in treating choroidal neovascularization associated with AMD [9, 67-69], diabetic retinopathy [19, 70] and macular edema associated with central retinal vein occlusion [71-73]. However, the fate of a lipophilic agent in the eye after administration is uncertain. Weijtens et al. (1999) injected 2.5 mg of dexamethasone, which is lipophilic, in the subconjunctival space and measured drug concentration in the aqueous humor and the vitreous at several time points. The maximum dexamethasone concentration in the aqueous and in the vitreous was 858 ng/ml in the vitreous at 2.5 hours post injection and 72.5 ng/ml in the aqueous at 3 hours post injection [28]. Only a small fraction of the injected dexamethasone was delivered to the eye tissue. In this study, it appeared difficult to deliver lipophilic and small size ocular drugs from the subconjunctival space to the subretinal region because of the formidable barriers such as the choroidal blood flow washout.

In previous animal experiments, PVA-based intravitreal implants showed some delivery of 2-methoxyestradiol to the posterior sub-retinal tissue. Robinson et al. [65] developed an intravitreal implant that released 2-methoxyestradiol and it was able to inhibit CNV in an animal model compared to the control. However, because of the complications of intravitreal implants, subconjunctival implants is an attractive alternative (See Table 1-3). Kim et al.

(2002) [63] investigated the intraocular distribution kinetics of 70 kDa fluorescein-conjugated dextran after subconjunctival injection in the rat eye. The fluorescein-conjugated dextran diffused transsclerally and dispersed throughout a large portion of the sclera, uvea, and cornea through the uveoscleral outflow pathways. Transscleral influx and intrachoroidal dispersion of 70 kDa fluorescein-conjugated dextran in the mouse eye was not precluded by either transcleral aqueous flow or by choroidal blood flow. In our study, H-110, a lipophilic agent, dispersed around the circumference of the eye (Figure 2-6) in the similar fashion as the fluorescein-conjugated dextran. H-110 reached the opposite pole of the eye 4.5 hours post implantation. Pure diffusion of H-110 alone cannot account for this distance at 4.5 hours. Therefore, a uveoscleral outflow mechanism may enhance the H-110 dispersion around the eye as in the case of fluorescein-conjugated dextran. Unlike fluorescein-conjugated dextran, little H-110 could reach the subretinal space. The choroidal blood flow was found to be a more formidable barrier to lipophilic and small size agents than hydrophilic and large size agents. However, in this study, we did not determine whether solubility or molecular size was the main factor in the elimination through the choroid.

In the *in vivo* implant studies, we found that it was more efficient to deliver H-110 from the vitreous to the subretinal space than from the subconjunctival to the retina. In our study, H-110 diffused into the retina uniformly (See Figure 2-7, 2-8 & 2-9). A previous study found that intravitreally injected fluorescein, which is hydrophilic, was eliminated across the retina by the active transport [62]. Based on the previous study, we assumed H-110 moved into the retina mainly by pure diffusion

because the retina is lipophilic and the retina was not a barrier to the delivery of H-110 to the subretinal space [46].

Our polyvinyl alcohol (PVA) based subconjunctival implant showed sustained release of H-110 for over one week following the initial rapid release. PVA has been our preferred choice for ocular implants because of its biocompability [65]. The initial rapid release might be due to the H-110 on the surface of the implant because H-110 might have diffused onto the surface with the water vapor during the drying process in the implant fabrication [74].

2.6 Conclusions

Delivering small size and lipophilic agents from the vitreous to the subretinal region was found to be more efficient than delivering from the subconjunctival space to the subretinal region because the choroid was a formidable barrier to the passage of a lipophilic fluorescent compound released from a sustained release device placed in the subconjunctival space of the rat.

CHAPTER 3. Controlled drug release from an ocular implant: real-time evaluation using magnetic resonance imaging

3.1 Objectives

The movement of small size and hydrophilic agents released from sustained release implant will be determined in the rabbit eye with magnetic resonance imaging (MRI) technology.

3.2 Introduction

Standard preclinical techniques of assessing ocular drug distribution, autoradiography and fluorescein labeling require euthanasia of different animals at variable time points with serial sectioning of the eye to reenact the movement of the drug molecules *in vivo* [75]. Standard techniques do not permit time serial studies and determination of drug diffusion gradients in the eye of individual animals. Fluorophotometry is limited to assessments of bulk fluorescein movement in the aqueous and vitreous humor [76].

In this chapter, we sought to develop a technique to evaluate the ocular distribution and elimination pathways of a drug surrogate from a sustained-release implant in normal rabbit eyes using magnetic resonance imaging (MRI) technology. We developed a sustained-release implant that releases the contrast agent gadolinium-diethylenetriaminopentaacetic acid (Gd-DTPA, molecular weight = 938 Daltons). These implants were evaluated separately in the subconjunctival space on the

episclera at the equator and in the vitreous cavity. Real-time movement of the drug surrogate was assessed with MRI.

3.3 Materials and methods

3.3.1 Implant fabrication

An episcleral implant was manufactured using the procedure as shown in Figure 3-1: 10% polyvinyl alcohol (PVA) (w/v) solution was formulated by placing 1.0 g of PVA (Celvol, Celanese Chemicals, Ltd., Dallas, TX) in 10 ml of molecular biology grade water (BIOfluids®, Biosource International, Camarillo, CA) in a 50 ml polypropylene conical tube (Falcon®, BD Biosciences, Franklin Lakes, NJ) and placed in a water bath at 100°C for 3 hours to dissolve all the PVA. The PVA solution was cooled down to room temperature and 0.71 ml of 0.5 M Gd-DTPA solution was added and stirred into the PVA mixture to produce a solution of 10% PVA and 25% Gd-DTPA (w/w/v). Eight ml was poured onto a glass plate which produced a thin film as it dried at room temperature. A biopsy punch (Acu•Punch® 4 mm, Acuderm Inc, Ft. Lauderdale, FL) was used on the dried film to make 4 mm diameter disks. Individual disks (8 total) were placed in a polytetrafluoroethylene mold, which has a 4.3 mm diameter and a 1.4 mm depth. The disks were coated with the remaining 10% PVA and 25% Gd-DTPA (w/w/v) solution. The dried implant was peeled out of the polytetrafluoroethylene mold and a total of 6.4 mg of Gd-DTPA was loaded into each episcleral implant.

An intravitreal implant was manufactured in a similar fashion as above

except less drug loading per implant was necessary to decrease the intensity of the Gd-DTPA signal in the vitreous (Figure 3-2). To accomplish this, a 15% PVA and 20% Gd-DTPA (w/w/v) solution was substituted and a smaller implant was made with 3 mm disks and mold dimensions of 3.2 mm diameter and 1.2 mm depth with a suture stub extension on one side of the implant for scleral fixation. A total of 3.7 mg of Gd-DTPA was loaded into each intravitreal implant.

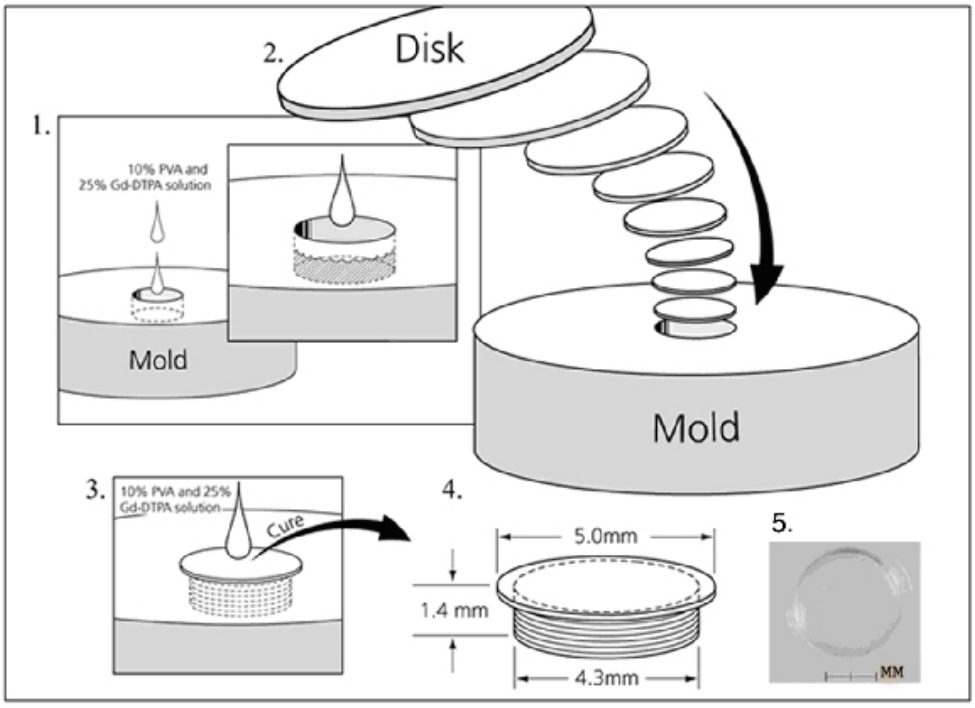

Figure 3-1. Fabrication procedure for the episcleral implant. 1: PVA/Gd-DTPA solution in mold 2: PVA/Gd-DTPA dry matrix discs inserted 3: complex cured 4: schematic of implant removed from the mold with dimensions 5: Photograph of the Gd-DTPA episcleral implant.

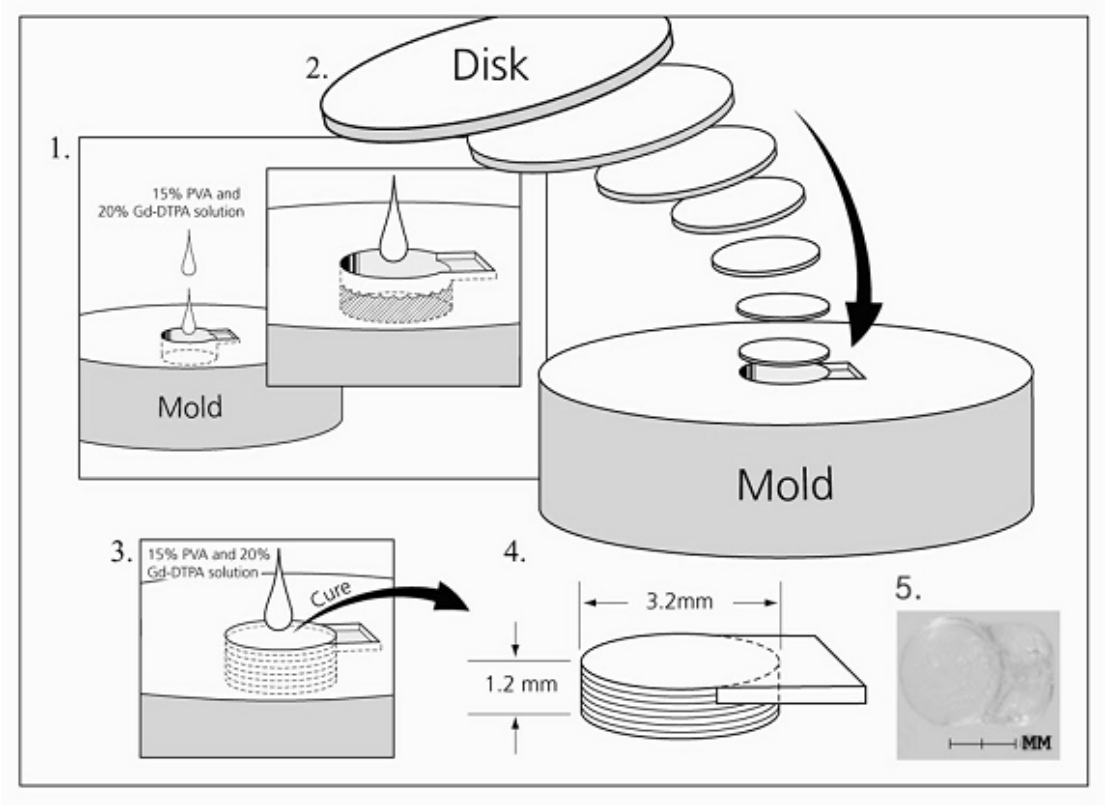

Figure 3-2. Fabrication procedure for the intravitreal implant. 1: PVA/Gd-DTPA solution in mold 2: PVA/Gd-DTPA dry matrix discs inserted 3: complex cured 4: schematic of implant removed from the mold with dimensions 5: Photograph of the Gd-DTPA intravitreal implant.

3.3.2 *In vitro* release rate determination

As previously reported [77], the release of Gd-DTPA from both the episcleral and intravitreal implants was equal from all external surfaces except at the suture platform in the intravitreal implant. For the batch of implants used in this study, bulk release was determined by placing the implants in 25 ml glass vials with

20 ml of phosphate buffered saline (PBS) (pH 7.4) and stirred with a magnetic bar at 150 rpm at room temperature. The solution was assayed every 10 minutes for one hour, every 30 minutes for the second hour, and hourly for the next 6 hours. The solution was completely replaced following each assay with fresh PBS to simulate sink conditions. The Gd-DTPA assays were performed using a spectrofluorometer (QuantaMaster, Photon Technology International, Lawrenceville, NJ) operated by FeliX (version 1.21, Photon Technology International). A calibration curve was made using a 275 nm excitation wavelength and a 312 nm emission wavelength and the lowest detectable concentration of Gd-DTPA was 4.69 ng/ml. The release rates were determined by calculating the amount of Gd-DTPA released in a given volume over time and recorded in mg per hour ± 1 S.D.

3.3.3 Magnetic resonance imaging

Dynamic MRI was used to image the rabbit eyes. All imaging experiments were performed on a 4.7 Tesla MRI system (Bruker Instruments, Billerica, MA). The images were analyzed using MATLAB (version 6.5, Mathworks Inc., Natick, MA) and Amira (version 2.3, TGS Inc., San Diego, CA).

3.3.3.1 *In vivo* experiments

New Zealand White (NZW) rabbits (n=3) weighing 2-3 kg were used (Covance Laboratories, Inc., Vienna, VA) and the procedures adhered to the guidelines from the Association for Research in Vision and Ophthalmology for animal use in research. Each rabbit was maintained under general anesthesia during

the 8-hour imaging period. The animals were initially anesthetized with ketamine hydrochloride (Fort Dodge, Inc., Fort Dodge, Indiana) 35 mg/kg intramuscular (IM) and xylazine (Phoenix Scientific, Inc., St. Joseph, MO) 5 mg/kg IM and an intravenous catheter was inserted into the marginal ear vein to administer fluids. An endotracheal tube was placed and anesthesia was maintained with 1 to 2% halothane or 1 to 2% isoflurane. During anesthesia, the rabbit's pulse, SpO_2, end-tidal CO_2, respiratory rate, anesthetic gas levels, and body temperature were monitored and maintained via a water pad connected to a heated recirculating pump. After adequate anesthesia and akinesia were obtained, a lid speculum was placed and the right pupil was dilated with 1 drop of phenylephrine hydrochloride 2.5% (Akorn, Inc., Decatur, IL) and tropicamide 1% (Alcon, Inc., Humacao, Puerto Rico). Proparacaine 1% ophthalmic drops (Allergan America, Hormigueros, PR) were used topically on the eye and an incision was made through the conjunctiva and tenon's fascia in the superotemporal quadrant at the equator of the globe. The equator of the rabbit eye was defined as the point at which the sclera starts the downward slope towards the optic nerve, approximately 5-6 mm posterior to the limbus.[78] The episcleral implant was placed directly on the episclera at the equator and the tenon's fascia and conjunctiva was reapproximated using 8-0 vicryl suture. For intravitreal placement, a 4 mm sclerotomy was performed at the equator, the implant was inserted into the vitreous cavity and sutured to the sclera using 8-0 vicryl suture. The sclerotomy was closed using 8-0 vicryl suture and the conjunctiva was reapproximated to the limbus using 10-0 vicryl suture. The rabbit was positioned in the scanner and the head was centered in a 10 cm diameter volume coil and imaged for 8 hours. Complete T_1-

weighted Fast Spin Echo 3D images were acquired over 20 minute intervals. The imaging parameters were Repetition time (TR)/ echo time (TE) = 267/9 ms, Field of View (FOV) = 9 cm × 9 cm × 9 cm, the acquisition matrix was 256 × 128 × 128, 2 averages, and echo train length was 8. An *in vivo* control eye (no implant) was imaged and a representative coronal section was recorded.

3.3.3.2 *Ex vivo* experiments

NZW rabbits were anesthetized as described above and euthanized with an intracardiac pentobarbital overdose (Beuthanasia-D Special, Scheming-Plough Animal Health Corp., Kemilworth, NJ). The right eye including the conjunctiva, tenon's fascia, extraocular muscles, and intraconal fat was removed with sharp dissection. The implants were placed on the episclera or vitreous cavity as described above. The eye was immediately wrapped with a 4 in × 4 in gauze pad moistened with phosphate buffered saline and placed in a sealed 50 ml conical tube. The tube was positioned in a 7.2 cm diameter volume coil and imaged every 10 minutes for 8 hours. The parameters were TR/TE = 259/6.6 ms, FOV = 5 cm × 5 cm × 4 cm, acquisition matrix size= 256 × 128 × 128, 1 average, and the echo train length was 8. An *ex vivo* control eye (no implant) was imaged and a representative coronal section was recorded.

3.3.4 Quantitative analysis of Gd-DTPA from MRI images

To measure Gd-DTPA concentrations directly from gray scale T_1-weighted MRI images, standard solutions of Gd-DTPA were scanned along with the rabbit eye. The following concentrations of Gd-DTPA were prepared in a 2% hydroxypropyl methylcellulose (METHOCEL®, Dow Chemical Company, Midland MI) solution: 1.0×10^{-1} M, 0.5×10^{-1} M, 1.0×10^{-2} M, 0.5×10^{-2} M, 0.25×10^{-2} M, 1.0×10^{-3} M, 0.5×10^{-3} M, 1.0×10^{-4} M, 0.5×10^{-4} M, 1.0×10^{-5} M, 0.5×10^{-5} M, and 1.0×10^{-6} M. Each of the 12 standard solutions were poured into 12 individual wells cut from a standard 96 well plate culture chamber and sealed with a silicone adhesive. Gray scale MRI images of the standard solutions were developed and average intensity value of each concentration was determined using the ImageJ (ver 1.27z, National Institutes of Health, USA).

3.4 Results

3.4.1 *In vitro* release rate

The *in vitro* release of both the episcleral (n=4) and intravitreal implants (n=4) demonstrated an initial burst with a declining diffusion phase (Figure 3-3). This release pattern is typical of a matrix implant whose release kinetics is governed by diffusion from dispersed drug in a polymer [79].

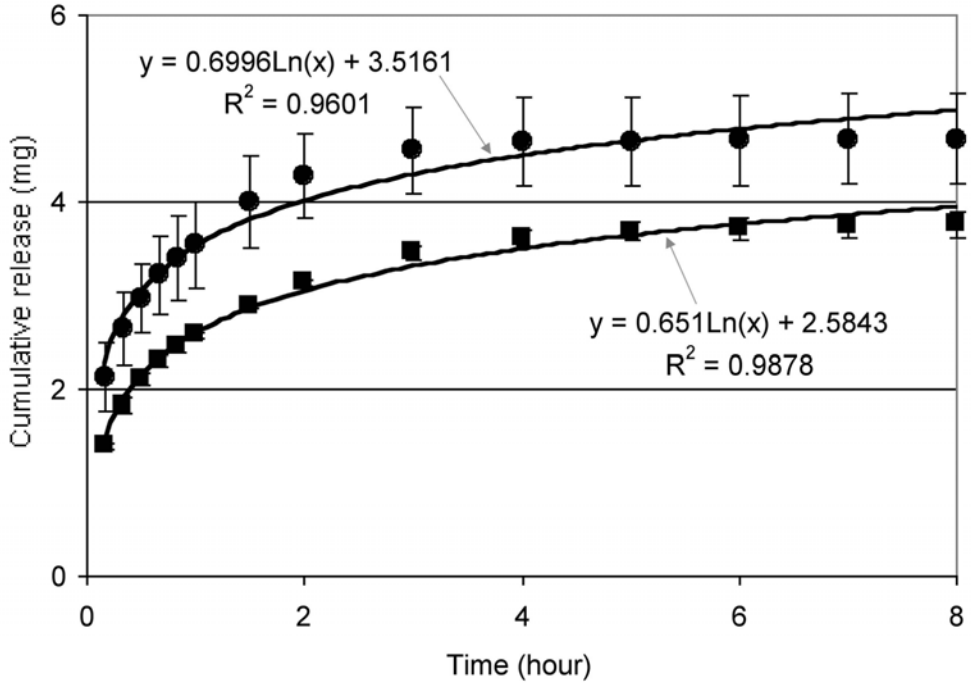

Figure 3-3. Cumulative release (mg ± 1 S.D.) over time of Gd-DTPA from episcleral (circle) and intravitreal (square) implants.

The episcleral implant released more total drug because of the increased drug loading in the manufacturing process. A total of 4.7 ± 0.49 mg and 3.8 ± 0.14 mg were released over 8 hours by the episcleral and intravitreal implants, respectively, with 99% of the drug that released occurring by 5 hours in the sink conditions of the *in vitro* assay.

3.4.2 Calibration curve for MRI quantitative analysis

The relationship of Gd-DTPA concentration and image intensity

values were determined during each experiment by scanning the standard Gd-DTPA solutions along with the eye. The lower detection limit of the Gd-DTPA was 0.5×10^{-5} M and the intensity signal initially increased with concentration up to 0.5×10^{-2} M (Figure 3-4). The intensity signal decreased with Gd-DTPA concentration beyond 0.5×10^{-2} M because of the T_2 shortening effects [80]. Therefore, area of very high drug concentrations immediately around the implant could not be quantified. Since Gd-DTPA has to be in an aqueous phase to generate a signal with T_1-weighted MRI images, no MRI signal emanated from within the implant.

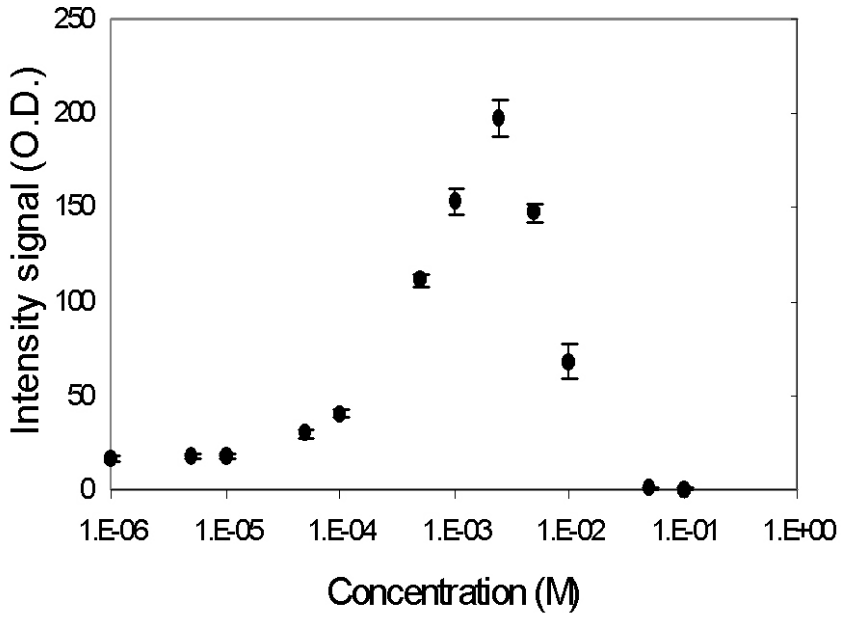

Figure 3-4. Calibration curve from standard solutions showing the relationship of Gd-DTPA concentration and image intensity values in O.D. (optical density) units. Each error bar represents the standard deviation of intensity values at each concentration solution.

3.4.3 MRI of *in vivo* and *ex vivo* control eyes

The *in vivo* MRI image of a control eye had little signal intensity in the vitreous and aqueous reflecting good T_1 saturation of the tissue water molecules (Figure 3-5(A)). The *ex vivo* MRI image of a control eye showed a higher signal relative to the surrounding tissue (Figure 3-5(B)). This is due in part to post mortem hardening of the tissue and a slightly different TR/TE value for the image. The effective background, however, was within experimental error for detecting Gd-DTPA and had less than 1% difference from the calibration standard in the image.

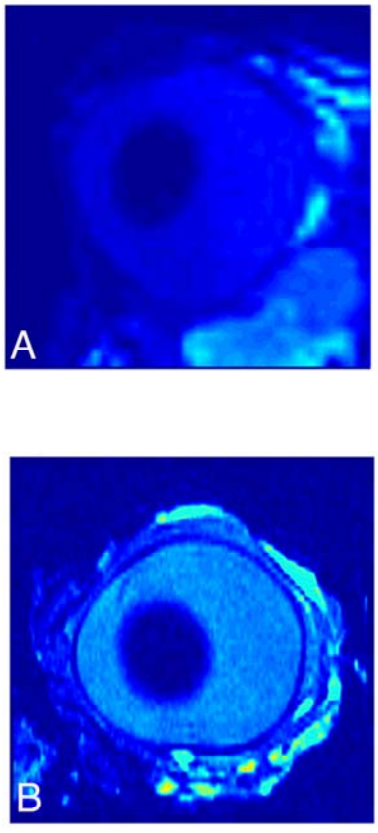

Figure 3-5. Control eyes (no Gd-DTPA implants); A. *in vivo* MRI scan (coronal image) and B. *ex vivo* MRI scan (coronal image)

3.4.4 Episcleral implant: ocular drug distribution

In the *in vivo* experiments with episcleral implants placed at the equator of the eye (n=3), Gd-DTPA signal was first observed in the vitreous and aqueous humor after a mean of 84.3 ± 12.7 minutes and 115.7 ± 28.4 minutes, respectively (Figure 3-6(A) & 3-6(B)). Over the 8 hour scan, the total mean cumulative amount of Gd-DTPA measured in the vitreous and aqueous humor was 2.7 ± 0.08 μg and 3.1 ± 2.1 μg, respectively. The mean cumulative amount that entered the vitreous and aqueous (i.e. 5.8 μg) was only 0.12% of the total cumulative amount released by the implant over an 8-hour period. No Gd-DTPA signal was present in the posterior segment of the eye. A gradual accumulation of Gd-DTPA was noted in the right buccal lymph node in 2 rabbits (Figure 3-7). In the *ex vivo* experiment with episcleral implants (n=2), one rabbit had an implant placed at the equator, the other between the equator and the optic nerve. The implant placed at the equator, Gd-DTPA signal was present in the vitreous within 30 minutes and in the anterior chamber within 60 minutes (Figure 3-6(C) & 3-6(D)). Gd-DTPA was present throughout the vitreous cavity and retina with a cumulative amount of 81.3 μg in the vitreous, and 67.8 μg in the aqueous humor, after 8 hours of scanning. In this same time frame, the more posterior implant delivered proportionately more Gd-DTPA into the vitreous (196.6 μg) compared with the aqueous humor (8.7 μg) (Figure 3-6(E) & 3-6(F)).

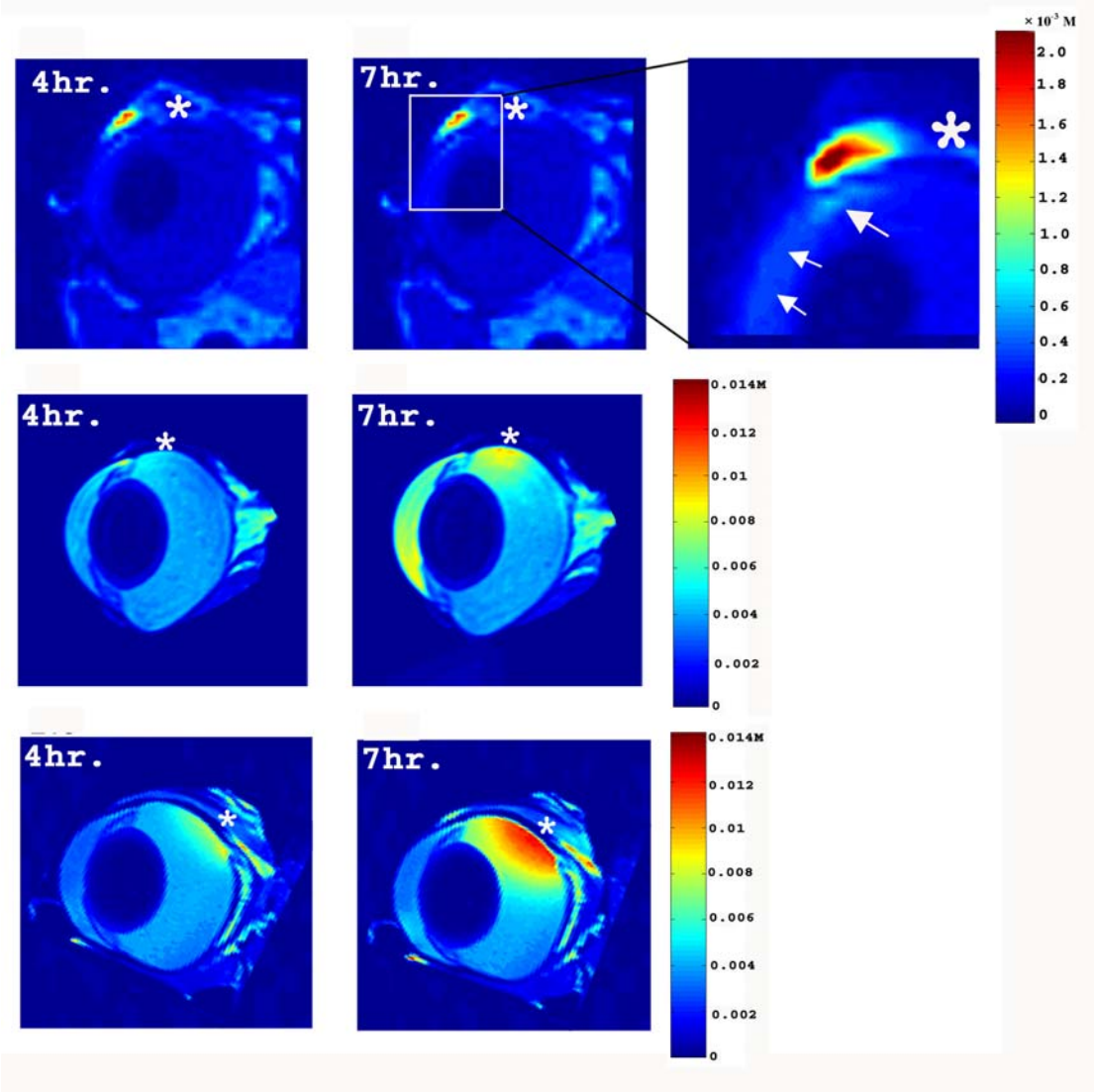

Figure 3-6. MRI scan (coronal images) with an episcleral implant in the right rabbit eye. Asterisk shows location of implant. Bar at the margin correlating Gd-DTPA concentration (M) with color in the image. (hr. = hour)

A. *In vivo* image 4 hours post-implant insertion at the equator. The Gd-DTPA signal is predominantly in the subconjunctival space.

B. *In vivo* image 7 hours post-implant insertion at the equator. Inset: A Gd-DTPA signal is present in the aqueous humor of the posterior chamber (large white arrow) and a weaker signal present in the anterior chamber (small white arrows).

C. *Ex vivo* image 4 hours post-implant insertion at the equator. A higher Gd-DTPA signal is present throughout the vitreous and aqueous humor compared with the *in vivo* eye in Figure 3-6 A.

D. *Ex vivo* image 7 hours post-implant insertion at the equator. Gd-DTPA is rapidly diffusing from the episcleral implant.

E. *Ex vivo* image 4 hours post-implant insertion between the equator and the optic nerve.

F. *Ex vivo* image 7 hours post-implant insertion between the equator and the optic nerve. Because of the posterior location of the implant, a higher Gd-DTPA signal is present in the vitreous cavity (and less in the anterior chamber) compared with an implant placed at the equator in Figure 3-6 D.

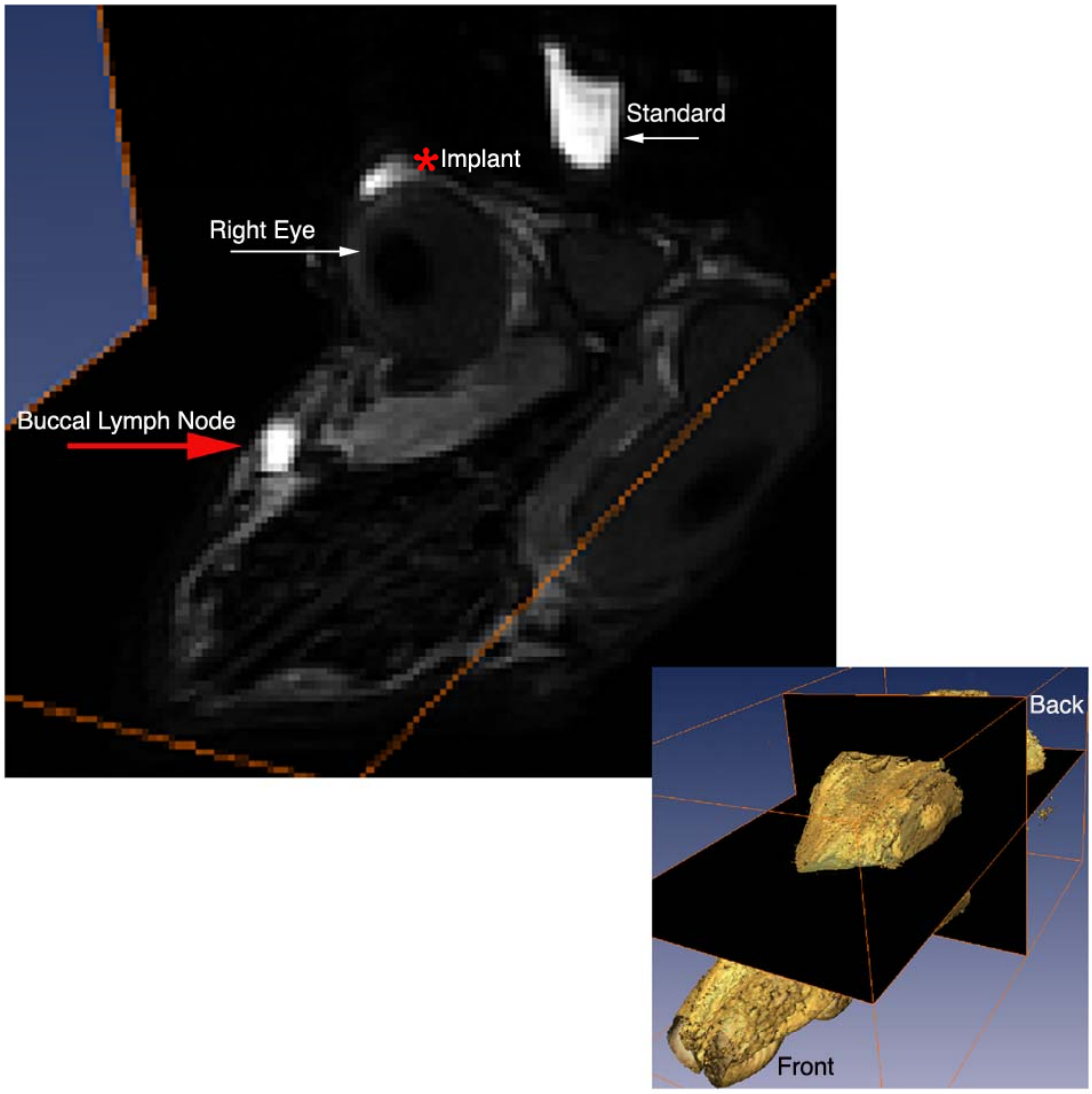

Figure 3-7. *In vivo* MR image of rabbit's head showing a combined axial and coronal image through the right eye. A reconstructed surface scan of the rabbit's head (lower right inset) shows the image slice orientation. The episcleral implant (red asterisk) right eye shows an adjacent Gd-DTPA signal. A high signal is present in the right buccal lymph node (labeled).

3.4.5 Intravitreal implant: ocular drug distribution

In vivo, Gd-DTPA immediately released into the vitreous and a concentration gradient was present in the vitreous cavity with higher levels present behind the lens and lower levels at the vitreoretinal interface (Figure 3-8(A) & 3-8(B)). There was no difference in the concentration of Gd-DTPA over the medullary rays, where retinal vessels are present, compared with the surrounding avacular retina. This Gd-DTPA concentration gradient was absent in the images of the *ex vivo* eyes. *In vivo*, there was a slightly higher Gd-DTPA signal at the vitreoretinal interface compared with the choroid with minimal signal observed in the sclera (Figure 3-9). In comparison, the *ex vivo* eyes showed relatively higher concentrations of Gd-DTPA at the vitreoretinal interface and low signals in the posterior retina and choroid (Figure 3-9). *In vivo*, there was a small Gd-DTPA signal present in the aqueous humor compared with the large signals in the *ex vivo* eyes. In the *ex vivo* eyes, the only clear passage of Gd-DTPA anteriorly appeared through the zonules immediately adjacent to the lens into the aqueous humor in the posterior chamber and tended to pool between the posterior iris and the anterior lens capsule.

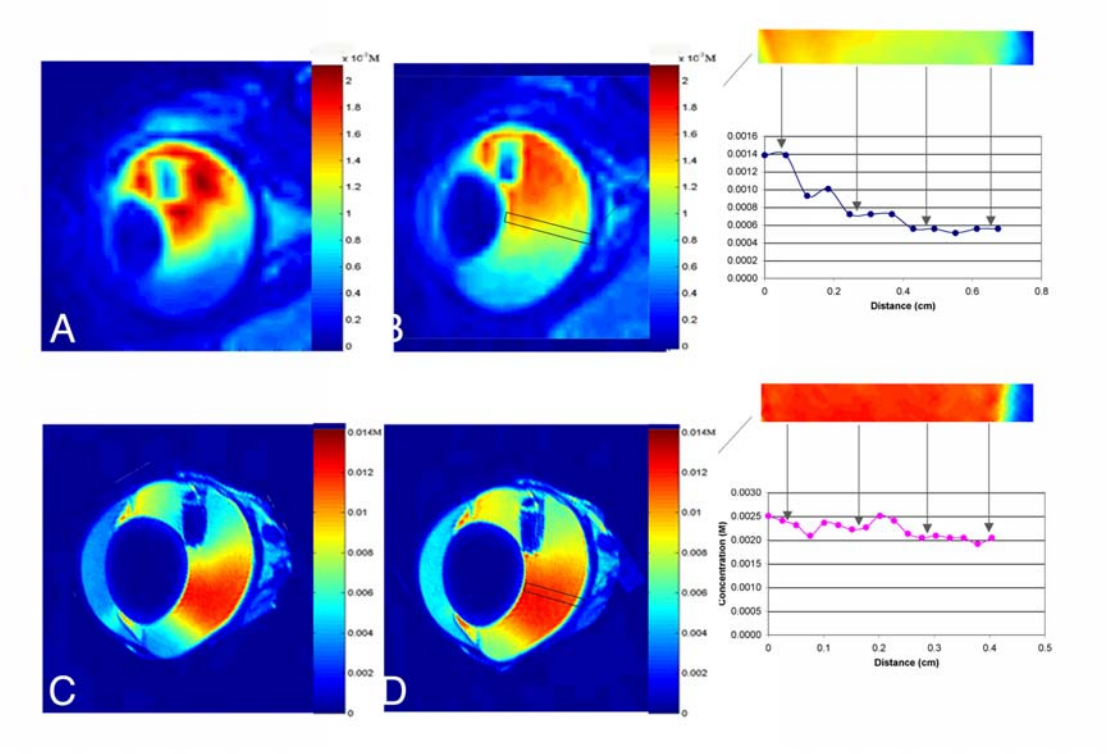

Figure 3-8. MRI scan (coronal images) with an intravitreal implant inserted through the equator of the right eye. Bar at the margin correlating Gd-DTPA concentration with color in the image. (hr. = hour)

A. *In vivo* image 4 hours post-implant insertion showing movement of Gd-DTPA in the vitreous cavity away from the implant.

B. *In vivo* image 7 hours post-implant insertion. The outlined area of the vitreous is magnified and shows a sharp decline in Gd-DTPA vitreous concentration (graph) from the posterior lens capsule to the retinal surface on the graph.

C. *Ex vivo* image 4 hours post-implant insertion showing Gd-DTPA movement into the inferior vitreous is more rapid compared with the *in vivo* images (Figure 3-8 A & 3-8 B)

D. *Ex vivo* image 7 hours post-implant insertion. The outlined area of vitreous is magnified and shows a shows a small decline in the Gd-DTPA vitreous concentration (graph) from the posterior lens capsule to the retinal surface.

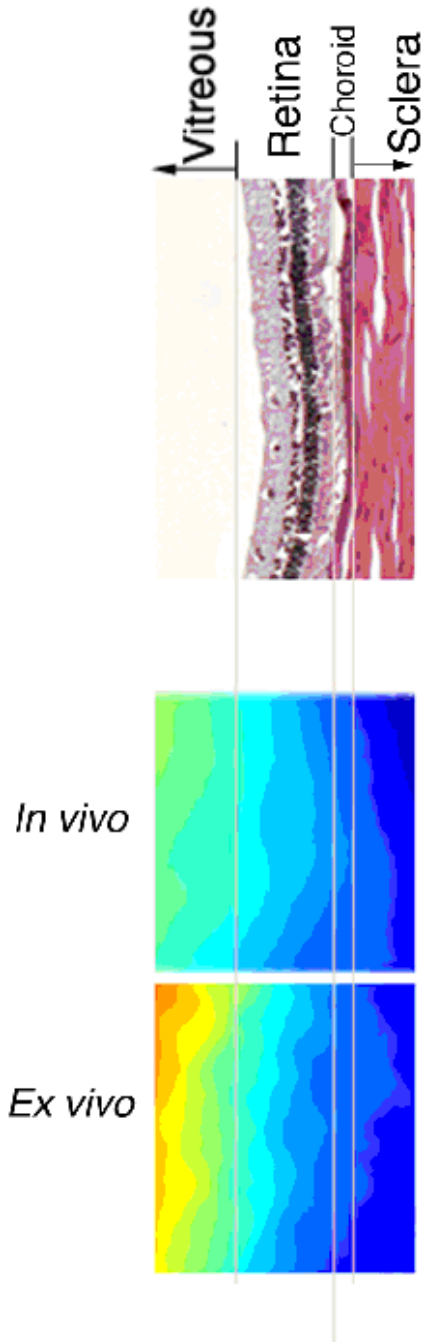

Figure 3-9. Magnified views of the region of the posterior vitreous, retina, choroid, and sclera in the outlined areas shown in Figures 3-8 B and 3-8 D. Above is a histologic section of a normal rabbit eye to identify the different ocular tissues in the MRI images (original magnification 100x, hematoxylin and eosin).

3.5 Discussion

Episcleral implants at the equator of the eye did not deliver a significant amount of Gd-DTPA into the vitreous and no Gd-DTPA was present in the posterior segment. An 8-fold increase in vitreous Gd-DTPA concentration occurred in the enucleated eyes suggesting that reducing the barriers to drug flux could increase drug movement from the episclera into the vitreous. These barriers include elimination pathways such as episcleral and conjunctival venous blood flow [78], conjunctival lymphatic drainage [81], choroidal blood flow [82], and counter-directional convection currents caused by the difference in hydrostatic pressures between the suprachoroidal tissue and the episcleral veins [48, 83]. Our study did not specifically identify the principal elimination pathway of Gd-DTPA movement from the episclera. In our study, the presence of a high concentration in the buccal lymph node, the proximal portion of the cervical lymph drainage system [84], was consistent with previous work showing radiolabeled compounds being eliminated from the subconjunctival space [85]. The relatively low flow rates of the lymph fluid in this region enables imaging of pooled Gd-DTPA in the lymph node [81]. Entry and elimination of Gd-DTPA from the episcleral veins is difficult to image because of the rapid dilution of Gd-DTPA as it enters the blood stream. The entry of Gd-DTPA into the aqueous appeared to be predominantly through the ciliary body region. Drug molecules transiting through the ciliary body from the episcleral would less likely be eliminated by venous drainage since flow rates are comparatively lower than the posterior choroid flow in most species [86], including the rabbit [87]. Other barriers to fluid and drug molecule flow from the episclera to the aqueous humor, such as

posteriorly directed fluid currents from uveoscleral flow, are negligible in the rabbit [88], and lymphatic drainage is absent in the ciliary body and choroid [82]. An advocate of fluid and drug molecule movement from the stroma of the ciliary into the aqueous humor is the non-pigmented cells of the ciliary epithelium where transport occurs through the tight junctions [89], by pinocytosis [90], and via osmotic gradients [86]. The passage of Gd-DTPA in the ciliary body region suggests that drugs targeting this region, such as aqueous humor production suppressants for glaucoma therapy, may be delivered using episcleral implants.

Implants placed directly in the vitreous cavity at the equator in live rabbits released Gd-DTPA produced a concentration gradient in the vitreous, lowest near the vitreoretinal interface. Based on previous experiments where fluorescein compounds were injected in the vitreous and sections of frozen eyes were examined, a gradual reduction in the vitreous concentration contours of sodium fluorescein from anterior to posterior was suggestive of a transretinal elimination pathway [62, 75]. The Gd-DTPA concentration gradient in the vitreous was abolished when the implants were imaged in the vitreous of enucleated eyes and the concentration was markedly reduced at the level of the RPE and the choroid. This suggested that the major transport mechanisms are inactivated when the eye was enucleated. Mechanisms that encourage transretinal fluid and drug molecule movement include higher hydrostatic pressures in the anterior vitreous compared with the episcleral space [91], oncotic pressure gradients created by the proteinaceous extracellular fluid of the choroid [86, 92], and rapid clearance via the choroidal blood flow [93]. The movement of Gd-DTPA released from an intravitreal implant through the neurosensory retina was

observed in both *in vivo* and *ex vivo* eyes, consistent with the lack of tight junctional barriers in the neurosensory retina [94]. Although choroidal tissue fluid can leave the eye via the sclera, either in or around perivascular spaces [85, 88, 95], in the *in vivo* intravitreal implant eyes, no Gd-DTPA was appreciated in the posterior sclera suggesting the elimination of Gd-DTPA was predominantly via the choroidal circulation.

In vivo, comparing the transport of Gd-DTPA released from an intravitreal implant in the vitreous by flow-induced convection, with that of diffusion, can be characterized with the Péclet number (Pé):

Pé= $V \cdot L / D$

where

V velocity of water in vitreous: 3.3×10^{-7} cm/sec [62]

L radius of the retina of rabbit**:** 1 cm [6]

D diffusion coefficient of Gd-DTPA in water: 3.8×10^{-6} cm^2/sec [96]

Pé = 0.087

This Péclet number suggests that the movement of Gd-DTPA in the vitreous was predominantly by diffusion, consistent with other studies examining the movement of small molecular weight compounds in the vitreous [83].

There was more rapid movement of Gd-DTPA in the aqueous and vitreous humor in the *ex-vivo* eyes with an intravitreal implant compared with the *in vivo* eyes because of the lack of transretinal clearance from the vitreous and loss of aqueous humor drainage. The *ex vivo* eyes showed a relative obstruction of Gd-DTPA

diffusion from the vitreous cavity to the posterior chamber, likely due to the dense vitreous condensation in this region [97, 98]. The pooling of Gd-DTPA in the posterior chamber of these eyes was due to the strong iris / lens apposition in rabbits where the iris acts like a one-way valve permitting anterior flow only [99].

There are a number of differences in the anatomy and physiology of the rabbit eye that have to be considered before extrapolating the results of this chapter to humans [78]. Although the permeability of rabbit and human sclera to a number of compounds is similar [25], the mean scleral thickness is less in the rabbit [78] compared with the human and this can have an effect on trans-scleral drug transport [100]. The choroidal vessel permeability and flow is different in rabbits compared with primates [82, 101, 102]. For example, the choroidal flow is 16% higher in rabbits compared with monkeys [103, 104] which may increase elimination of drug transiting to the vitreous released from an episcleral implant. Although there are minor variations in choroidal blood flow within the same eye of the rabbit, major variations occur in primates where flow in the macula is a log unit higher than in the retinal periphery [105], and this may have an impact on the transit of drug molecules into the eye from an episcleral implant. Another important difference between rabbits and humans is the degree of retinal vascularization; the rabbit possessing a merangiotic retina (i.e. partially vascularized retina) and the human a holangiotic retina (i.e. completely vascularized retina). In rabbit, the MRI images in the region of the retinal vessels of the medullary rays showed no difference in signal compared with other areas of avascular retina. Since retinal blood flow is a fraction of choroidal blood flow [106], the amount of Gd-DTPA being eliminated via the retinal circulation

may not be significant or it may be below the resolution of this MRI technique. Clearance of drugs via the retinal circulation may be more a factor in humans where the retinal vascularization is complete.

There are limitations in the interpretation of the data in this study. Gd-DTPA concentrations could only be quantified between 0.5×10^{-5} M and 0.5×10^{-2} M which did not allow for quantification of the high Gd-DTPA concentrations around the implant. Furthermore, with the resolution of the MRI system being in the micromolar range, Gd-DTPA in lower concentrations would not have been identified in the ocular tissues. The post-mortem effect of the ocular tissues on drug movement was not specifically examined in this study. However, *in vitro* studies of accessing ocular tissue drug transport suggest that isolated sclera from rabbits and humans and flat mount preparations of the retinal pigment epithelium and choroid [107] can remain structurally [100] and functionally [25] viable for a number of hours. Although the blood flow is terminated once an eye is enucleated, endothelial cell tight junctions can remain functionally intact for several hours following an ischemic insult to the endothelial cells *in vitro* [108]. In addition, the fact that Gd-DTPA movement through the retina was significantly delayed with an accumulation of Gd-DTPA in the vitreous of the enucleated eyes with the intravitreal implants suggests that the outer blood-retinal barrier, i.e. the tight junctions between RPE cells, remained intact. Another limitation of this study is we examined the movement of a single drug surrogate, at one concentration, from the implants. Since the molecular weight, hydrodynamic radius, and the solubility of a compound in water influences the ocular penetration of a compound [25, 100], Gd-DTPA, a low molecular weight and

hydrophilic compound, does not have general applicability to the movement and transport of all drugs in the eye. However, improvements in drug labeling techniques with metal ion chelates with a variety of therapeutic compounds have begun to revolutionize assessments of drug distribution throughout the body using MRI [109, 110] and applying these new technologies will improve the general understanding of drug movement in the eye as a function of molecular weight, hydrodynamic radius, and solubility.

3.6 Conclusions

Episcleral implants at the equator of the eye did not deliver a significant amount of Gd-DTPA into the vitreous and no compound was present in the posterior segment. An 8-fold increase in vitreous Gd-DTPA concentration occurred in the enucleated eyes suggesting that there are significant barriers to the movement of drugs from the episcleral space into the vitreous *in vivo*. Dynamic MRI using Gd-DTPA, and potentially metal ion/drug complexes, may be useful in understanding the spatial relationships of ocular drug distribution and clearance mechanisms in the eye.

CHAPTER 4. Transport of drugs released from an intravitreal implant by comparing magnetic resonance imaging data to a finite element mathematical model

4.1 Objectives

Several parameter values will be calculated by comparing simulation data to experimental data and the concentration distribution of model drugs released from an intravitreal implant at several cases will be estimated with the developed mathematical eye model.

4.2 Introduction

MRI has been utilized to investigate the anatomy and pathology of the eye non-invasively [31, 35, 37, 111]. We employ MRI to overcome limitations in autoradiography and fluorescence, which do not yield real-time information and require tedious dissection procedures, and to determine non-invasively the real-time movement of a drug surrogate, gadolinium-diethylenetriaminopentaacetic acid (Gd-DTPA) released from a polymer-based intravitreal implant.

In this chapter, we developed a finite element mathematical eye model to help analyzing MRI experiment data and calculated several physiological parameters by comparing simulation data to MRI experimental data. With the developed mathematical model, we estimated concentration of Gd-DTPA in the vitreous at several situations.

4.3 Materials and methods

4.3.1 Intravitreal implant design

An intravitreal implant was manufactured using the procedure as shown in Figure 3-2: 15% polyvinyl alcohol (PVA) (w/v) solution was formulated by placing 1.5 g of PVA (Celvol, Celanese Chemicals, Ltd., Dallas, TX) in 10 ml of molecular biology grade water (BIOfluids®, Biosource International, Camarillo, CA) in a 50 ml polypropylene conical tube (Falcon®, BD Biosciences, Franklin Lakes, NJ) and placed in a water bath at 100°C for 3 hours to dissolve all the PVA. The PVA solution was cooled down to room temperature and 0.80 ml of 0.5 M Gd-DTPA solution was added and stirred into the PVA mixture to produce a solution of 15% PVA and 20% Gd-DTPA (w/w/v). Eight ml was poured onto a glass plate which produced a thin film as it dried at room temperature. A biopsy punch (Acu·Punch® 3 mm, Acuderm Inc, Ft. Lauderdale, FL) was used on the dried film to make 3 mm diameter disks. Individual disks (7 total) were placed in a polytetrafluorethylene mold, which has a 3.2 mm diameter and a 1.2 mm depth. The disks were coated with the remaining 15% PVA and 20% Gd-DTPA (w/w/v) solution. The dried implant was peeled out of the polytetrafluoroethylene mold and a total of 3.7 mg of Gd-DTPA was loaded into each intravitreal implant.

4.3.2 *In vitro* release rate

In vitro release rate experiments were performed on the fabricated implants over an 8 hour period, which was equivalent to the MRI experiment time period. Implants were placed in 25 ml glass vials with 20 ml of phosphate buffered

saline (PBS) (pH 7.4) and stirred at 150 rpm at room temperature. The solution was assayed ever 10 minutes for the first hour, every 30 minutes for the second hour, and then hourly up to 8 hours. The PBS solution was completely replaced with fresh PBS at each sample time to simulate sink condition. Gd-DTPA assays were performed using a spectrofluorometer (QuantaMaster, Photon Technology Internation, Lawrenceville, NJ) at excitation wavelength 275 nm; emission wavelength 312 nm. The release rates were determined by calculating the amount of Gd-DTPA released over time and recorded as mg per hour.

4.3.3 Magnetic resonance imaging

4.3.3.1 Standard solutions for quantitative analysis of MRI images

To compare successive MRI images from day to day and to calibrate the amount of Gd-DTPA in the vitreous and in the aqueous humor, standard solution of known Gd-DTPA concentration were always scanned along side the rabbit eyes. The standard solutions were prepared by adding varying amounts of 0.5 M Gd-DTPA solution to 2 % hydropropyl methylcellulose (HPMC) (METHOCELL®, Dow Chemical) solution to make 1.0×10^{-1}M, 0.5×10^{-1}M, 1.0×10^{-2}M, 0.5×10^{-2}M, 0.25×10^{-2}M, 1.0×10^{-3}M, 0.5×10^{-3}M, 1.0×10^{-4}M, 0.5×10^{-4}M, 1.0×10^{-5}M, 0.5×10^{-5}M, and 1.0×10^{-61}M calibration solutions. Each of the 12 calibration solutions was sealed with silicone into 12 individual wells cut from a standard 96 well plate culture chamber (VWR international, Bridgeport, NJ, USA). Gray scale images of the standard solutions were developed and the average intensity value of each concentration was determined using imageJ software (version 1.27z, National

Institutes of Health, Bethesda, USA). A concentration curve of image intensity versus Gd-DTPA concentration was generated.

4.3.3.2 *In vivo* experiment

All imaging experiments were performed *ex vivo* and *in vivo* on New Zealand White rabbits in a 4.7 Tesla magnet equipped with a Bruker Avance console (Bruker-biospin, Billerica, MA). The procedures adhered to the guidelines from the Associated for Research in Vision and Ophthalmology for animal use in research. All analyses and manipulations of images were performed using MATLAB (version 6.5, Mathworks Inc., Natick, MA, USA) and AMIRA (version 2.3, TGS Inc., San Diego, CA, USA). Each rabbit was maintained under general anesthesia during the entire imaging period. The animals were induced with xylazine (5–10 mg/kg) and ketamine (35-50 mg/kg IM to effect) and an IV catheter was inserted into the marginal ear vein to administer fluids. An endotracheal tube was placed and anesthesia was maintained with 1-2% halothane or 1-2% isoflurane. The conjunctiva was opened with a stab incision (using a Beaver blade), and an intravitreal implant was placed into the vitreous chamber. The implant was sutured to the sclera; the sclera and conjunctiva were closed with suture. After completing this preparation, the rabbit was positioned in the MRI. T_1-weighted MRI studies were performed using a 10 cm diameter volume coil and a Fast Spin Echo sequence. MRI scanning parameters were repetition time (TR)/echo time (TE) = 200/9.0 ms, with a 9 cm × 9 cm × 9 cm field of view (FOV), and a 256 × 128 × 128 acquisition matrix size for the *in vivo* experiment. A complete 3D data set was acquired every 20 minutes. During

the study, pulse, blood oxygenation (SpO_2), end-tidal CO_2, respiratory rate, anesthetic gas levels, and body temperature were monitored.

4.3.3.2 *Ex vivo* experiment

Eyes were enucleated from euthanasized rabbits. The conjunctiva was opened approximately 2 mm posterior from the limbus. The exposed sclera was opened with a stab incision (using a Beaver blade), and an intravitreal implant was placed into the vitreous chamber. The implant was sutured to the sclera; the sclera and conjunctiva were closed with suture. After placing the implant in the vitreous, the eye was placed in a 50 ml centrifugal tube, on a wet (sterile saline) sterile 4 inch × 4 inch gauze pad, to keep the eye moisturized. After completing this preparation, the tube was immediately positioned in the MRI. The eye was scanned every 10 minutes for 20 hours using a 72 mm diameter volume coil and a Fast Spin Echo sequence. MRI scanning parameters were TR/TE = 200/6.6 ms, FOV = 5 cm × 5 cm × 4 cm, echo train length = 8 ms, 256 × 128 × 128 acquisition matrix size, and 2 averages.

4.3.4 3-D computer simulation

A 3-D finite element mathematical model of the eye was developed using FEMLAB software (version 2.3, Consol Inc., Burlington, MA, USA) to help analyze MRI images and understand the transport of Gd-DTPA released from an intravitreal implant. The geometry of the mathematical model of the eye was based on the physiological dimensions of a rabbit eye [6] and was composed of the vitreous, the lens, the posterior surface of the eye, and the implant (Figure 4-1(A)). In this

initial model, the posterior surface is described as a “lumped” region consisting of a combination of the sclera-choroid-retinal barrier. A total of 21174 finite element meshes were generated automatically by the FEMLAB software (Figure 4-1(B)).

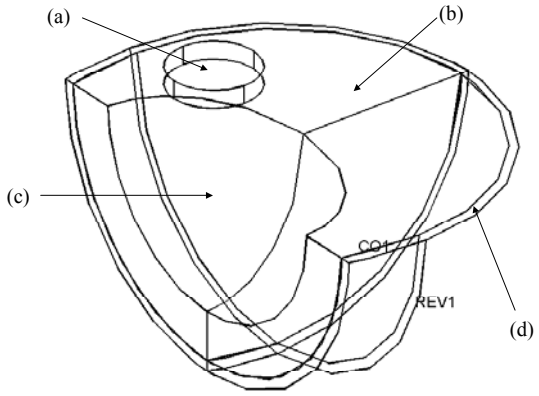

(A)

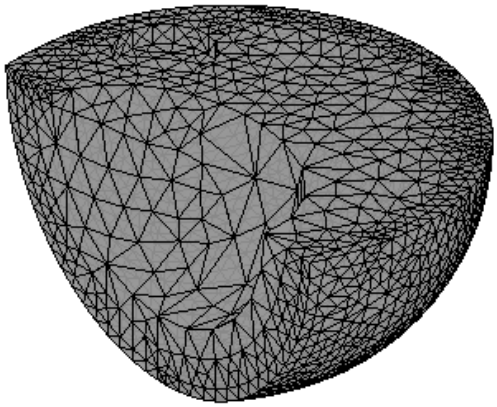

(B)

FIGURE 4-1. (A) Geometry of mathematical eye model. (a): intravitreal implant; (b): vitreous, (c): lens site, and (d): sclera-choroid-retina barrier. (B) 21174 finite element meshes.

To determine the velocity distribution of the fluid movement through the eye, Darcy's law was applied to the vitreous compartment and to the sclera-choroid-retinal membrane [91]:

$$\vec{U} = -\frac{K}{\mu}\nabla p \tag{1}$$

where, $\vec{U}$ is the velocity of the fluid, K is the hydraulic conductivity of the vitreous or sclera-choroid-retinal membrane, μ is the viscosity of the fluid, and ∇p is the pressure gradient. Values of the hydraulic conductivity for vitreous gel and the sclera-choroid-retinal membrane and for the viscosity of the aqueous fluid were derived from the literature (see Table 4-1). Pressures of 15 mmHg and 10 mmHg were applied to the hyloid and the outer sclera, respectively, to achieve a 5 mmHg pressure drop between these elements [112]. The lens and the implant were considered to be impermeable to fluid flow; so, a zero velocity fluid flow boundary condition was applied throughout the lens and the implant. To calculate the concentration distribution of the released Gd-DTPA in the vitreous region and the sclera-choroid-retinal membrane, the following diffusion-convection equation was solved [48]:

$$\rho\ \frac{dC}{dt} - \nabla \bullet (D\nabla C) + \vec{U} \bullet \nabla C = 0 \tag{2}$$

where, ρ is the density of fluid, D is the diffusion coefficient of Gd-DTPA in the vitreous, $\vec{U}$ is the velocity of fluid in the vitreous, and C is the concentration of Gd-DTPA. To expedite computation, the steady state vitreous velocity distribution of the fluid was first calculated from the Darcy's law and that velocity vector field was

exported into and superimposed on the diffusion-convection equation to determine concentration distribution of Gd-DTPA in the vitreous.

Table 4-1. Parameter values used in the simulation study.

Parameter	Value	Reference
Density of aqueous humor	1 g cm^{-3}	Friedrich et al., 1997
Viscosity of aqueous humor	6.9×10^{-3} g cm^{-1} sec^{-1}	Friedrich et al., 1997
Pressure at the hyaloid	15 mmHg	Missel, 2002
Pressure at the episclera	10 mmHg	Missel, 2002
Hydraulic conductivity in the sclera	1.5×10^{-11} cm^2 Pa^{-1} sec^{-1}	Xu et al., 2002
Hydraulic conductivity in the vitreous	2.4×10^{-6} cm^2 Pa^{-1} sec^{-1}	Xu et al., 2002
Diffusivity of Gd-DTPA in the vitreous	?	Estimated from this study
Permeability of Gd-DTPA in the sclera	?	Estimated from this study

A mass flux boundary condition was imposed on the surface of implant to simulate the *in vitro* release (Figure 4-2). At the outer boundary of the sclera-choroid-retinal region (episclera), a zero concentration boundary condition was applied. This would represent a rapid "sink" condition, possibly resulting from rapid clearance by

choroidal blood flow. A continuity condition was applied at the interface between the vitreous and sclera-choroid-retinal membrane region of the eye both in the flow velocity calculation and in the diffusion convection calculation. The current model does not include an anterior segment. In order to account for the loss of drug to the anterior segment, a boundary condition was used at the hyloid membrane that represented drug clearance to the anterior region. The clearance was represented in the model as flux boundary condition of the drug concentration at the hyloid membrane times the aqueous humor turnover rate divided by the hyloid area [48]:

$$\text{Flux of drug clearance} = -\left(f / A\right) \times C$$

where, A is the hyaloid area, f is the turnover rate of aqueous humor, and C is the concentration at the hyloid membrane. The Gd-DTPA clearance value equaled 6.16×10^{-5} [cm/ sec] $\times$ C. Other parameter values that were used for the mathematical eye model are listed in Table 4-1. Model simulations were compared to MRI concentration data on a relative quantitative basis. The following procedure was followed. Individual X-Y voxel positions were averaged over ten adjacent Z-plane MRI image slices, each 350 micron thick, near the center axis of the eye to obtain an X-Y planar concentration profile for Gd-DTPA averaged over a 3.5 mm Z thickness. The averaging smoothed out slight image irregularities in any given 350 micron image slice and provided a concentration profile from the lens to the retina the X-Y plane to compare to the simulation concentrations in a similar plane. Concentration values were normalized relative to that at the lens surface to account for variations in the implant release rates [4]. Relative concentration profiles from lens surface to retina were compared to simulation data.

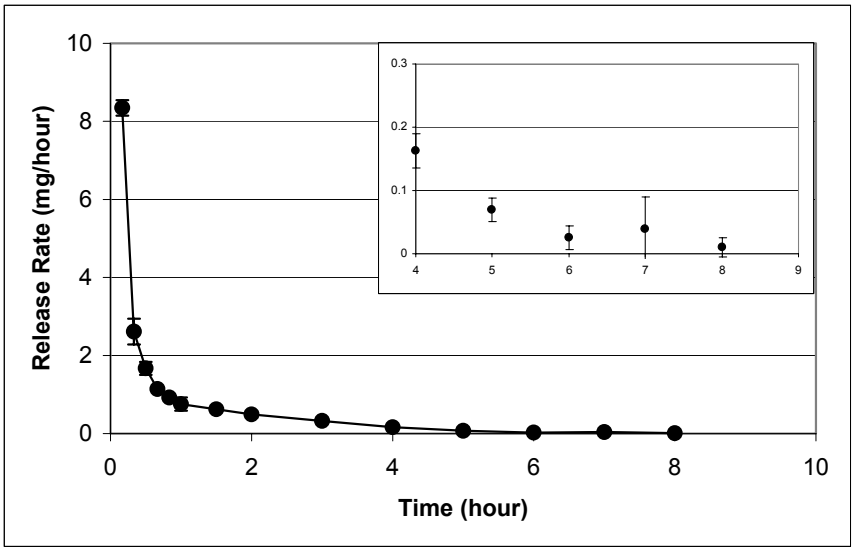

(A)

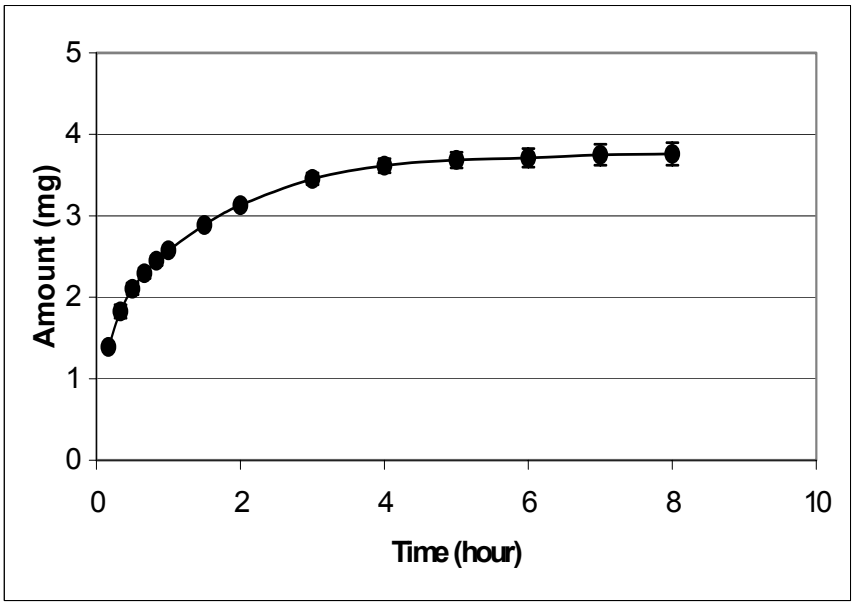

(B)

FIGURE 4-2. (A) Release rate of Gd-DTPA from intravitreal implants; (B) cumulative amount of released Gd-DTPA.

4.4 Results

4.4.1 MR images:

(A) *In vivo*

Figure 4-3 shows the MRI intensity images in a rabbit eye at 1.5, 2.7, 4.1, and 7.7 hour following insertion of an intervitreal Gd-DTPA matrix implant. The dark rectangle outlines the implant location and appears black due to the saturation T_2 effects of the high Gd-DTPA concentration in the implant. The large oval-shaped dark region to the lower right of the implant is the rabbit lens which is impermeable to Gd-DTPA and appears black due to insignificant concentration. Gd-DTPA can be seen to disperse through large regions of the vitreous compartment as time progresses. There is a definite concentration gradient as one recedes away from the implant. A distinct concentration gradient is maintained with the *in vivo* system for up to nearly 8 hour post-implantation. Some Gd-DTPA was evident at the incision site which may have occurred by the implant contacting moist tissue during insertion or by some leakage or diffusion of Gd-DTPA back to the incision area. Very little signal intensity is seen in the anterior chamber of the *in vivo* eye in Figure 4-3. Also, a dark ring is observed around the posterior segments of the eye in an area of the retina-choroid-sclera which may represent an undetectable, low Gd-DTPA concentration.

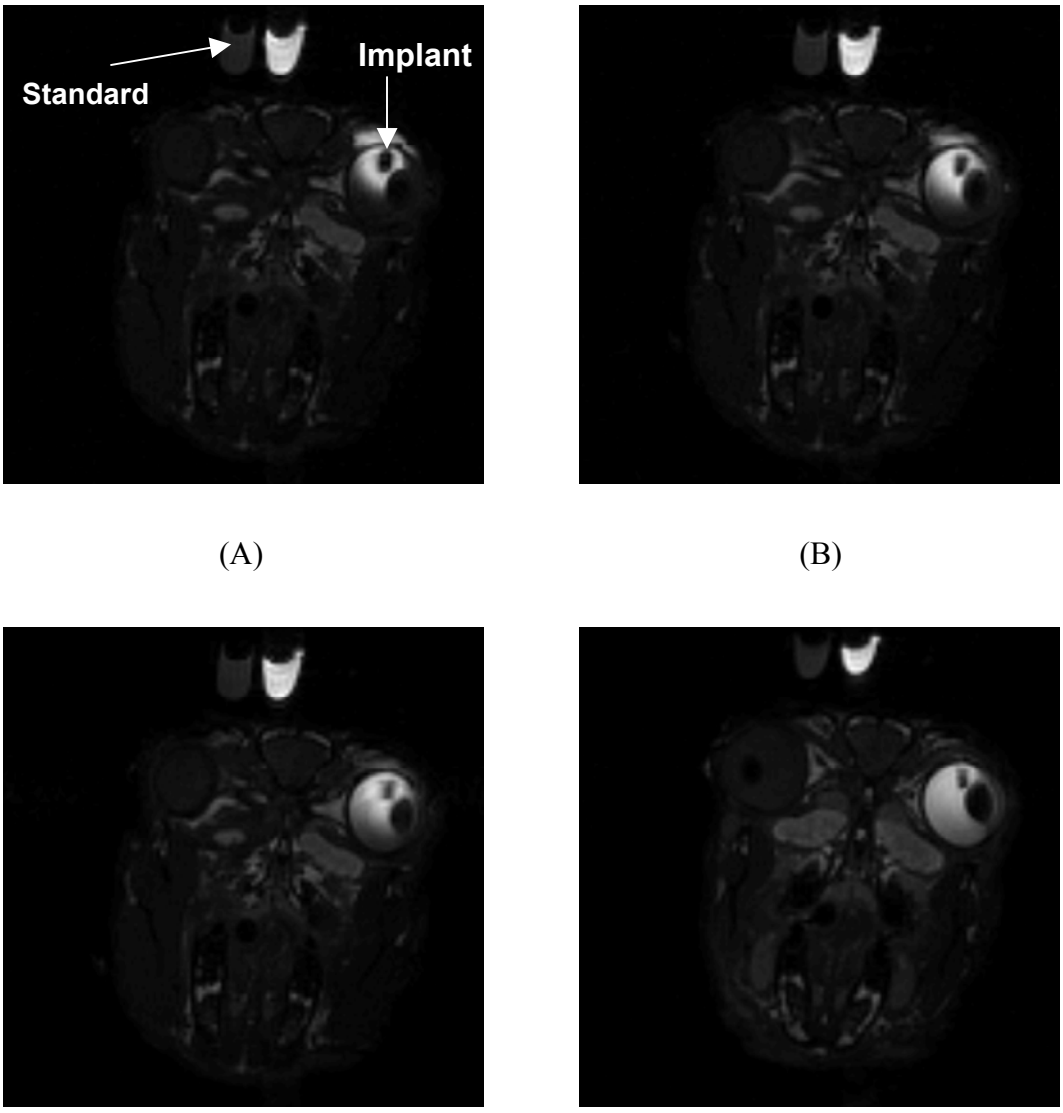

FIGURE 4-3. *In vivo* intravitreal implant MR images. (A) 1.5 hour post implantation, (B) 2.7 hour post implantation, (C) 4.1 hour post implantation, and (D) 7.7 hour post implantation.

(A) *Ex vivo*

Figure 4-4 shows the MRI images in an *ex vivo* rabbit eye at 1.2, 2.6, 4.6, and 10.1 hour post implantation. These images show more spatial resolution near the eye since a surface coil was placed closer to the eye during these *ex vivo* experiment. The PVA implant is clearly visible as the thin rectangular dark region. The large rabbit lens is impermeable to Gd-DTPA and remains dark. The Gd-DTPA is seen to diffuse in both anterior (toward the aqueous chamber) and posterior (toward the retina) direction. Since there is no clearance by aqueous outflow in the *ex vivo* eye, Gd-DTPA begins to diffuse through the hyloid membrane. In contrast to the *in vivo* case, Gd-DTPA can accumulate in the aqueous compartment. At 10.1 hour, the image intensity within the implant actually appears to brighten since the implant's Gd-DTPA concentration is diminishing below the saturation values (black image). The image intensity at 10.1 hours shows a substantially more uniform concentration distribution from the back of the lens toward the retina with essentially no gradient as one proceeds distal to the implant. This *ex vivo* distribution represents a distinct contrast to the *in vivo* data and most likely occurs due to the lack of transport of Gd-DTPA through the retina-choroid-sclera layer in the *ex vivo* eye.

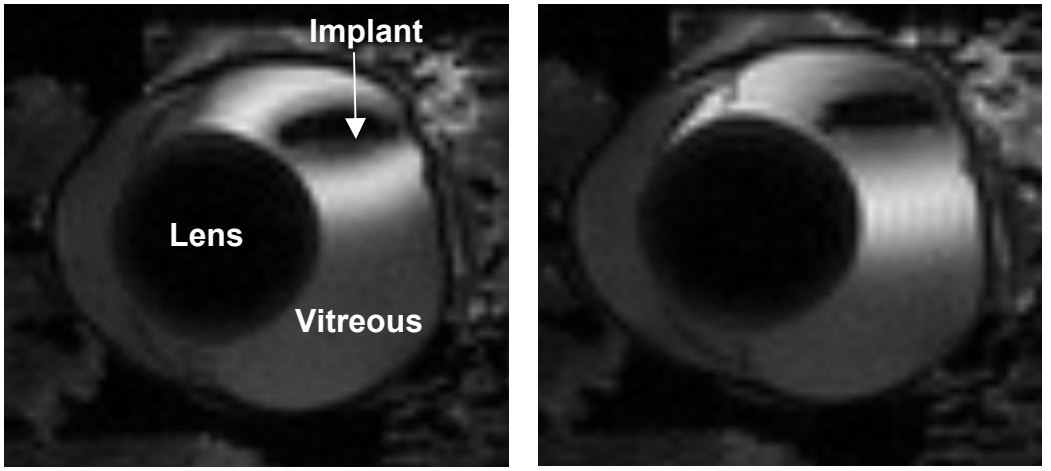

(A) (B)

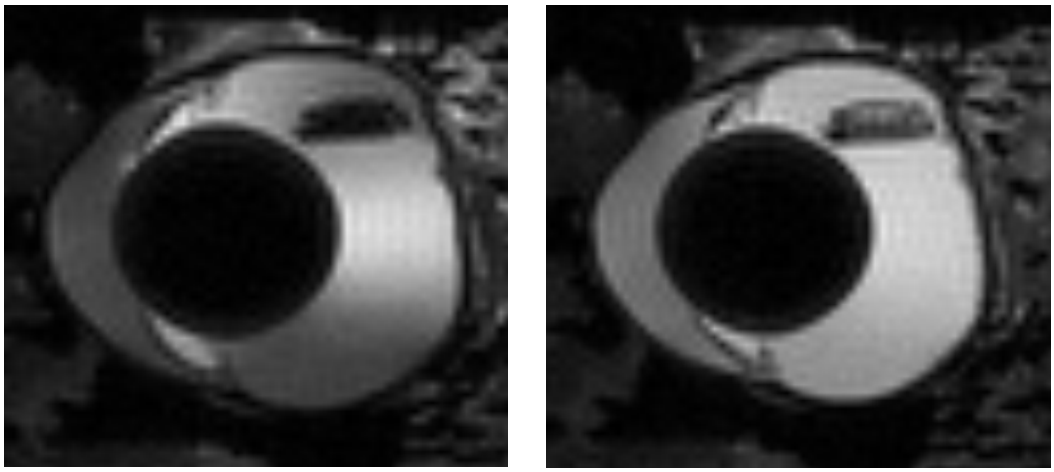

(C) (D)

FIGURE 4-4. *Ex vivo* intravitreal implant MR images. (A) 1.2 hour post implantation, (B) 2.6 hour post implantation, (C) 4.6 hour post implantation, and (D) 10.1 hour post implantation.

Figure 4-5 and 4-6 show the *in vivo* and *ex vivo* profiles of Gd-DTPA concentration calculated from the intensity images along a line drawn from the lens to the retina. For the *in vivo* case, the concentration profile for Gd-DTPA from the lens to the retina appears to approach a quasi steady state by 7.32 hour post implantation and there is a persistent concentration gradient at the retina surface. For the *ex vivo* experiment, the concentration profile becomes relatively flat by 6.68 hour and subsequently remains without a gradient.

Figures 4-7 and 4-8 show the *in vivo* and *ex vivo* MRI experimental Gd-DTPA concentration profiles taken along the vertical line from the middle of the vitreous to side opposite to the implant. In Figure 4-7, there is still a significant drop in Gd-DTPA concentration from the implant side of the vitreous compartment (x-axis 0 cm) to the far (x-axis 1.0 cm) side at the longest experimental time point of 7.7 hour. A similar situation exists for the *ex vivo* case, as shown in Figure 4-8, except that by 10.1 hours, the concentration on the far side (1.5 cm) brings to rise somewhat.

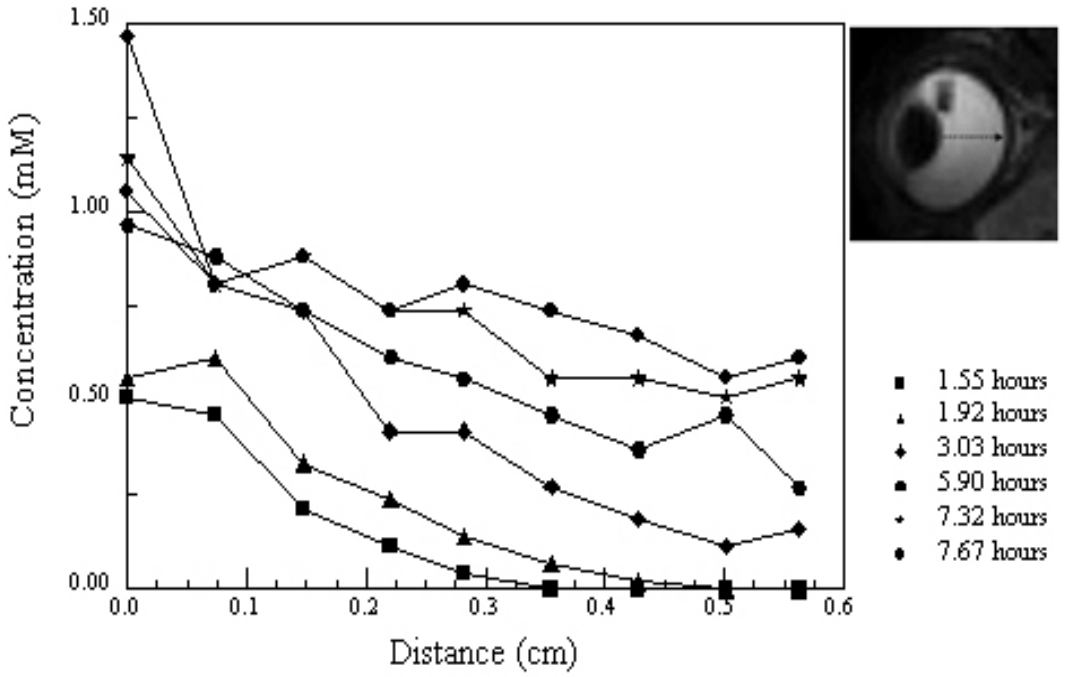

FIGURE 4-5. Concentration distribution of Gd-DTPA from the lens to the retina in *in vivo* MRI experiment and (B) *ex vivo* MRI experiment.

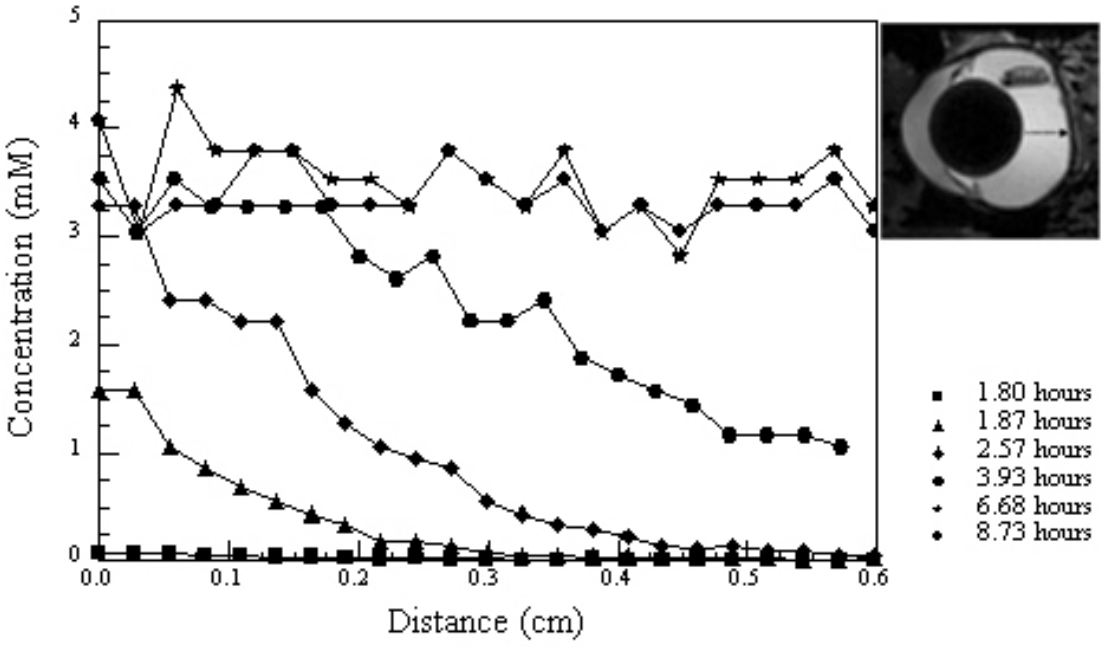

FIGURE 4-6. Concentration distribution of Gd-DTPA from the lens to the retina in *ex vivo* MRI experiment.

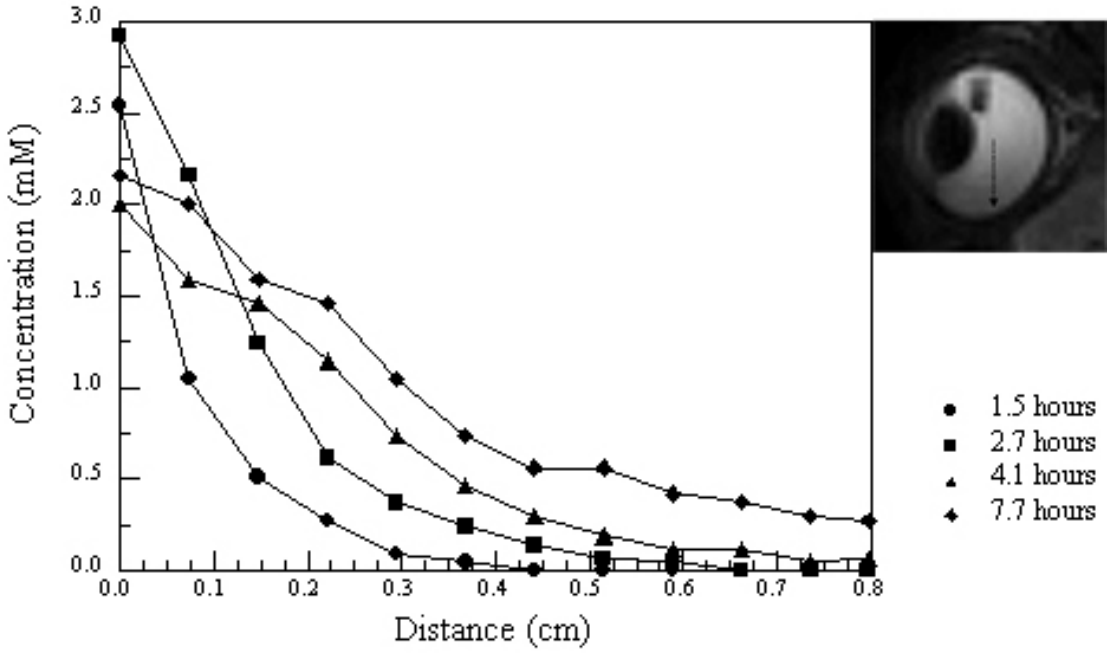

FIGURE 4-7. Concentration distribution of Gd-DTPA from the middle of the vitreous to the other side of the vitreous in *in vivo* MRI experimental data.

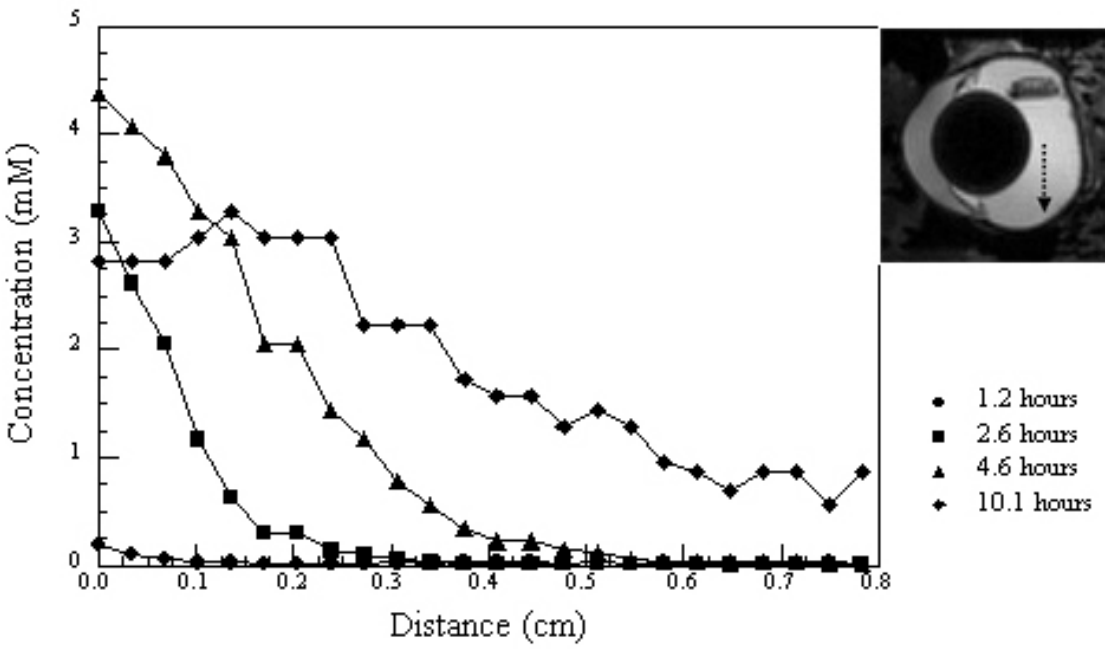

FIGURE 4-8. Concentration distribution of Gd-DTPA from the middle of the vitreous to the other side of the vitreous in *ex vivo* MRI experimental data.

4.4.2 3-D computer simulation

From the mathematical eye model, the velocity distribution of the fluid convection in the vitreous compartment was calculated. Figure 4-9 shows a steady state, gray scale velocity contour with arrows marking velocity directions. The fluid flows from the hyloid membrane toward and then out through the retina-choroid-sclera membrane. The average velocity through the retina-choroid-sclera surface is reported by Missel [48] to be approximately 3.52×10^{-7} cm/sec and that near the optical nerve is reported by Araie [62] to be 3.9×10^{-7} cm/sec. This version of the model does not include explicitly flow from the ciliary body toward the anterior compartment. The movement of Gd-DTPA to the anterior compartment was described with a clearance term consisting of aqueous humor turnover divided by hyloid area in the Methods section.

The vitreous diffusion coefficient and retina-choroid-sclera barrier permeability was determined by a trial and error process that optimized agreement between the MRI data and the simulation. In this process, the diffusivity value of Gd-DTPA in vitreous was initially set at 3.8×10^{-6} cm^2/sec according to Gordon et al. [96]. Then, by a series of trial simulations, we obtained a model of diffusion coefficient through the 0.03 cm thick retina-choroid-sclera membrane for the 3.0×10^{-7} cm^2/sec. This translates to an equivalent permeability of 1.0×10^{-5} cm/sec. Subsequently, the vitreous diffusion coefficient was readjusted to a value of 2.8×10^{-6} cm^2/sec to improve the final fit between simulation and MRI concentration data. The fitting was optimized by visual inspection of Figure 4-10.

Figure 4-11 shows surface plots from model simulation of the concentration

distribution of Gd-DTPA in the vitreous at several time points. Qualitatively, the model shows a time course and a pattern of drug dispersion similar to those suggested in *in vivo* images. Few representative concentration profiles determined by the simulation are plotted in Figures 4-12 and 4-13. These profiles, along a horizontal axis from the back of the lens to the retina, also shows similar qualitative behaviors to the MRI data in Figures 5 and 6 for the *in vivo* and *ex vivo* cases. In Figure 4-12, the concentration increases at the lens surface (x = 0 cm) with time and subsequently decreases as the release rate from the implant diminishes. At the retina surface (x = 0.65 cm), a concentration gradient is always evident. In Figure 4-13, where the permeability is set to zero to simulate the *ex vivo* case, the concentration profile approaches uniformity over time from the lens to the retina and then reaches the steady state distribution.

From instructional purposes, some concentration profiles under hypothetical steady state conditions were determined with the finite element model. The actual experimental Gd-DTPA release rate was time varying and steady state could not be achieved. For steady state simulations, a constant release rate of 0.1 mg/hour was used. This release rate represents a nominal average value of hypothetical *in vivo* and *ex vivo* experiments with the implant. Figures 4-14 A through D show hypothetical concentration profiles along an axis from the back of the lens to the retina at different times as predicted by the model for four different values of the retina-choroid-sclera permeability coefficients, 1.0×10^{-4} cm/sec, 1.0×10^{-5} cm/sec (the predicted *in vivo* value), 1.0×10^{-6} cm/sec, and zero (the assumed *ex vivo* value). At a low permeability, 1.0×10^{-6} cm^2/sec and especially at zero permeability, the concentration

gradient at the retina surface almost vanished. The longest time point for a profile shown in Figure 4-14 is 20 hour, which appears to represent steady state since there is no little further change in the profile with time in the case of retina-choroid-sclera permeability coefficient of 1.0×10^{-4} cm/sec.

A theoretical representation by computer simulation of concentration profiles along a vertical axis (Figure 4-7 and 4-8) from the implant to the opposite side of the vitreous compartment is shown in Figure 4-15 for a condition representing the *in vivo* case (permeability = 1×10^{-5} cm^2/sec) and in Figure 4-16 for the *ex vivo* case (permeability = zero). Even as steady state appears to be achieved by 20 hour in the simulations in the *in vivo* case, concentrations opposing the implant continue rising slightly at 20 hour in the *ex vivo* case.

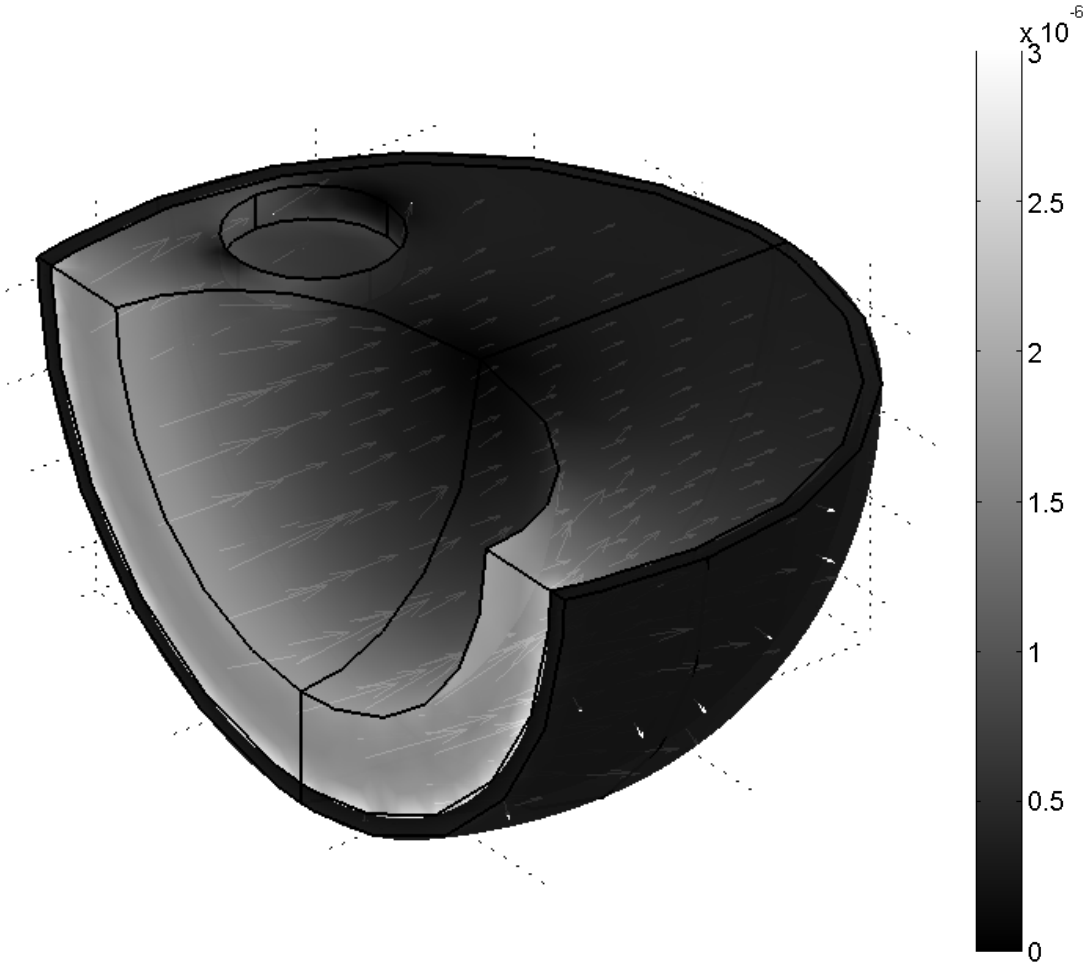

FIGURE 4-9. Mathematical study results: The steady-state velocity distribution of aqueous humor in the vitreous.

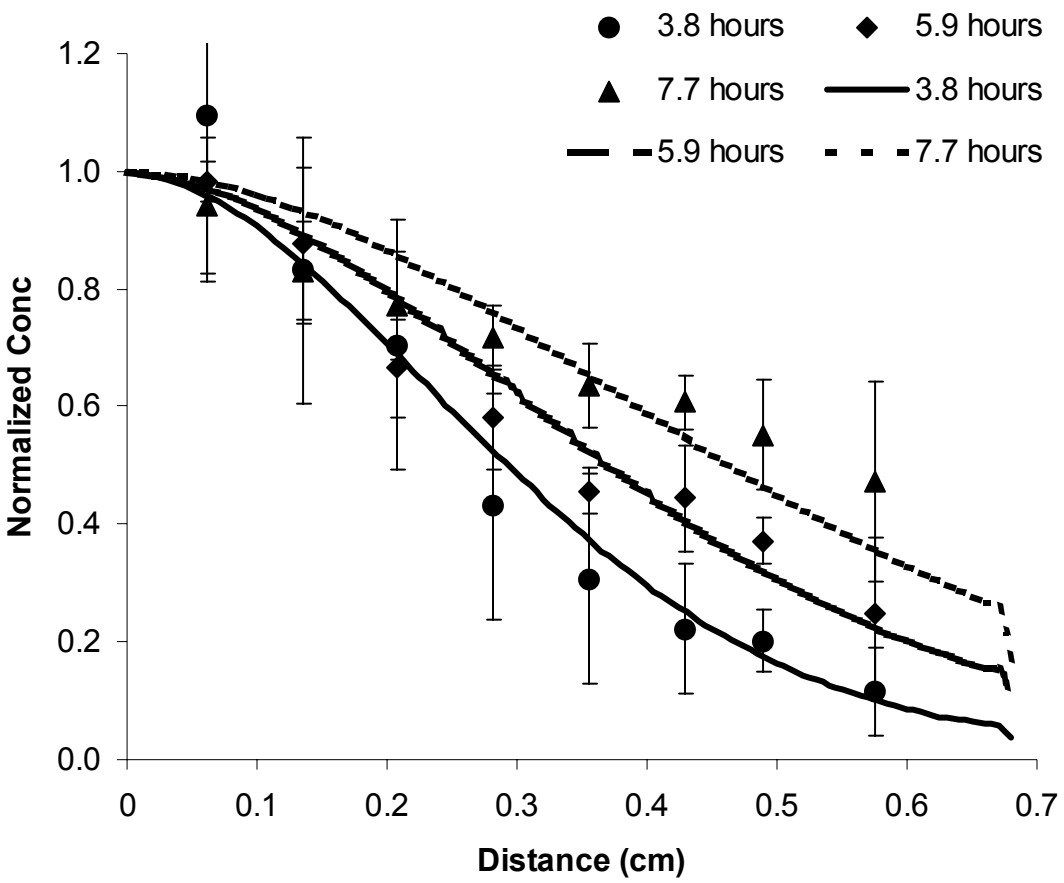

FIGURE 4-10. Comparison between *in vivo* MRI experiment and simulation with 3.0 $\times 10^{-7}$ cm^2/sec for diffusion coefficient in the posterior segment of the eye and 2.8×10^{-6} cm^2/sec in the vitreous. Concentration from the lens to the retina was divided by that next to the lens to calculate the normalized concentration.

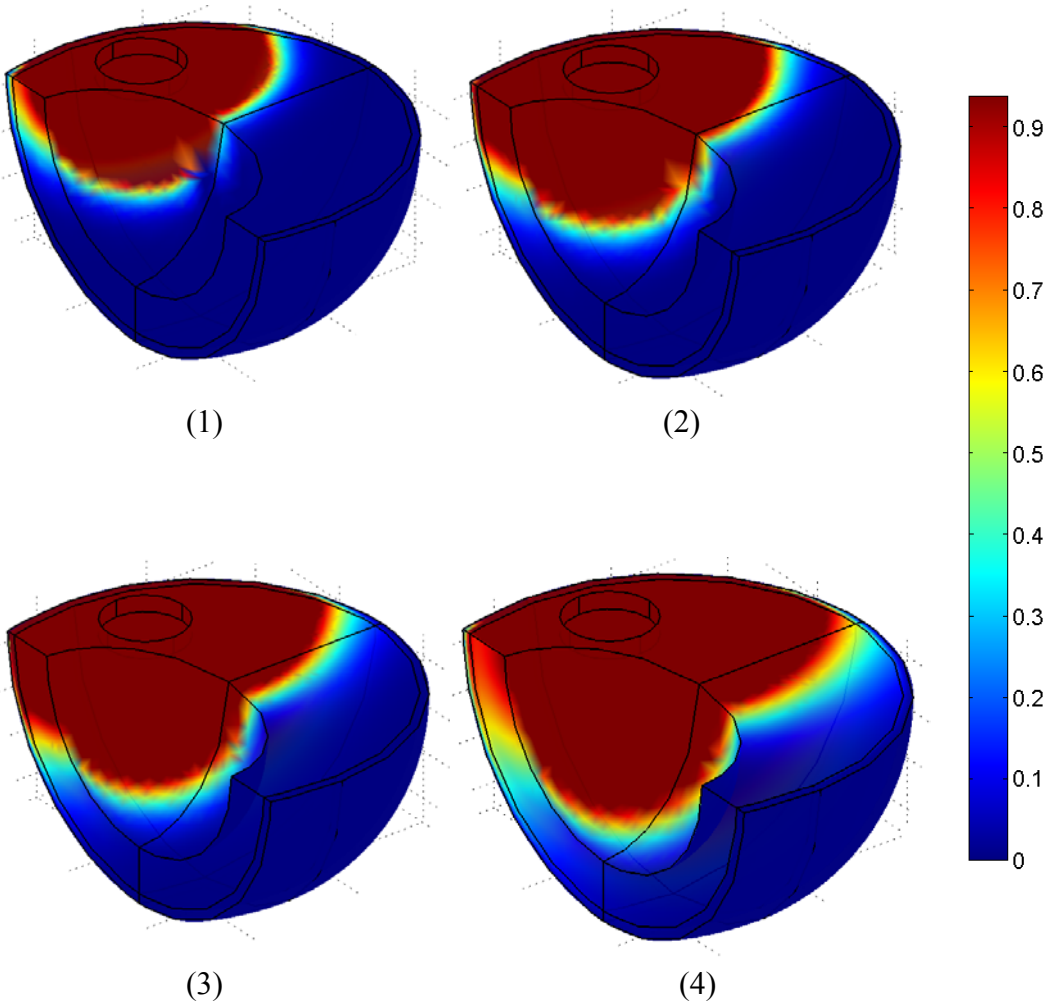

FIGURE 4-11. Mathematical study results: (1), (2), (3), and (4) show concentration distribution at 1.50 hour, 2.68 hour, 4.12 hour, and 7.67 hour post implantation. Unit of the colorbar is mg/cm^3.

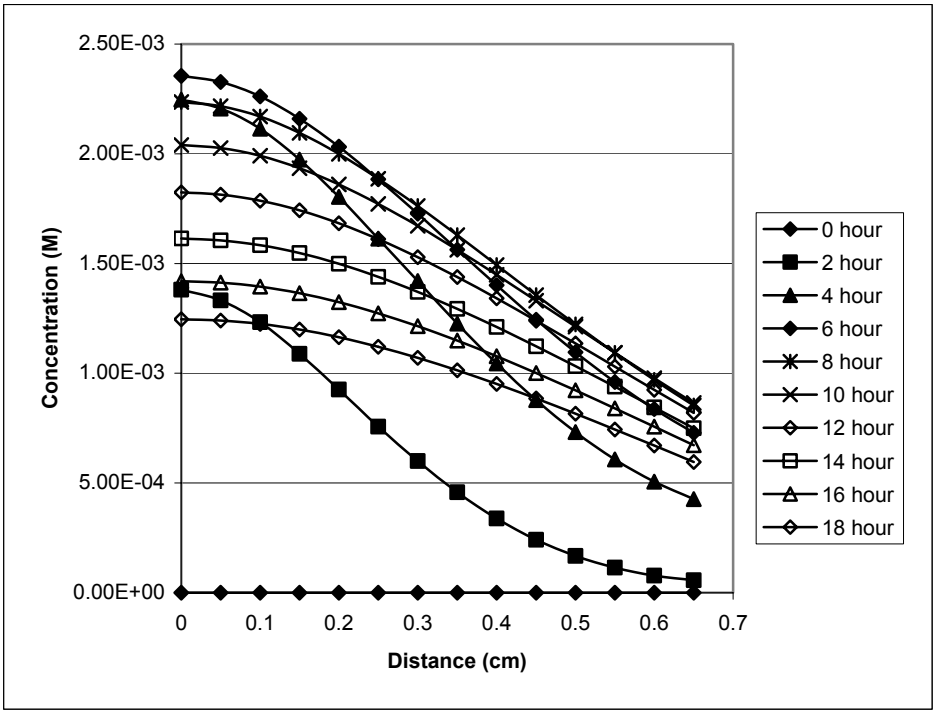

FIGURE 4-12. Simulated concentration distribution profiles from the back of the lens to the retina with the *in vitro* release rate in *in vivo* case.

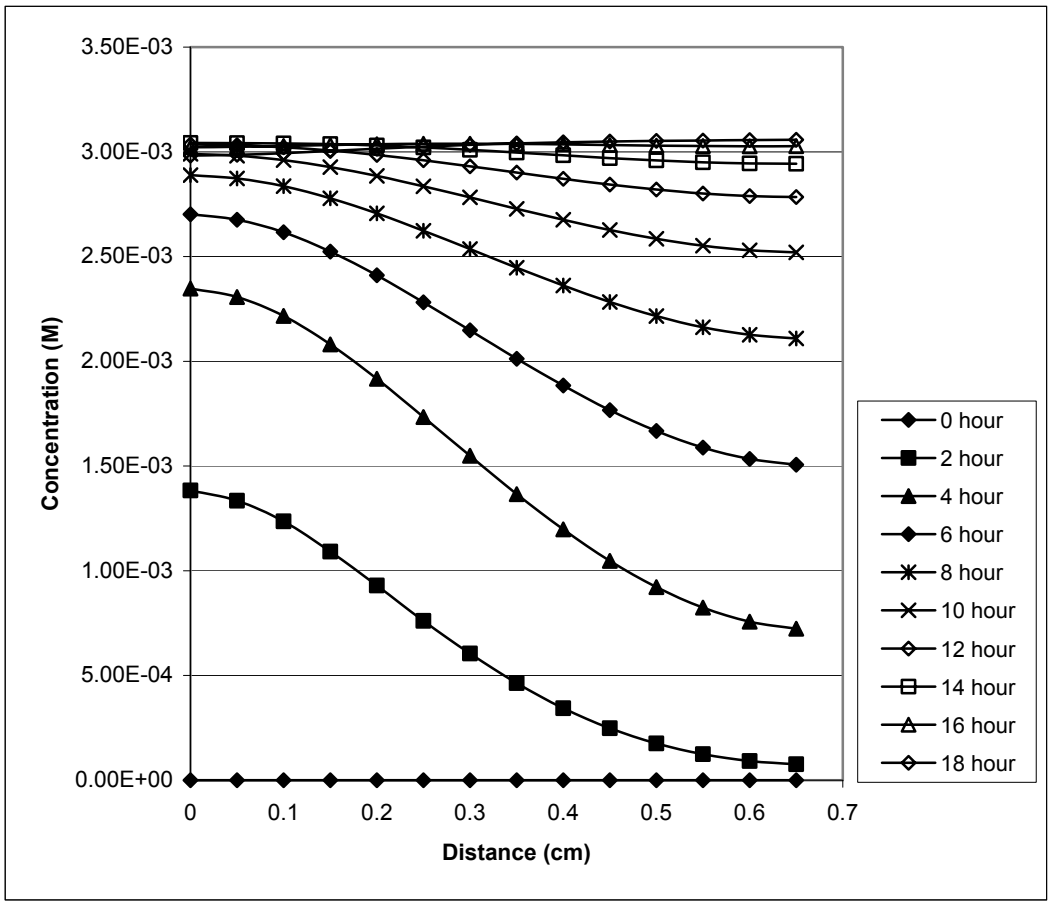

FIGURE 4-13. Simulated concentration distribution profiles from the back of the lens to the retina with the *in vitro* release rate in *ex vivo* case.

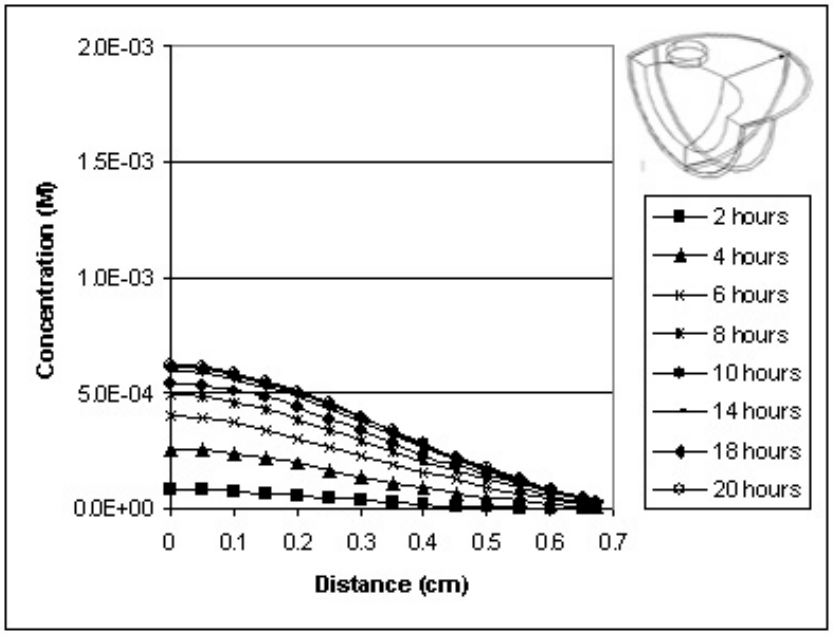
2.0E-03
1.5E-03
1.0E-03
5.0E-04
0.0E+00
Concentration (M)
0
0.1
0.2
0.3
0.4
0.5
0.6
0.7
Distance (cm)
2 hours
4 hours
6 hours
8 hours
10 hours
14 hours
18 hours
20 hours

(A)

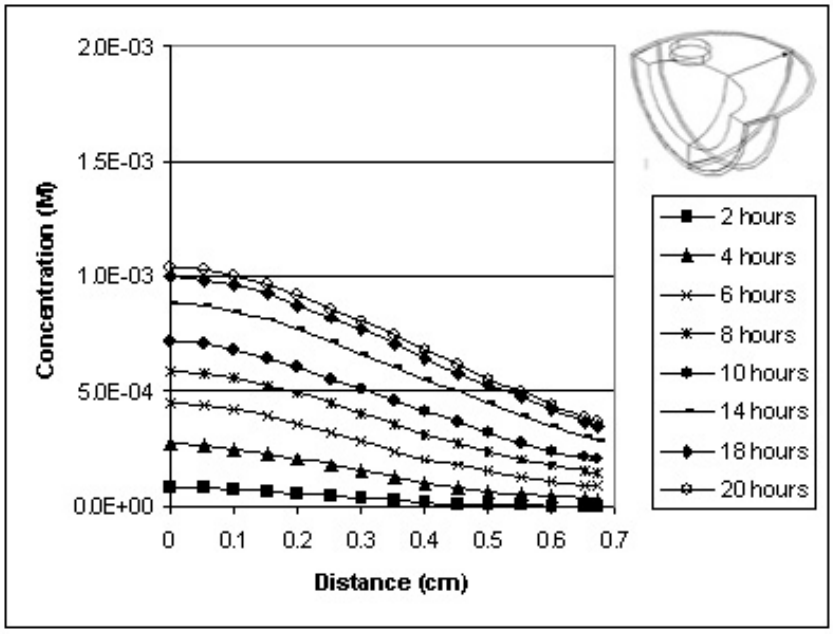
2.0E-03
1.5E-03
1.0E-03
5.0E-04
0.0E+00
Concentration (M)
0
0.1
0.2
0.3
0.4
0.5
0.6
0.7
Distance (cm)
2 hours
4 hours
6 hours
8 hours
10 hours
14 hours
18 hours
20 hours

(B)

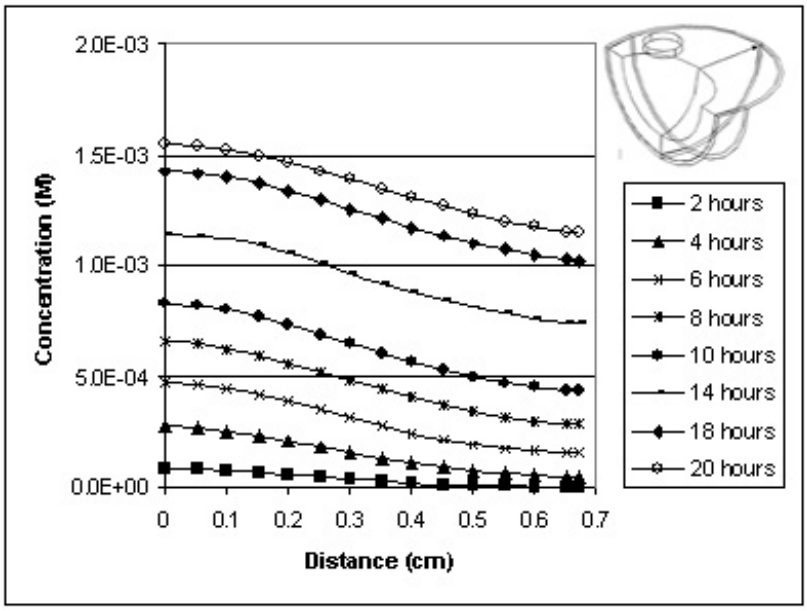
2.0E-03
1.5E-03
1.0E-03
5.0E-04
0.0E+00
Concentration (M)
0
0.1
0.2
0.3
0.4
0.5
0.6
0.7
Distance (cm)
2 hours
4 hours
6 hours
8 hours
10 hours
14 hours
18 hours
20 hours

(C)

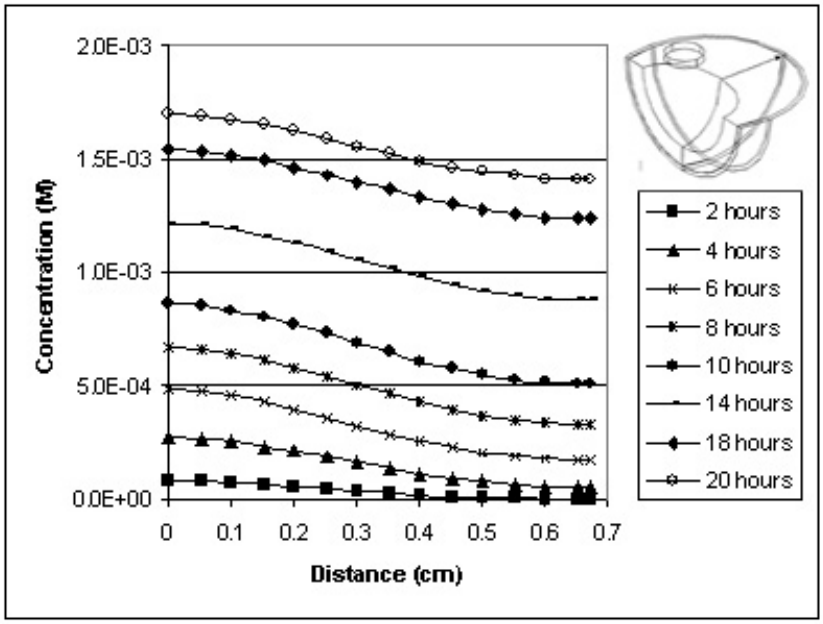
2.0E-03
1.5E-03
1.0E-03
5.0E-04
0.0E+00
Concentration (M)
0
0.1
0.2
0.3
0.4
0.5
0.6
0.7
Distance (cm)
2 hours
4 hours
6 hours
8 hours
10 hours
14 hours
18 hours
20 hours

(D)

FIGURE 4-14. Simulated concentration profiles with time along an axis from the back of the lens to the retina simulated for four different values of the R-C-S permeability coefficients; (A) 1.0×10^{-4} cm/sec, (B) 1.0×10^{-5} cm/sec, (C) 1.0×10^{-6} cm/sec, and (D) 0 cm/sec with a release rate of 0.1 mg $hour^{-1}$.

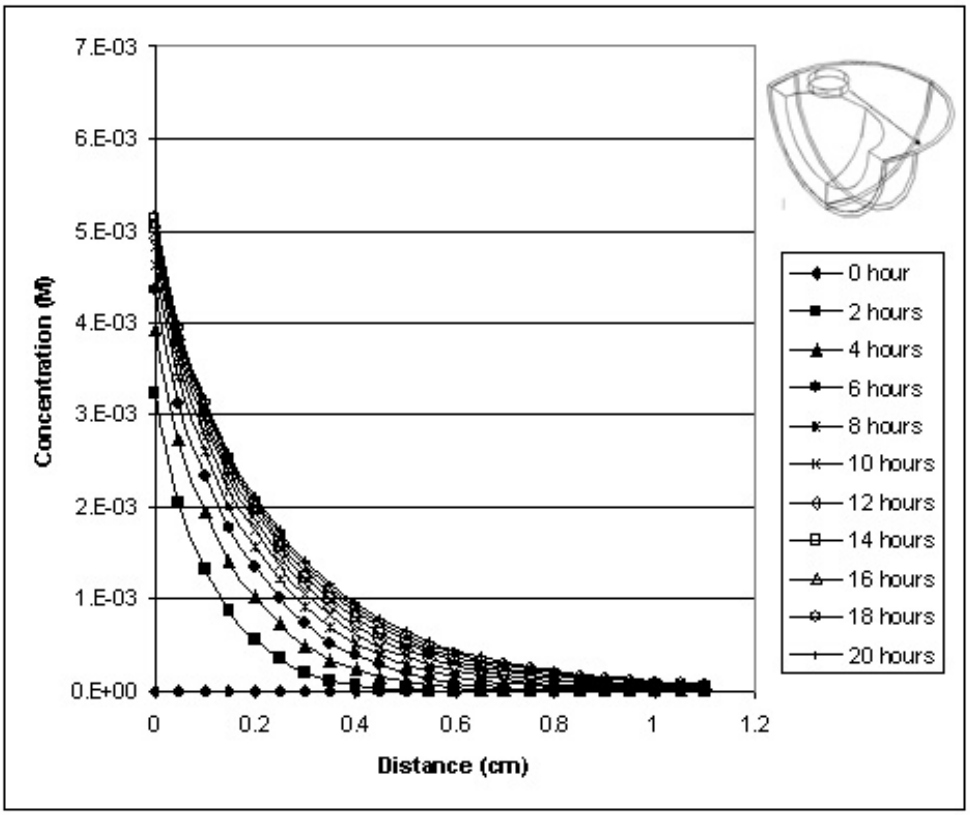

FIGURE 4-15. Simulated concentration profiles with time along an axis from the implant to the other side of the vitreous *in vivo* case.

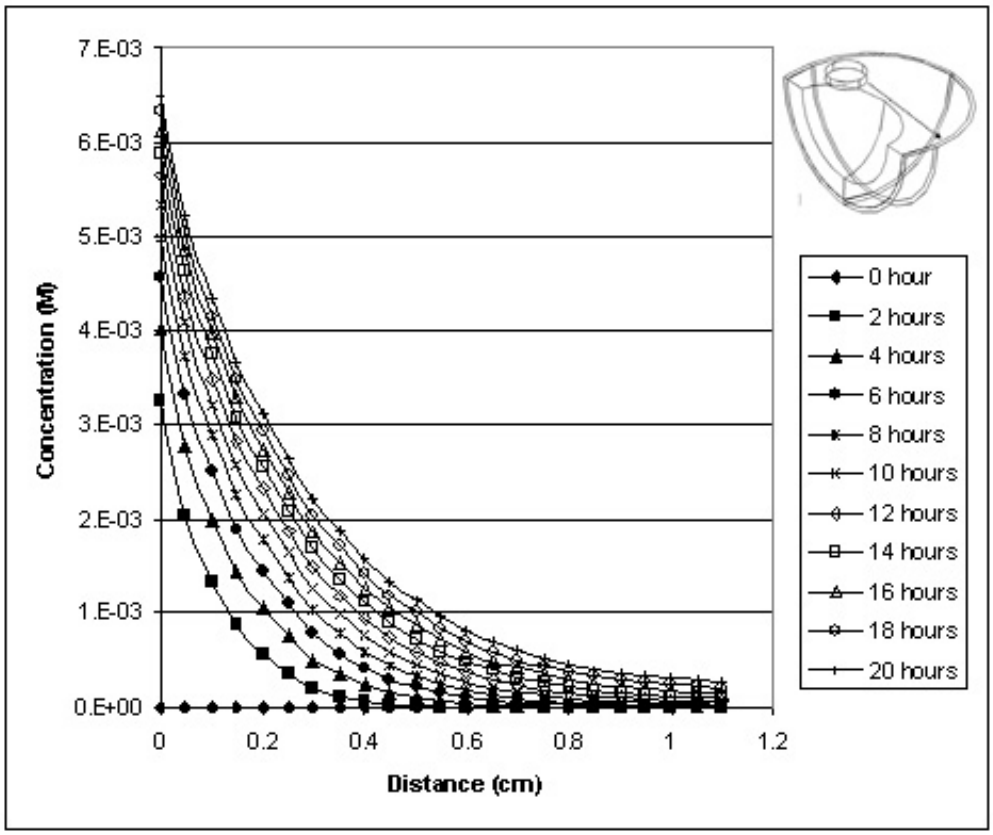

FIGURE 4-16. Simulated concentration profiles with time along an axis from the implant to the other side of the vitreous for *ex vivo* case with a release rate of 0.1 mg/hour.

4.5 Discussion

Information on the movement of drugs in the eye is important in determining efficient drug delivery routes, developing new drug delivery methods, and delivering drugs within the desired concentration ranges to the target site with minimal side effects. In this study, we investigated the movement of a small hydrophilic drug surrogate, Gd-DTPA (molecular weight = 958), released from an implant that was placed in the vitreous cavity of White New Zealand rabbits in both *in vivo* and *ex vivo* experiments. The transport of the Gd-DTPA was monitored by MRI and quantification of Gd-DTPA concentrations over time was obtained. The Gd-DTPA vitreous concentration profiles in rabbit eyes were correlated with a finite element mathematical model of the rabbit eye. Results of the mathematical analyses were the estimation of transport parameters in the rabbit eye such as vitreous diffusion coefficients and retinal-choroidal-scleral permeability (Table 4-2).

Table 4-2. Results of mathematical analyses.

A finite element mathematical model
• diffusion coefficient of Gd-DTPA in the vitreous: 2.8×10^{-6} cm^2/sec
• permeability of Gd-DTPA in R-C-S membrane: 1.0×10^{-5} cm/sec

MRI has proven to be a very useful tool for analyzing drug delivery in the eye. The technique is non-invasive and gives results in 3-D and in real time. Lizak et al. [113] used a modified fast spin echo sequence technique to image human lenses and was able to detect differences between normal and cataractous eyes. Previous studies reported the use of T_1- weighted MRI imaging for analyzing the diffusion of Gd-DTPA through PVA hydrogels [96] and for measuring bioreactor perfusion [114]. These studies analyzed MRI experimental data quantitatively with the relationship between T_1 relaxed values and concentration using inversion recovery MR imaging technique. Kolodny et al. [111, 114, 115] used MRI to study the eye. They concluded that plasma-derived proteins bypass the posterior chamber of the eye and enter the anterior chamber directly via the iris root. Their analysis was based on MRI images following intravenously injected Gd-DTPA rather than specific proteins. Several studies used contrast enhanced MRI to investigate the breakdown of the blood-retinal barrier created by chemical induction or by photocoagulation.[37, 116, 117] Berkowitz et al. (1991) produced panretinal photocoagulation in pigmented rabbits and reported a "leakiness" parameter to describe the increase in the permeability of the retina by comparing the brightness of Gd-DTPA images from the vitreous [116]. Berkowitz et al. (1992) and Sen et al. (1992) used contrast enhanced MRI to study the chemical-induced breakdown of two separate components of the blood-retinal-barrier: the outer barrier composed of the retinal pigment epithelial cells (RPE) and the inner barrier consisting of the retinal vascular endothelial cells. From their results, they calculated a "modified" permeability-area parameter and they concluded that the RPE disruption resulted in a greater increase in retinal

permeability than vascular disruption. They also reported a retinal permeability-area product parameter for control rabbits of 8.8×10^{-6} cm/sec [117], which compares quite favorably with our estimate of the retina-choroid-sclera layer Gd-DTPA permeability parameter of 1.0×10^{-5} cm/sec which was used in our finite element model. This model retina-choroid-sclera permeability is equivalent to a diffusion coefficient of 3.0×10^{-7} cm^2/sec through a retina-choroid-sclera layer of 0.03 cm thickness.

Our best fit model diffusion coefficient value for Gd-DTPA in the vitreous compartment was 2.8×10^{-6} cm^2/sec. This value compares to a free aqueous diffusion coefficient of 3.8×10^{-6} cm^2/sec as calculated by the Stokes-Einstein equation for a sphere [96] and 2.7×10^{-6} cm^2/sec calculated by the Wilke-Chang empirical theory using a specific volume of 0.77 ml/gm [118]. The vitreous is a porous medium composed of approximately 99% (w/w) water and 1% collagen fibers [119]. The close agreement of the model vitreous diffusion coefficient with those estimated from free diffusion theory would suggest that the collagen matrix provides minimal hindrance to diffusion of the relatively low molecular weight Gd-DTPA. Missel [48] assumed a diffusion coefficient for the retina-choroid-sclera region in his mathematical model that was one sixth of the vitreous diffusion coefficient. Applying this one sixth scaling factor to our model vitreous diffusion coefficient of 2.8×10^{-6} cm^2/sec results in an estimate of an retina-choroid-sclera diffusion coefficient of 4.7×10^{-7} cm^2/sec which compares to the 3.0×10^{-7} cm^2/sec derived from our finite element model.

The previous reports in the literature of image enhanced MRI studies of the eye were done with intravenous injections of Gd-DTPA. To our knowledge, our study is the first quantitative report of transport in the eye for compounds delivered by intravitreal implants. The concurrence of our permeability parameter derived from intravitreal delivery with that of Sen et al. [117] following intravenous injections would imply asymmetrical trans-retinal transport for Gd-DTPA. This result supports the assertion of Berkowitz [116] that transport of Gd-DTPA is by passive diffusion and not active transport.

Other mathematical simulations of drug delivery to the eye have been published. Ohtori and Tojo [120] reported a computer simulation of drug delivery to the eye from intravitreal injections using dexamethasone sodium m-sulfobenzoate (DMSB) as the model drug. They concluded that the major route of elimination was via the posterior aqueous humor, especially for hydrophilic drugs, but that the retina-choroid-sclera membrane, because of its large area, cannot be overlooked, especially for lipophilic drugs. Tojo and Isowaki [44] presented a pharmacokinetic model for intravitreal drug delivery based on an analysis of diffusion in a cylindrical vitreous body model. They modeled source terms for drug delivery that mimicked reservoir-type and matrix-type release of gancyclovir and the release of DMSB from biodegradable polymer rods. They showed good agreement between average vitreous concentration data and model simulations, but their study did not include spatial determination of drug concentration. Freidrich et al. [4] presented a sophisticated finite element model of the rabbit eye. Their analysis included fluorescein transport, which is highly permeable through the retina, and fluorescein glucuronide transport,

which poorly permeates the retina. Examination of the fluorescien simulations shows significant concentration gradients normal to the retinal surface, but for fluorescien glucoronide, these gradients are absent and shows instead concentration contours lines that are perpendicular to the retina. Their simulations are in agreement with the data of Aureie and Maurice [62] and reflect the findings or our Gd-DTPA MRI data and simulations for the *in vivo* and *ex vivo* experiments. That is to say, in our *in vivo* experiment, Gd-DTPA is apparently permeable through the retina-choroid-sclera layer and shows a sustained concentration gradient at the retinal surface. In our *ex vivo* experiments, there is no permeation of the Gd-DTPA through the retina-choroid-sclera layer, and this results in the absence of a concentration gradient at the retinal surface.

None of the previous models discussed above include convective flow through the vitreous compartment. The relative importance of convective fluid flow in vitreal drug movement is an unsettled issue in drug transport studies in the eye. Our model includes convection velocities in the vitreous which were calculated from normal intracoular pressures at the hyloid membrane (15 mm Hg). The fluid velocities vary somewhat as one traverses from the hyloid membrane toward the posterior segments of the vitreous near the retina since there is an expanding cross sectional area for flow. A nominal velocity for flow through the retina-choroid-sclera barrier in our model is 3.5×10^{-7} cm/sec. This compares favorably with a value of 3.9×10^{-7} cm/sec reported by Araie and Maurice [62] and 3.5×10^{-7} cm/sec reported by Missel [48]. Missel concludes that hydraulic flow is not likely to be of clinical significance for movement of low molecular weight drugs, especially if they are efficiently cleared

in the choroid. Likewise, our computer simulations show that reducing the convective flow to zero in the model produces essentially no change in the Gd-DTPA concentration profiles within the vitreous, suggesting that diffusion is the dominant mechanism for transport in our system. Xu et al. [91] calculated numbers to be 0.4 for a human eye and 0.024 for a mouse eye. The Péclet number reflects the relative importance of flow versus diffusion in transport. Using a nominal velocity at the retinal surface of 3.5×10^{-7} cm/sec, a diffusion coefficient of 3.8×10^{-6} cm^2/sec in the vitreous, and a nominal length scale of 1.0 cm for the diameter of the vitreous cavity of a rabbit eye, we calculate a Péclet number (vL/D) of approximately 0.09 which implies a dominance of diffusion over flow in affecting the concentration distribution of the Gd-DTPA in the vitreous. Xu's velocity estimate for the Péclet number was based on a Darcy's Law calculation using the combined resistance to flow calculated from the vitreous and scleral hydraulic conductivities, but any contribution to flow resistance from the retinal layer was ignored. They obtained a velocity value of 1.0×10^{-6} cm/sec which is about three times higher than our model value and the values reported by Missel [48].

The implant was placed in one side of the vitreous near the hyloid membrane, not in the middle of the vitreous because of surgerical difficulty, and the intensity gradient of Gd-DTPA across the vitreous from the middle of the vitreous to the other side of the vitreous was shown in the MRI images (see Figures 4-7 and 4-8). The previous simulation study showed asymmetric distribution of the model drug released from an intravitreal implant, which was position near the hyloid membrane, at steady state [48]. The our MRI experimental data showed that the concentration of Gd-

DTPA was 8.6×10^{-4} M at the other side of the vitreous about 10 hours post implantation in *ex vivo*, but it was 2.7×10^{-4} M about 7 hour post implantation in *in vivo*. In our simulation study, estimated steady state concentration gradient of Gd-DTPA from the implant to the other side of the vitreous was found to be stiffer in *in vivo* than in *ex vivo* because of elimination across the retina-choroid-sclera membrane. Both the release rate and the position of the implants in the vitreous were found to affect the distribution of the therapeutic agents in the vitreous. These are both important in delivering therapeutic agents within the desired clinical level to the target site.

Other techniques are available for transport studies in tissue, such as fluoremtry and autoradiography, but these procedures have limitations such as being one-dimensional, requiring animal sacrifice followed by serial sectioning at various time points, and in some cases, being difficult to quantify. Microdialysis has also been reported for analysis of vitreous drug concentrations in the eye.[42]

One potential drawback to the MRI method is the limited availability of actual drug compounds with paramagnetic properties detectable by MRI. Gd-DTPA (gadolinium diethylenetriaminepentaaceticacid) is a water soluble, MRI image enhancing agent with a molecular weight of approximately 958. It was selected because its molecular weight is similar to drugs of interest in ophthalmologic delivery; it is water soluble; and it is a standard MRI enhancing agent which is approved for use in animals and humans. Recently, larger varieties of compounds are becoming more available that are MRI contrast enhancing through chemical

conjugation of paramagnetic substances, including a series of high molecular weight compounds [121].

4.6 Conclusions

Diffusion coefficient and permeability of Gd-DTPA in the vitreous and in the RCS membrane were determined to be 2.8×10^{-6} cm^2/sec and 1.0×10^{-5} cm/sec, respectively by comparing simulation data to MRI experimental data. Implantation site was found from simulation studies to be one of important factors at controlling concentration of drugs released from an intravitreal implant in the vitreous.

CHAPTER 5. Compartmental pharmacokinetic analysis of magnetic resonance imaging experimental data

5.1 Objectives

Compartmental pharmacokinetic studies will be performed to understand the movement of Gd-DTPA released from an intravitreal implant or a subconjunctival implant in the rabbit eyes.

5.2 Introduction

Development of efficient drug delivery methods requires an understanding of the distribution of applied drug in the eye. Pharmacokinetics is defined as the quantitative analysis of the processes of drug absorption, distribution, and elimination that determine the time course of drug action [43]. The previous studies described the distribution of therapeutic agents injected intravitreally or released from an ocular implant in the vitreous using the finite element mathematical eye models [4, 44-46, 120]. Even though the previous studies succeeded in predicting the spatial distribution and calculating the total amount of therapeutic agents in the vitreous at several time points, the mathematical models were complicated and several parameter values were demanded to run the model.

Worakul et al. (1997) [40] summarized lumped pharmacokintic models depicting the distribution of ocular agents in the anterior segment of the eye. Several previous studies have been done to understand the elimination and the distribution of injected therapeutic agents in the vitreous using compartmental

pharmacokinetics [42, 122, 123]. To our knowledge, no lumped compartmental pharmacokinetic study has been performed to determine the elimination rate of therapeutic agents released from an ocular implant in the vitreous and the subconjunctival space.

In this chapter, we calculate the elimination rate of MRI contrast agent, Gd-DTPA, released from both the intravitreal implant and the subconjunctival implant to determine the main elimination pathways in the rabbit eye with lumped compartment pharmacokinetic models.

5.3 Materials and methods

5.3.1. Intravitreal implant MRI experiments

In order to obtain estimates of the average Gd-DTPA clearance rates from the eye, a simplified, lumped two-compartment model of the eye was developed to perform a pharmacokinetic analysis. Figure 5-1 shows a schematic of the lumped model for intravitreal implant MRI experiment. Gd-DTPA is assumed to be cleared across the retina-choroid-sclera barrier (k_1), transferred from the vitreous to the aqueous compartment across the hyloid membrane (k_2), and eliminated from the aqueous compartment to some region that is outside the eye (k_3). Drug is released into the vitreous compartment from the implant at a rate R. *In vitro* release rate of Gd-DTPA from intravitreal implant was used for R. The mass balance equations determined for the vitreous and aqueous compartments are:

$$\frac{dM_v}{dt} = -(k_1 + k_2)M_v + R \qquad (5\text{-}1)$$

$$\frac{dM_a}{dt} = -k_3 M_a + k_2 M_v \qquad (5\text{-}2)$$

where, M_v and M_a are amounts [mg] of Gd-DTPA in the vitreous and in the aqueous humor chamber, respectively. k_1, k_2, and k_3 are transfer coefficients [hour^{-1}] for the elimination pathways of Gd-DTPA.

Experimental values for the total amount of Gd-DTPA in the vitreous and aqueous compartments at each time point were determined from the concentration MRI images of the eye by outlining the vitreous and aqueous regions of interest in all the image slices that constitute a particular eye. Each voxel concentration was then multiplied by the voxel volume and summed over all the slices that constitute particular region of interest, e.g. the vitreous or anterior compartment, at each time point. This analysis yielded data for the total Gd-DTPA amount, M_v and M_a, in the vitreous and aqueous compartments over time. Equations 5-1 and 5-2 were regressed against these data to determine the optimum values of the transfer coefficients with the Matlab optimization toolbox (version 2.3, Mathworks Inc., Natick, MA, USA).

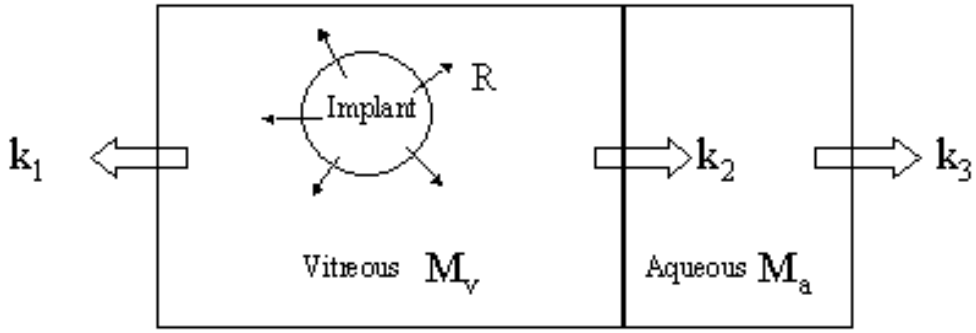

Figure 5-1. A schematic of the lumped two-compartment model of the eye for an intravitreal implant.

k_1: transfer coefficient across the retina-choroid-sclera barrier [$hour^{-1}$].

k_2: transfer coefficient from the vitreous to the aqueous humor compartment across the hyloid membrane [$hour^{-1}$].

k_3: transfer coefficient from the aqueous compartment to some region that is outside the eye [$hour^{-1}$].

R: release rate from an intravitreal implant [mg/hour]

M_V: amount of Gd-DTPA in the vitreous [mg].

M_a: amount of Gd-DTPA in the aqueous compartment [mg].

5.3.2. Subconjunctival implant MRI experiments

A simplified, lumped three-compartment model of the eye was developed to analyze the ocular drug distribution from a subconjunctival implant at the equator *in vivo*. Figure 5-2 shows a schematic of the pharmacokinetic lumped model. In the subconjunctival implant experiment, Gd-DTPA is assumed to be transferred from the subconjunctival space directly into the aqueous humor (k_1) and into the vitreous humor (k_2), eliminated from the aqueous humor through Schlemm's canal to the aqueous veins (k_3) and from the vitreous into the aqueous humor (k_4), and cleared from the subconjunctival space (i.e. movement into the episcleral veins and conjunctival lymphatics) (k_5). Gd-DTPA is released into the subconjunctival space from the implant at a rate *R(t)*. The mass balance equations for the subconjunctival implant experiment are:

$$\frac{dM_a}{dt} = k_1 M_s + k_4 M_v - k_3 M_a \qquad (5\text{-}3)$$

$$\frac{dM_v}{dt} = k_2 M_s - k_4 M_v \qquad (5\text{-}4)$$

$$\frac{dM_s}{dt} = -(k_1 + k_2 + k_5) M_s + R \qquad (5\text{-}5)$$

where, M_a, M_v, and M_s are amount [mg] of Gd-DTPA in the aqueous humor, the vitreous, and the subconjunctival compartment, respectively. k_1, k_2, k_3, k_4, and k_5 are transfer coefficients [hour^{-1}] for elimination pathways of Gd-DTPA. Experimental values for the total amount of Gd-DTPA in the vitreous and aqueous compartments at each time points were determined and the above three equations were regressed by the same method as the case of intravitreal implant MRI experiment. The amount of

Gd-DTPA at the subconjunctival space was estimated from the results of the pharmacokinetics.

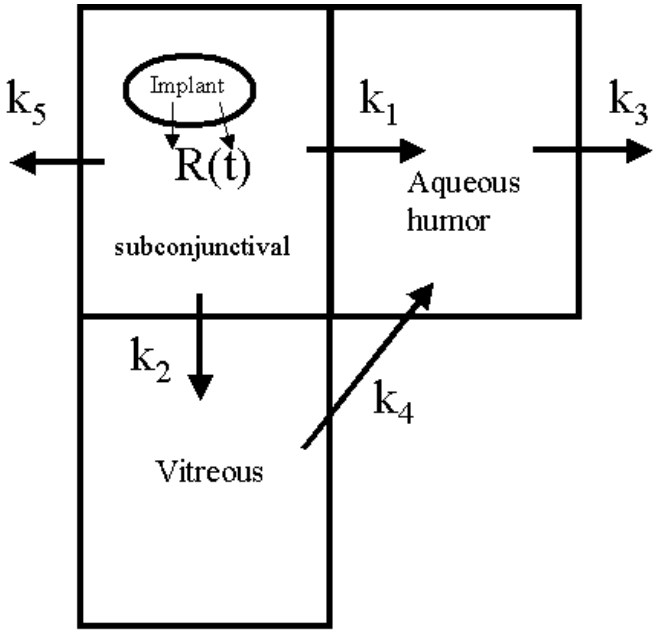

Figure 5-2. A schematic of the lumped two-compartment model of the eye for a subconjunctival implant.

k_1: transfer coefficient from the subconjunctival space directly into the aqueous humor.

k_2: transfer coefficient from the subconjunctival space directly into the vitreous humor.

k_3: transfer coefficient from the aqueous humor through Schlemm's canal to the aqueous veins.

k_4: transfer coefficient from the vitreous into the aqueous humor.

k_5: transfer coefficient from the subconjunctival space (i.e. movement into the episcleral veins and conjunctival lymphatics).

R(t): release rate of Gd-DTPA from the subconjunctival implant.

5.4. Results

5.4.1. Intravitreal implant MRI experiments

A lumped compartment, pharmacokinetic analysis (PK) of the Gd-DTPA distribution was performed as an adjunct to the finite element model. With the PK model, we were able to obtain overall average clearance parameters for the Gd-DTPA elimination by the hypothesized major routes: (1) transport through the retina-choroid-sclera membrane, (2) movement across the hyloid / cliary body region, and (3) washout by aqueous humor from the anterior chamber. The total amounts of Gd-DTPA in the vitreous chamber and in the anterior aqueous humor chamber was determined from an analysis of the MRI concentration images as described in the Methods section. The experimental Gd-DTPA amounts in the vitreous chamber and in the anterior aqueous chamber are shown as the circles in Figures 5-3 and 5-4 respectively. The two compartment pharmacokinetic model described in Figure 1, which utilized Equations (5-1) and (5-2), was used to obtain values of the clearance constants k_1, k_2, and k_3 that optimized the fit between the simulation and experimental data by a regression method. The resultant values were $k_1 = 0.088$ hour^{-1}, $k_2 = 0.009$ hour^{-1}, and $k_3 = 0.362$ hour^{-1}. Used these values in the model, the simulated amount of Gd-DTPA in the vitreous and aqueous humor are shown by the solid lines in Figure 5-3 and 5-4. The amount of Gd-DTPA present in the anterior chamber is typically 40 times less than that in the vitreous compartment. The amount of Gd-DTPA reaches a plateau at about 5 hour and then gradually clears from the vitreous. The *in vitro* release data shows that the implant has released most of the Gd-DTPA by 2 hour.

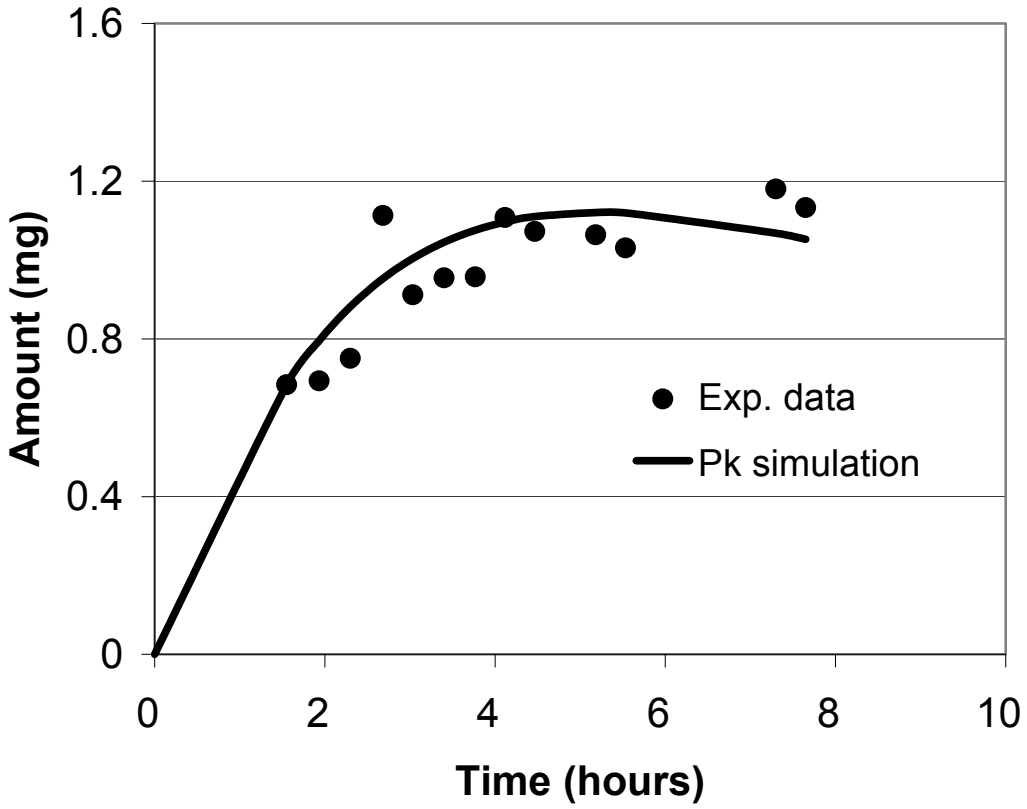

Figure 5-3. Amount of Gd-DTPA released from an intravitreal implant in the vitreous from MRI experiments (dots) and pharmacokinetic analysis (the solid lines).

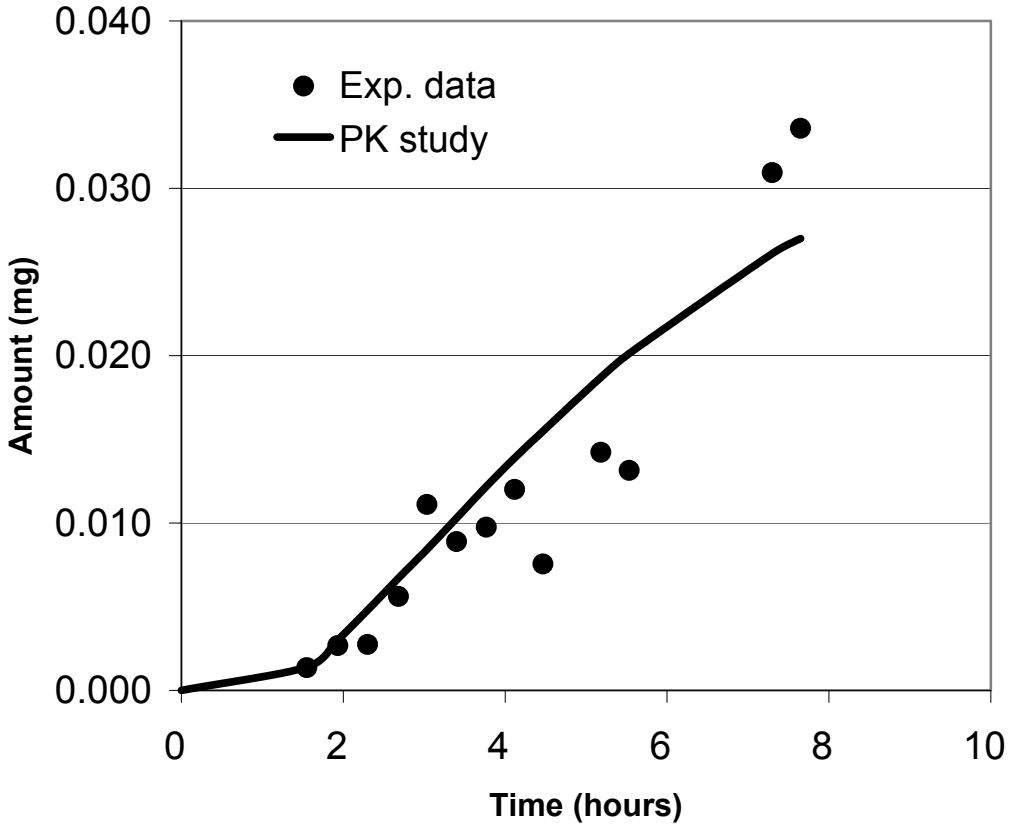

Figure 5-4. Amount of Gd-DTPA released from an intravitreal implant in the aqueous humor from MRI experiments (dots) and pharmacokinetic study (the solid lines).

5.4.2. Subconjunctival implant MRI experiments

We obtained information on the amount of Gd-DTPA in the vitreous and the aqueous humor, not in the subconjunctival space. Because of the shortage of information, we could the ratio between one another but not absolute transfer coefficient values. The experimental Gd-DTPA amounts in the vitreous chamber and in the anterior aqueous chamber are shown as the circles in Figure 5-5 and 5-6, respectively. The three compartment pharmacokinetic model descried in Figure 5-2 the values of the transfer coefficients k_1, k_2, k_3, k_4, and k_5 to be 0.0056 hour^{-1}, 0.0076 hour^{-1}, 0.018 hour^{-1}, 0.082 hour^{-1}, and 4.73 hour^{-1}, respectively. Used these values in the model, the simulated amount of Gd-DTPA in the vitreous and aqueous humor are shown by the solid lines in Figures 5-5 and 5-6. The amount of Gd-DTPA in the subconjunctival space was estimated from Equation (5-5) and shown in Figure 5-7. The amount of Gd-DTPA in the subconjunctival space peaked at the beginning because of the initial release burst in *in vitro* release rate and then decreased so fast from the subconjunctival space into the outside of the eye. The ratio of transfer coefficient from the subconjunctival space to the vitreous to that from the subconjunctival space to the aqueous humor was found to be 1.35. In this model, the Gd-DTPA transferred from the subconjunctival space to the vitreous was assumed to be eliminated into the aqueous humor because most of Gd-DTPA transferred from the subconjunctival space into the vitreous was observed near the hyloid membrane, not in the middle of the vitreous so that Gd-DTPA in the vitreous was assumed to be swept by the aqueous humor flow into the aqueous humor chamber [124].

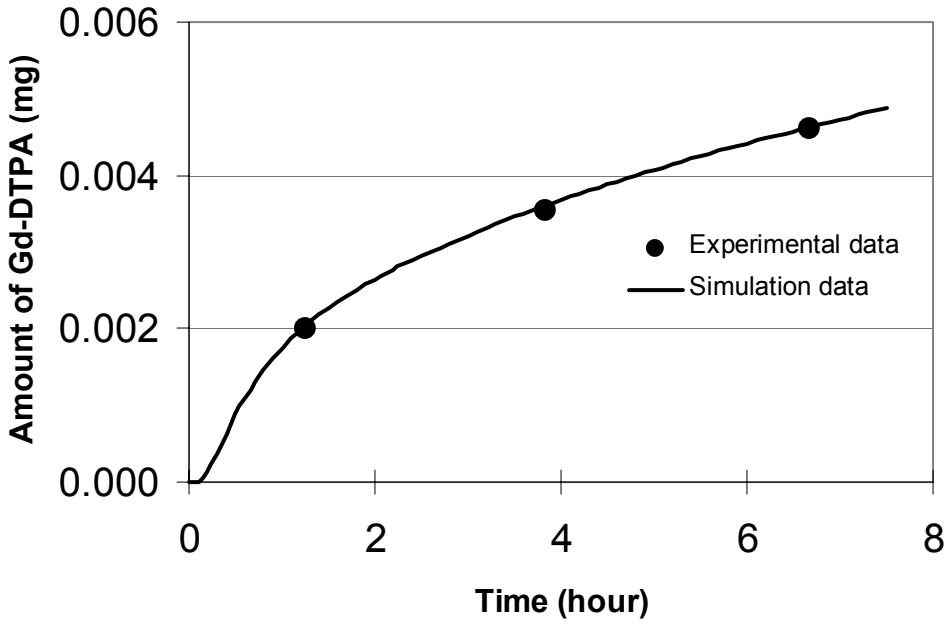

Figure 5-5. Amount of Gd-DTPA released a subconjunctival implant in the aqueous humor from MRI experiments (dots) and pharmacokinetic study (the solid lines).

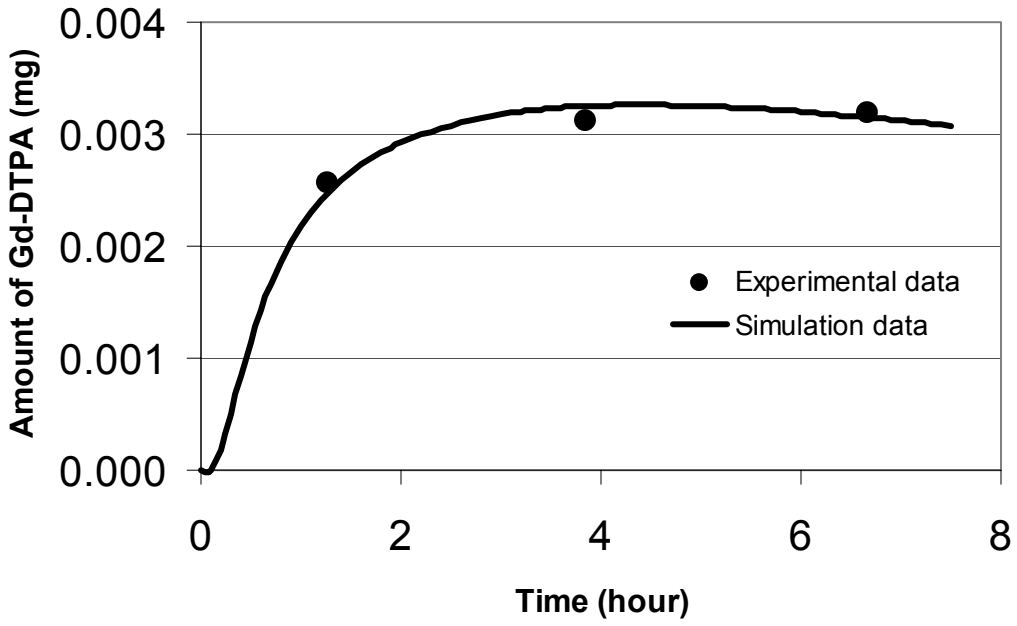

Figure 5-6. Amount of Gd-DTPA released from a subconjunctival implant in the vitreous from MRI experiments (dots) and pharmacokinetic study (the solid lines).

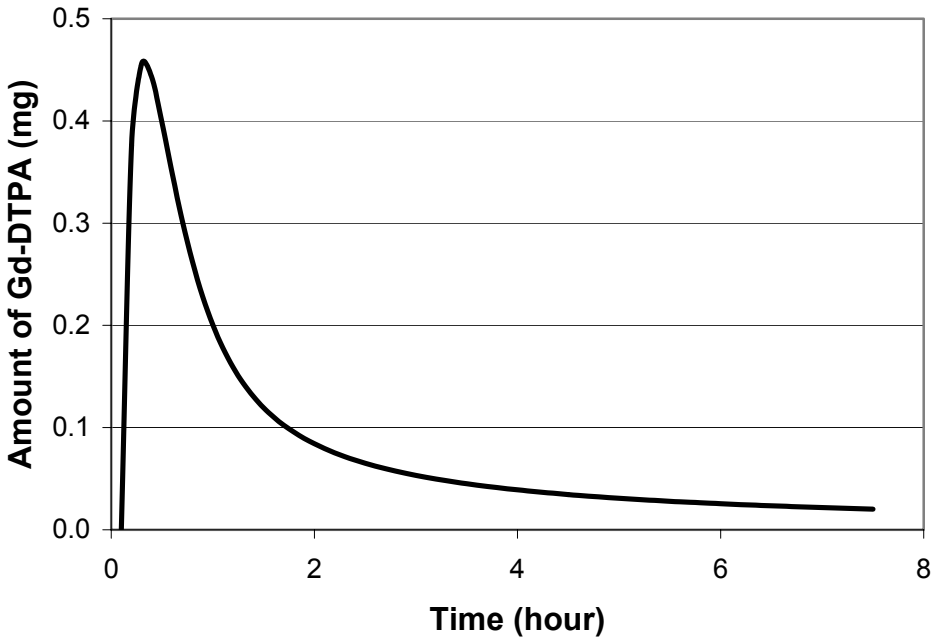

Figure 5-7. Estimated amount of Gd-DTPA in the subconjunctival space from the pharmacokinetic study.

5.5 Discussion

The two compartment pharmacokinetic PK model was a more simplified approach to quantitatively tracking the disposition of the Gd-DTPA in the vitreous and aqueous compartments than the finite element mathematical eye model mentioned in Chapter 4. It is based on the amount of Gd-DTPA summed over the compartment volume and does not utilize spatial variations of amount. In the lumped compartment pharmacokinetics for an intravitreal MRI experiment, the kinetic constants resulting from the best fit of the PK simulations to the summed experimental MRI amount data also showed a dominant elimination path of Gd-DTPA to be via the retina-choroid-sclera barrier compared to the anterior elimination through the aqueous chamber. The PK kinetic constant for elimination through the retina-choroid-sclera (0.088 $hour^{-1}$) was about 10 fold greater than that for elimination via the anterior aqueous path (0.009 $hour^{-1}$). Comparison of these PK kinetic parameters to other relevant physiologic values or to equivalent finite element model parameters gave only modest agreement. For example, the k_3 parameter (0.362 $hour^{-1}$) in Figure 5-1 can be compared to the aqueous humor drainage in rabbits of 0.64 $hour^{-1}$, which is calculated as the aqueous humor production rate of 0.16 ml $hour^{-1}$ [5] divided by the aqueous humor volume of 0.25 ml [125]. Also, the PK constant representing elimination through the retina-choroid-sclera barrier (k_1) in Figure 5-1 times the vitreous volume (V) can be compared to the finite element retina-choroid-sclera permeability-area product (P×A), or in other words, $k_1 = P \times A \times V^{-1}$. This $P \times A \times V^{-1}$ product is $(1.0 \times 10^{-5}$ cm/sec) × (1.91 cm^2) × (0.32 $cm^3)^{-1}$ = 0.21 hr^{-1} compared to a k_1 of 0.088 hr^{-1} in Figure 5-1. There are a number of factors that may

relate to these discrepancies. For example, to calculate drug fluxes, the Figure 5-1 PK model utilizes the total amount of Gd-DTPA in compartments instead of the distributed amount in the finite element model. Also, the values of the PK kinetic constants estimated from a best fit of Equations 5-1 and 5-2 to the averaged concentration data depend on the value assumed for the source term, *R*, in the PK model which represents the drug release rate. The *R* term was based on the *in vitro* release studies. There may be differences between the *in vitro* and *in vivo* release rates. Finally, errors in the calculation of the average Gd-DTPA concentrations used in the PK model can occur from incorrect estimates of the Gd-DTPA concentration from the MRI images at the extreme high and low concentrations values e.g. near the implant and in the aqueous compartment, respectively. In any event, both the finite element (Chapter 4) and the PK model suggest that Gd-DTPA is eliminated predominately through the retina-choroid-sclera barrier in the *in vivo* experiments.

In lumped compartment pharmacokinetics for the subconjunctival implant MRI experiment, we found that Gd-DTPA was quickly eliminated from the subconjunctival space. However, we could not identify the pathway of Gd-DTPA elimination from the subconjunctival space, but collectively, in Figure 5-2 these pathways have an elimination coefficient (k_5) 3-log units higher than that for particle movement into the vitreous (k_2). This Figure 5-2 PK study found that delivering therapeutic agents from the subconjunctival space into the inside of the eye was inefficient because of active elimination mechanism such as the choroidal blood flow. In Chapter 2, lipophilic therapeutic agent, H-110, released from a subconjunctival implant could not be delivered to the subretinal space across the choroid. From the

subconjunctival H-110 study and the subconjunctival Gd-DTPA study, we concluded the choroidal blood flow is a formidable barrier to the low molecular weight therapeutics from the subconjunctival space into the subretinal space.

In the MRI images, we could not determine the amount of Gd-DTPA in the subconjunctival space because the difference between the subconjunctival space and the standard solution. No information on the amount of Gd-DTPA in the subconjunctival space prevented the determination of the absolute value. Only relative values showing the ratio of one elimination rate constant to another could be determined.

Pharmacokinetic studies with lumped compartments gave useful information on the fate of the drugs and is important in determining an efficient delivery route of therapeutics in the eye.

5.6 Conclusions

Elimination of Gd-DTPA released from an intravitreal implant from the vitreous was found from the two-compartment pharmacokinetic study to be about 10 times greater than transport from the vitreous to the aqueous humor. Elimination of Gd-DTPA from the subconjunctival space to external of the eye was determined from the three-compartment pharmacokinetic study to be about 1000 times more dominant than transport into the vitreous.

CHAPTER 6. Pharmacokinetic study of traimcinolone acetonide injected intravitreally.

6.1 Objectives

A pharmacokinetic model will be developed to analyze triamcinolone acetonide experimental data and decide optimal injection doses in human cases.

6.2 Introduction

Intravitreal administration of triamcinolone acetonide has been used widely in ophthalmology for the treatment of diabetic retinopathy [19, 70], uveitis [126-129], pseudophakic cystoid macular edema [130, 131], choroidal neovascularization associated with AMD [9, 67-69], and macular edema associated with central retinal vein occlusion [71-73].

To maximize the benefits of intravitreal injected triamcinolone acetonide to the posterior segment eye diseases, it would be desirable to determine the length of time that therapeutic levels are maintained. Up to now, several pharmacokinetic studies have been done on the clearance following intravitreal injection of a single dose triamcinolone acetonide [132-134]. However, these studies do not permit estimation of clearance for other doses. In addition, the studies do not provide the basis for estimating the optimal dosing for clinical efficacy.

The purpose of this study was to aid in optimizing the administration of

triamcinolone acetonide by developing a guide for predicting the clearance in patients over a range of doses from pharmacokinetic studies in rabbits.

6.3 Materials and methods

6.3.1 TAC-PF formulation

Triamcinolone acetonide USP grade (Voight Global Distribution, LLC, Kansas City, MO) was prepared as a sterile 40 mg/ml or 160 mg/ml suspension in normal saline for injection USP (B. Braun Medical Inc., Irvine, Ca) in single use vials by the Clinical Center Pharmacy Department at the National Institutes of Health. Hydroxypropylmethylcellulose 0.5% USP was added to increase the viscosity of the formulation and enable the drug particles to stay in suspension for a minimum of 20 minutes after shaking allowing time to draw an accurate dose.

6.3.2 Intravitreal TAC-PF animal experiment

Fifty-two New Zealand White rabbits of either sex weighing 2-3 kg were used (Covance Laboratories, Inc., Vienna, VA) and the procedures adhered to the guidelines from the Association for Research in Vision and Ophthalmology for animal use in research. Food and water were supplied to the rabbits *ad libitum*. Animals were anesthetized with ketamine hydrochloride (Fort Dodge, Inc., Fort Dodge, Indiana) 35mg/kg IM, xylazine (Phoenix Scientific, Inc., St. Joseph, MO) 5mg/kg IM, and proparacaine 1% ophthalmic drops (Allergan America, Hormigueros, PR) were used topically on the right eye. After adequate anesthesia and akinesia were obtained, a lid speculum was placed and the right eye was injected 3 mm behind

the surgical limbus in the superotemporal quadrant with 0.1 ml (4 mg or 16 mg) TAC-PF. Rabbits were euthanized with a pentobarbital overdose (Beuthanasia-D Special, Schering-Plough Animal Health Corp., Kenilworth, NJ) at intervals of 1 hour, 7 days, 14 days, 28 days, 42 days, 56 days, and 119 days for the 4 mg injection or 1 hour, 7 days, 27 days, 70 days, 131 days, and 238 days for the 16 mg injection. The eyes were enucleated and immediately frozen at –70˚ C for later dissection and drug extraction.

The eyes were dissected while frozen by first removing the cornea with a razor blade and the aqueous humor, ciliary body/ iris, lens, and vitreous were isolated. A 5 × 5 mm section of sclera/choroid and retina was removed en bloc adjacent to the optic nerve. The TA was extracted from the tissues by the addition of sufficient amount of HPLC grade acetonitrile to dissolve the remain TA (Burdick & Jackson, Inc., Muskegon, MI) and then the TA-acetonitrile solution was sonicated with a model GEX 600 Ultrasonic processor (Thomas Scientific, Swedesboro, NJ) set at level 3.5 for 1 minute for aqueous and vitreous humor. The samples were incubated for 24 hours at room temperature and spun down in a GS-6R centrifuge (Beckman Coulter Inc., Fullerton, CA) for 30 minutes at 8,000 rpm and the supernatants were submitted for HPLC analysis. The drug assays were performed using a Hewlett Packard HP1100 HPLC system (Agilent Technologies, Palo Alto, CA) equipped with a Diode Array detector, an auto-sampler, a quaternary, and an HP Kayak workstation which controlled the operation of HPLC and analyzed the data. A Beckman Ultrasphere C-18 column (5 μm, 250 × 4.6 mm)(Beckman Coulter, Inc., Fullerton CA) was used for separation and the wavelength for detection was set at 254 nm. The

flow rate employed was 1.0 ml/min with a mobile phase of 60% of water and 40% of acetonitrile by volume. The retention time of TAAC was 7.0 minutes and the TAAC detection limit was 10 ng/ml.

6.3.3 Pharmacokinetics of TAC-PF in the vitreous

On the assumption that the elimination rate at any specific time depends on amount in the combined vitreous and depot, the experimental data were regressed with the following equation:

$$\frac{dM}{dt} = -k \times M^{n} \tag{6-1}$$

where, t [day] is time in days and M [mg] represents the amount of triamcinolone acetonide in the depot plus the vitreous. k [day^{-1}] is an elimination rate constant. n is a constant to characterize the nonlinear dependence of clearance on the dose of triamcinolone acetonide. The elimination rate constants for 4 mg injection and 16 mg injection, k_4 and k_{16}, and n value in Equation (6-1) were found by regressing animal experimental data of 4 mg injection and 16 mg injection simultaneously using MATLAB Optimization toolbox (version 2.3, The MathWorks, Inc., Natick, MA, USA).

The ratio of the elimination rate constants was determined with the following relationship (See Appendix I):

$$\frac{k_4}{k_{16}} = \left(\frac{Dose_4}{Dose_{16}} \right)^{m} \tag{6-2}$$

From the calculated k_4, k_{16}, and doses, $Dose_4$ = 4 mg and $Dose_{16}$ = 16 mg, a value for *m* value was determined. The above Equation (6-2) allowed estimating the elimination for other intravitreal triamcinolone acetonide doses.

A half-life of intravitreal injected triamcinolone acetonide was calculated with the following equation (See Appendix II):

$$t_{1/2} = \frac{1}{k} \times \left(\frac{1}{n-1} \right) \times M_0^{1-n} \times \left[2^{n-1} - 1 \right] \qquad (6\text{-}3)$$

6.4 Results

Triamcinolone acetonide, is a lipophilic corticosteroid. It forms a depot in the vitreous when injected intravitreally (Figure 6-1). In Figure 6-1, the white spot represents the depot of triamcinolone acetonide in the vitreous.

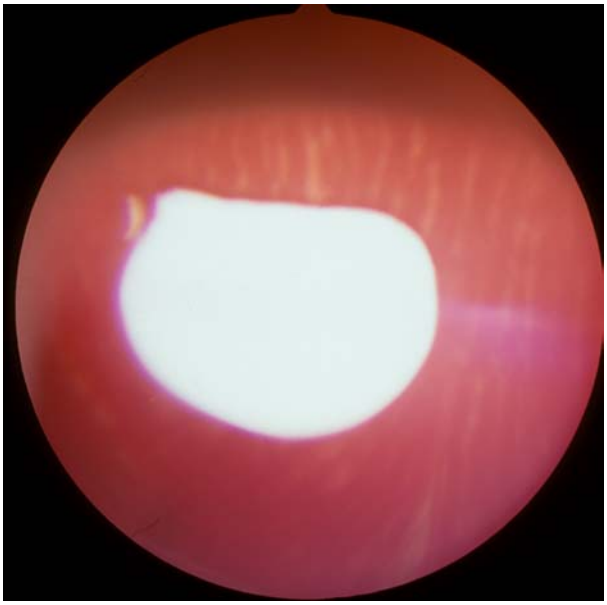

Figure 6-1. TAC-PF depot in the rabbit vitreous 1 day post implantation. A white spot marks the TAC-PF depot in the vitreous; red background is the rabbit retina.

Pharmacokinetics:

In the experiment, a small amount of injected triamcinolone acetonide was observed to leak back through an injection needle hole. It was difficult to estimate the small leakage and so we could not confirm that exactly 4 mg or 16 mg triamcinolone acetonide was injected.

The amount of triamcinolone acetonide extracted from the vitreous at each time point is shown in Figure 6-2 (4-mg intravitreal injection) and Figure 6-3 (16-mg intravitreal injection). The data from 4 mg (k_4) and 16 mg (k_{16}) triamcinolone acetonide injections were regressed with the Equation (6-1) to find the elimination rate constants k_4 and k_{16}, and the exponent n. The resulting values were k_4=0.0245 [day^{-1}], k_{16}=0.0069 [day^{-1}], and n=1.41. The regression curves are shown as solid lines in Figure 6-2 and Figure 6-3. The elimination of water-soluble drugs from the vitreous follows linear one-compartment pharmacokinetic behavior with a value in Equation (6-1) of n=1. Because poorly soluble intravitreal injected triamcinolone acetonide sediments to from a depot, the drug is not distributed homogenously in the vitreous.

Using the k_4 and k_{16} values determined by regressing by Equation 6-1 was found that m=-0.91 from Equation (6-2). Using Equation (6-2) to extrapolate to other doses, we predict rate constant values for 1-mg and 8-mg dose injections, k_1 and k_8 to be 0.087 [day $^{-1}$] and 0.013 [day^{-1}], respectively. Using the estimated k_1 and k_8 values and Equation (6-1) allowed us to predict the time course of intravitreal injected TA in the vitreous for doses of 1 mg injection and 8 mg (Figure 6-4).

The half-life of each intravitreal injection dose was calculated with

Equation (6-3) and was found to follow the following relationship with injection dose (Figure 6-5):

$$\text{Half-life [days]} = 9.20 \times \text{Injection amount [mg]}^{0.508}$$

Results of this pharmacokinetic study are summarized at Table 6-1.

Table 6-1. Summary of pharmacokinetic study.

Injection amount	Mass transfer coefficient (k) [day^{-1}]	Half-life [days]
1 mg	0.0870	9.2
4 mg	0.0245	18.6
8 mg	0.0130	26.5
16 mg	0.0069	37.6

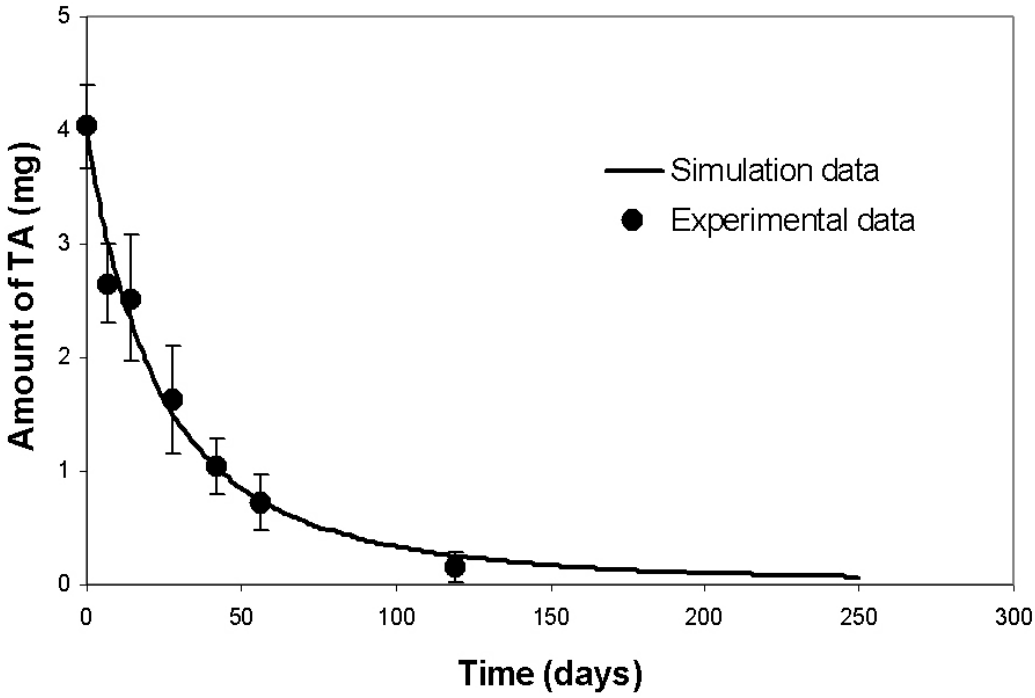

Figure 6-2. 4 mg TA intravitreal injection experimental data (dots) and regression with a Equation 6-1 (line).

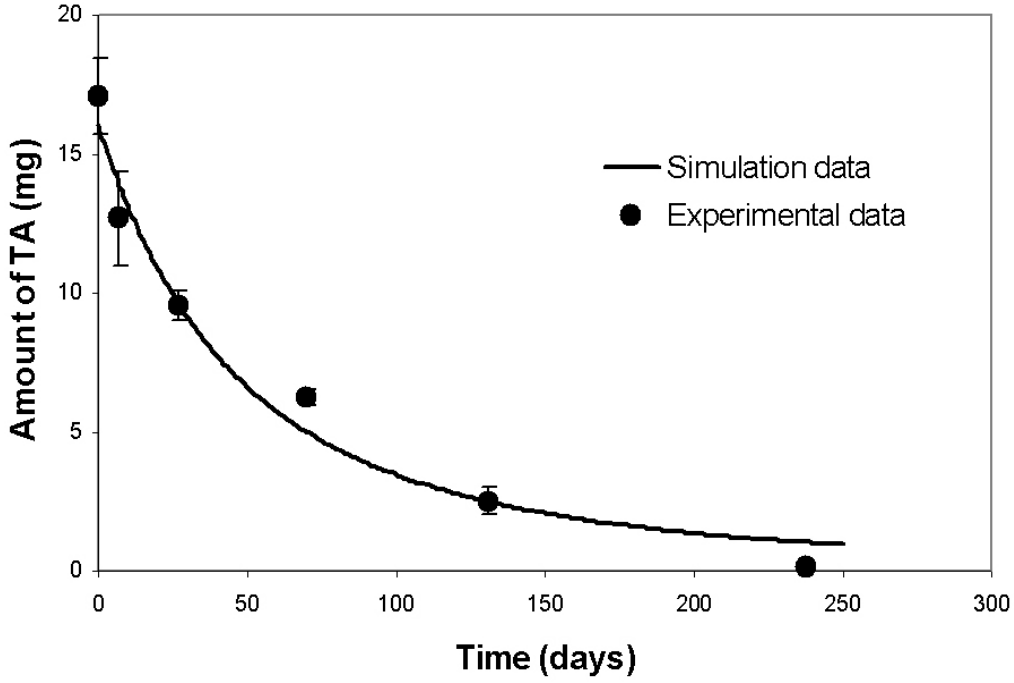

Figure 6-3. 16 mg TA intravitreal injection experimental data (dots) and regression with a Equation 6-1 (line).

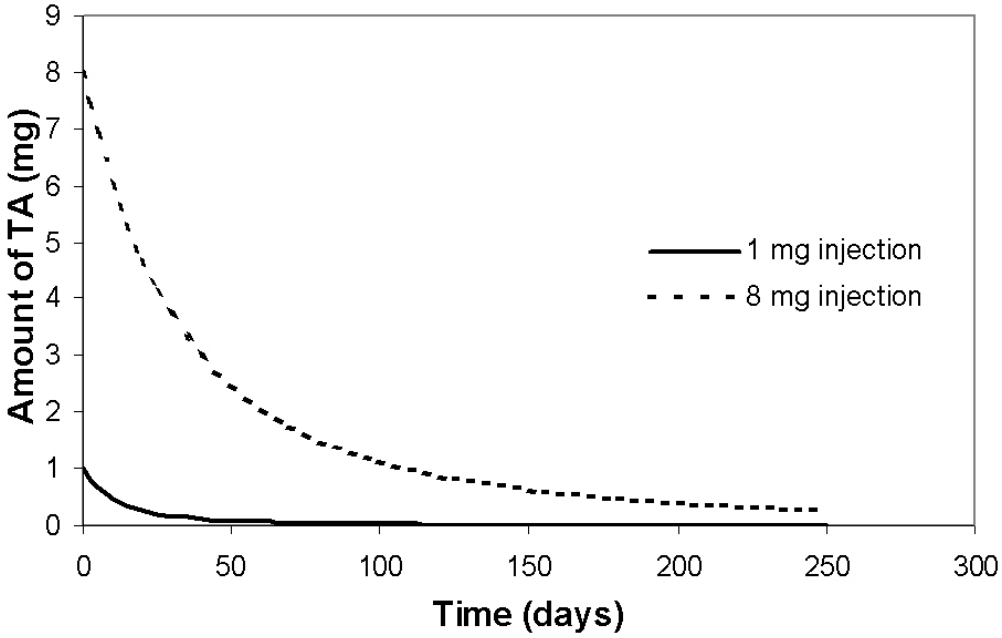

Figure 6-4. Estimated amount of TA in the vitreous in 1 mg injection (solid line) and 8 mg injection (dotted line).

Figure 6-5. The relationship between the calculated half-life of TA in the vitreous and the injection amount.

6.5 Discussion

Diseases affecting the posterior segment of the eye, age-related macular degeneration (AMD) and diabetic retinopathy, are the main causes of blindness in developed countries. Although topical administration such as eye drop accounts for nearly 90% of the currently accessible market formulations for drug application [15], less than 5% of topically applied therapeutic agent passes through the cornea because of tear flow drainage, dilution by blinking, corneal diffusion resistance, and aqueous humor washout [15, 16, 44]. Systemic administration of biologically active agents often fails to deliver to some target sites at therapeutic levels because of the blood-retina barrier and the blood-aqueous barrier [1]. For effective treatment, large systemic doses are often required, which can cause systemic adverse effects. Therefore, intravitreal injection is a current method being used to deliver drugs directly to the posterior segment of the eye [70, 71]. However, one of disadvantages of intravitreal injection is rapid elimination from the vitreous [46]. Schindler RH et al. [132] reported that cortisone was washed out of the eye within approximately 24 hours after a single intravitreal injection. To prolong the duration of intravitreal injected triamcinolone acetonide, the use of the crystalline form of triamcinolone acetonide, which formed a depot in the vitreous (Figure 6-1), was suggested [135]. When crystalline triamcinolone acetonide was injected into the vitreous, it condensed into a small region to form a depot because of rapid diffusion of the saline vehicle from the suspension and lipophilicity of triamcinolone acetonide [132]. Jonas JB [136] detected triamcinolone acetonide in the human aqueous humor up to 6 months after 25 mg intravitreal instillation. Scholes GN et al. [133]

determined the half-life of 0.4 mg intravitreal injected triamcinolone acetonide to be 1.6 days in rabbit eyes and detected 66 ± 19 μg in the rabbit vitreous with HPLC 13 days post injection. The authors clinically observed triamcinolone acetonide depot in the vitreous by indirect ophthalmoscopy up to average 23.3 days after 0.4 mg intravitreal injection. Following intravitreal injection of 0.5 mg triamcinolone acetonide [132], 6.5 days average retention of the drug in eyes that underwent a combined vitrectomy and lensectomy, 16.8 days average retention in eyes that underwent vitrectomy only, and 41 days average retention in normal rabbit eyes was reported, which meant clearance of triamcinolone acetonide from the vitreous depends on ocular condition. In our experiment, we could clearly observe a white triamcinolone acetonide depot in all of isolated frozen vitreous (n=4) 56 days post 4-mg triamcinolone acetonide injection and 131 days post 16-mg triamcinolone acetonide injection; however, in two of four isolated frozen vitreous 119 days post 4-mg injection and two of four isolated frozen vitreous 238 days post 16-mg injection. All of triamcinolone acetonide injected rabbit eyes were found to contain HPLC detectable amount in the vitreous by 119 days post 4-mg injection and 238 days post 16-mg injection.

It is important to know for clinical use how long after a single intravitreal injection the concentration of triamcinolone acetonide in the vitreous remains above the therapeutic index. In our experimental data analysis, the elimination rate of triamcinolone acetonide (*dM/dt*) was found to depend on the amount of triamcinolone acetonide in the vitreous raised to the power, n=1.41 ($M^{1.41}$) because triamcinolone acetonide did not distribute homogenously in the vitreous but formed a depot. Since

we could not use our previous ocular pharmacokinetic studies in rabbit [41] to calculate half-life of each injection, a unique pharmacokinetic analysis was developed to characterize the clearance from the vitreous of depot formulation for steroid types of drugs. Assuming that all of administered drug will be eliminated after five half-lives, it was estimated that 4 mg or 16 mg intravitreal injected triamcinolone acetonide should be for 93 days or 188 days, respectively. To keep within detectable amount of triamcinolone acetonide for one year with two times injections in rabbit eyes, doses of 16 mg triamcinolone acetonide are required.

Determination of the elimination pathways for intravitreal injected drugs is important. Intravitreal injected ocular therapeutics are thought to be eliminated either across the retinal surface or via drainage out of the anterior chamber depending on solubility [46]. Most intravitreal injected hydrophilic agents or hydrophobic agents were concluded to be eliminated via the annular gap between the lens and the ciliary body or through the retina-choroid-scleral membrane, respectively [40]. In our experiment, a triamcinolone acetonide depot was observed to position in the posterior vitreous near the retina and no triamcinolone acetonide was detected in the harvested aqueous humor. This suggests that the major route of elimination for traimcinolone acetonide is across the retina barrier in the rabbit eye. In a previous study [134], triamcinolone acetonide concentrations in human aqueous humor of 2.2 – 7.2 μg/ml were measured following 4-mg intravitreal injection. The authors concluded intravitreal injected traimcinolone acetonide was eliminated mainly via the anterior route. These discrepancies are related to several factors. There are a number of differences in the anatomy and physiology of the rabbit eye. The choroidal vessel

permeability and flow is different in rabbits compared with primates [82, 101, 102]. For example, the choroidal flow is 16% higher in rabbits compared with monkeys, which may increase elimination of triamcinolone acetonide across the retina in rabbit [103, 104]. The previous study [134] has been done in the eyes of elderly patient whose vitreous is often liquefied. Liquefied vitreous humor circulates by convection and the ocular globe movement and helps dissolve the triamcinolone acetonide crystal faster and disperse more easily into the anterior chamber than in normal eyes. However, considering the high partition coefficient of lipophilic agents into the cell membranes of the retina and the very low aqueous solubility of triamcinolone acetonide, it is doubtful that a major elimination of intravitreal injection triamcinolone acetonide is via the anterior route.

The elimination of intravitreal triamcinolone acetonide can be considered to involve three steps; dissolution from a depot into the vitreous, diffusion in the vitreous, and elimination across the retina. The rate of clearance across the retina is assumed to be proportional to the vitreal concentration of dissolved drug at interface with the retina. The elimination rate constant for this step is, $k_R = P \times A \times V^{-1}$ in which V = 1.5 ml is the volume of the rabbit vitreous [41], A is the superficial surface area of the vitreous-retina interface, 1.22 cm^2 [120] and P is apparent permeability of the blood-retinal barrier corresponding to this area. Friedrich has estimated the range of permeability value to be of the order of 10^{-7} to 10^{-4} cm^2/sec [47]. The lower limit corresponds to hydrophilic solutes that are poorly permeable. As a lipophilic solute, triamcinolone acetonide would likely be associated with a high permeability value. The upper limit on the rate constant is $k_R = (1.0 \times 10^{-4}$ cm/sec$) \times (1.22$ $cm^2) \times (1.5$ $cm^3)^{-1}$

= 7.03 [day^{-1}]. The diffusion rate of triamcinolone acetonide in the vitreous can be characterized by the following parameter, $k_D = D/r^2$, where D is diffusion coefficient in the vitreous and r is the radius of the rabbit vitreous. For triamcinolone acetonide with a molecular weight of 434.5 Da, the diffusion coefficient is estimated to be 5.6×10^{-6} [cm^2/sec] [47]. For r = 0.72 cm [120], the diffusion rate constant of triamcinolone acetonide in the vitreous, k_D, was calculated to be 0.9 [day^{-1}]. The dissolution rate of triamcinolone acetonide from a depot into the vitreous, k_S can be calculated from the following equation:

$$\frac{1}{k} = \frac{1}{k_S} + \frac{1}{k_D} + \frac{1}{k_R}$$

where, k represents the overall rate constant for elimination from the eye. In the case of 4 mg or 16 mg triamcinolone acetonide intravitreal injection, dissolution rate into the vitreous, k_D, was calculated to be 0.0253 or 0.0070 [day^{-1}]. In comparison to the rate constant for diffusion in the vitreous and permeation across the retina, the dissolution from a depot into the vitreous was found to be the slowest step in the elimination of triamcinolone acetonide from the eye. The overall rate of elimination was found to depend upon the amount of triamcinolone acetonide injected. This result suggests that the rate of elimination is independent of the vitreous volume. This conclusion is supported by the previous study [134] who measured the half-life of 4-mg intravitreal injected triamcinolone acetonide in the human vitreous to be 18.6 days, which is comparable to our result of 18.6 days.

6.6 Conclusions

The empirical pharmacokinetic equations were developed and used to analyze triamcinolone acetonide intravitreal injection animal experimental data. It was determined that animal experimental data about intravitreally injected triamcinolone acetonide forming a depot in the vitreous can be applied to human cases with ignorable error because the elimination limiting step of triamcinolone acetonide from the vitreous is the dissolution from the depot into the vitreous. 16 mg intravitreal injection of triamcinolone acetonide was found to be required to keep the therapeutic concentration in the vitreous with two times intravitreal injection a year in human cases.

CHAPTER 7. Summary and recommendations

7.1 Summary

The movement of drug surrogates, H-110 (small size and lipophilic) and Gd-DTPA (small size and hydrophilic) released from sustained release implants in the eye was studied with fluorescent and MRI.

Using the fluorescent technology, the movement of H-110 in the tissue level could be analyzed only qualitatively. On the other hand, we could analyze the movement of MRI contrast agent, Gd-DTPA in the vitreous quantitatively by referring to concentration calibration standards as well as qualitatively. However, we could not accurately determine the distribution of Gd-DTPA within the finer structure of some tissues such as the retina because of the MRI detection limitation and resolution with the current MR setup.

In the intravitreal H-110 study, H-110 released from a HPMC based implant reached the outer plexiform cell layer by 3 hour post implantation and the subretinal region 1 day post implantation most likely by diffusion. In the subconjunctival H-110 study, some H-110 released from an implant could be detected at the subretinal space 3 day post implantation. It is felt that H-110 can be eliminated by uptake into the choroidal blood flow. H-110 was observed to distribute circumferentially around the sclera, the conjunctiva, and then to the cornea. From this study, we conclude that lipophilic and low molecular weight therapeutics (H-110) can be delivered more efficiently from the vitreous into the subretinal space than from the subconjunctival space into the subretinal space because of enhanced retina

transport of lipophilic material and because of elimination by the choroidal blood flow.

In the *in vivo* MRI experiment with a subconjunctival implant, some Gd-DTPA could be detected in the aqueous humor and the anterior vitreous. A large portion of the released Gd-DTPA is thought to be eliminated through the episcleral and conjunctival venous blood flow, conjunctival lymphatic drainage, choroidal blood flow, and the episcleral veins as reported in literatures. A high concentration of Gd-DTPA was detected in the buccal lymph node in our study (Figure 3-7). However, we could not detect Gd-DTPA in the choroid because of resolution limits and the rapid dilution of Gd-DTPA through the choroid. According to our three-compartment pharmacokinetic model, Eliminating Gd-DTPA from the subconjunctival space was 100 times faster than transferring into the vitreous or the aqueous humor.

In the *in vivo* intravitreal MRI experiment, we found that a concentration gradient was established from the back of the lens to the posterior retina. In contrast, in the intravitreal *ex vivo* MRI experiment, a concentration gradient did not exist within the vitreous. We believe that this is due to the diffusion of Gd-DTPA across the retina and then elimination by choroidal blood flow in the *in vivo* case, but is not present in the *ex vivo* case. The permeability of Gd-DTPA through the retina-choroid-sclera membrane was calculated to be 1.0×10^{-5} cm/sec based on the MRI experimental data and the computer simulation data. The diffusion coefficient of Gd-DTPA in the vitreous was determined to be 2.8×10^{-6} cm^2/sec, which is in agreement with the previous studies.

In the intravitreal MRI two-compartment pharmacokinetic study, released Gd-DTPA was eliminated 10 times faster across the retina than through the aqueous humor flow. Because of the elimination mechanism of Gd-DTPA from the vitreous, which results in a concentration gradient from the near implant region to the more distal region in the vitreous at steady state, implantation position in the vitreous in controlling the concentration of therapeutics at the target site is of prime importance.

From the H-110 fluorescent experiment and the Gd-DTPA experiment, we found that delivering both small size hydrophilic and small size lipophilic agents from the subconjunctival space into the subretinal space was less efficient than delivering from the vitreous to the subretinal space because of several barrier mechanisms.

A pharmacokinetic study was performed to calculate the half-life of a preservative-free formulation of triamcinolone acetonide (TAC-PF) in the New Zealand White rabbit to determine an injection schedule in human clinical trials. In indirect ophthalmoscopic study, it was observed that intravitreally injected triamcinolone acetonide did not disperse in the vitreous homogeneously, but formed a depot. Several previous compartmental pharmacokinetic analyses have been developed with an assumption that an applied agent distributes homogenously within the vitreous compartment. Our pharmacokinetics was unique in that it accounted for the depot effect. In the animal studies, we found the half-lives of 4 mg and 16 mg intravitreal injections to be 18.6 days and 37.6 days, respectively. With this animal experimental data and our mathematical analysis for microparticulated steroid

therapeutics, the half-lives of 1 mg and 8 mg intravitreal injections were estimated to be 9.2 days and 26.5 days, respectively. With the above calculated half-life data, the relationshiop between amount of TAC-PF injection and half-life in the vitreous was found to follow the following relationship:

$$(\text{Half-life[days]}) = 9.2 \times (\text{Amount of injected TAC-PF [mg]})^{0.508}$$

In this study, we determined that the rate-limiting step for elimination of triamcinolone acetonide was dissolution from the depot into the vitreous and not the diffusion in the vitreous or elimination across the retina.

7.2 Recommendations for future research

In this study, we determined the movement of small size drug surrogates, H-110 (lipophilic) and Gd-DTPA (hydrophilic), delivered by sustained release implants in the eye. Several macromolecular anti-angiogenic agents such as vascular endothelial growth factor (VEGF) receptor chimeric protein, tissue inhibitor of metalloproteinase (TIMP)-1 (28 kDa), TIMP-2 (24 kDa), pigment epithelium-derived factor (50 kDa) have been tested in the clinics for treating ocular disorders of the posterior segment of the eye [63]. However, more information about the movement of macromolecular compounds in the eye is needed since it is important to develop unique delivery method and to control the concentration at the target site. Because of the improvement of labeling technology, Gd-DTPA can be conjugated to macromolecular materials such as lysozyme (14.3 kDa), trypsinogen (24 kDa), ovalbumin (45 kDa), and bovine serum albumin (67 kDa). The movement of macromolecular compounds has been studied in cartilage [137]. IgG antibody was

conjugated with Gd or Mn and the relxation properties were tested to confirm that the conjugated compounds were reasonable for MRI study [138]. To my knowledge, no MRI study has yet been done in the eye with macromolecules labeled with paramagnetic metal. Investigation to understand the movement of macromolecules released from sustained release implants in the eye using the MRI is one recommendation for future work. By comparing the movement of small size materials with macromolecules, the effect of molecular size on the movement of agents in the eye will be confirmed.

Our mathematical eye model consisted of only the lens, the vitreous, and the posterior segment of the eye (the retina-choroid-sclera membrane). In this study, the mathematical model did not include certain anterior segments of the eye such as the posterior segment of the aqueous humor, the anterior segment of the aqueous humor, and the cornea. In addition, the retina, the choroid, and the sclera were simplified in the current model into only one lumped region because of limited information about each membrane. Future work can be aimed at improving and extending the mathematical model to add an anterior chamber and to separate the posterior region into sclera, choroid, and retina. Such an improved model will allow for simulations of subconjunctival delivery of drugs with prediction of drug concentrations in each subconjunctival tissue.

Nowadays, both microparticles and nanoparticles have been intensively studied to deliver ocular therapeutics for an extended time period without complicated surgery. A previous study represented the movement of flucorescent conjugated nanoparticles injected intravitreally in the eye, rather than drugs released

from the particles [139]. Average particle size of our TAC-PF was 4 μm (not reported in this dissertation). However, triamcinolone acetonide dissolved, not released into the vitreous. In addition, the TAC-PF formed a depot in the vitreous, not dispersed. It is difficult to apply the pharmacokinetics of TAC-PF to biodegradable microparticles or nanoparticles cases. To determine the movement of microparticles or nanoparticles injected intravitreally or subconjunctivally, further pharmacokinetic studies are recommended as possible future work.

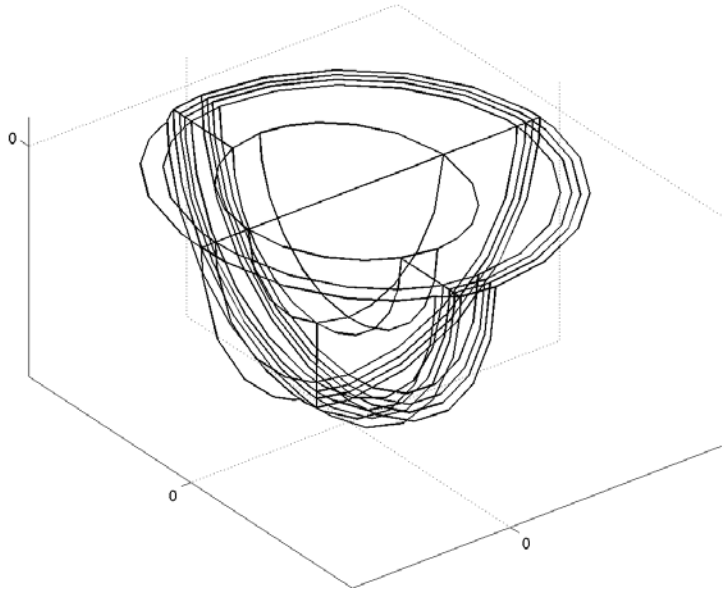

(A)

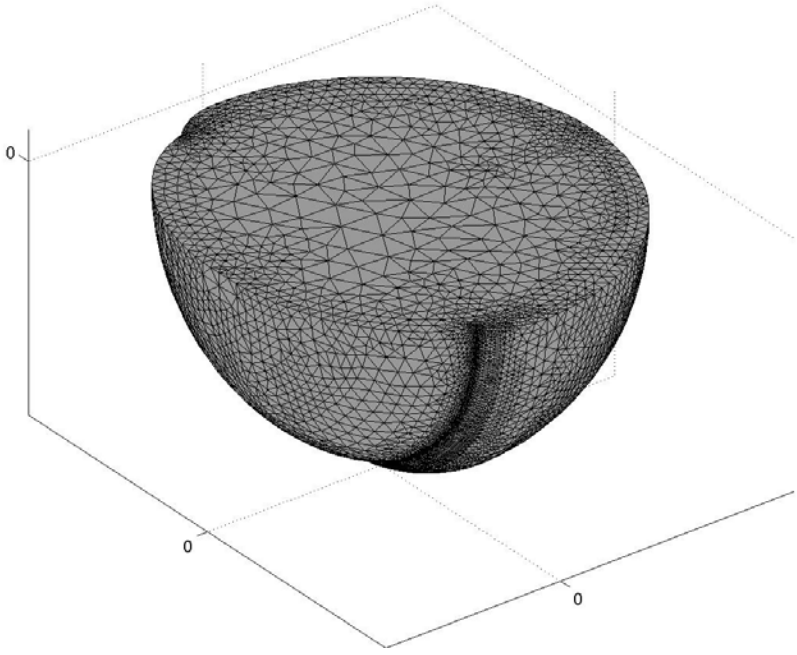

(B)

Figure 7-1. Complicated mathematical eye model for future works.

APPENDICES

[APPENDIX I]

With the assumption that the limiting step for clearance of triamcinolone acetonide from a depot into the vitreous is dissolution, the elimination rate can be expressed with the following equation:

$$r = \frac{dM}{dt} = -P \times A \times C_0 \qquad \text{(I-1)}$$

where, P, A, and C_0 denote the permeability, the surface area of a depot, and the concentration of dissolved triamcinolone acetonide in the aqueous phase within the depot, respectively.

In addition, the surface area of depot is assumed to be proportional to the amount

of triamcinolone acetonide in a depot:

$$A = K \times M^n \qquad \text{(I-2)}$$

where, K is a proportional constant. In sheet geometry and a spherical geometry, n must be 0 and 2/3, respectively.

Substituting (I-2) into (I-1) gives for the

4-mg injection

$$r_4 = \frac{dM}{dt} = -k_4 \times M^n \quad \text{where } k_4 = P \times C_0 \times K_4 \qquad \text{(I-3)}$$

and for the 16-mg injection

$$r_{16} = \frac{dM}{dt} = -k_{16} \times M^n \quad \text{where } k_{16} = P \times C_0 \times K_{16} \qquad \text{(I-4)}$$

Assuming the area coefficients, in turn, depend upon the initial mass of the depot

to a power m, $K=L\times M_i^m$, leads to

$$k_4 = P \times C_0 \times L \times M_4^m \quad \text{(I-5)}$$

$$k_{16} = P \times C_0 \times L \times M_{16}^m \quad \text{(I-6)}$$

Taking the rates of (I-5) to (I-6) gives,

$$\frac{k_4}{k_{16}} = \left(\frac{M_4}{M_{16}} \right)^m \quad \text{(I-7)}$$

in which M_4 = 4 mg and M_{16} = 16 mg.

[APPENDIX II]

The elimination of triamcinolone acetonide from the vitreous is governed by the following equation:

$$\frac{dM}{dt} = -k \times M^{n} \qquad \text{(II-1)}$$

By multiplying both sides with $M^{-n} \times dt$, the equation (1) is written by the following equation, again.

$$\frac{1}{M^{n}} dM = -k \times dt \qquad \text{(II-2)}$$

To calculate half-life of triamcinolone acetonide in the vitreous, the both sides of Equation (II-2) was integrated.

$$\int_{M_0}^{\frac{M_0}{2}} \frac{1}{M^{n}} dM = -k \times \int_{0}^{t_{1/2}} dt \qquad \text{(II-3)}$$

where, M and M_0 represent amount at a specific time and an initial time, respectively. $t_{1/2}$ means the time when amount of injected triamcinolone acetonide becomes to be half.

Finally, Equation (II-3) can be simplified to be as follows:

$$t_{1/2} = \frac{1}{k} \times \left(\frac{1}{n-1} \right) \times M_0^{\,1-n} \times \left[\left(\frac{1}{2} \right)^{1-n} - 1 \right] \qquad \text{(II-4)}$$

Equation (II-4) shows that half-life depends on both the elimination rate constant

and injected amount.

BIBLIOGRAPHY

1. Duvvuri, S., S. Majumdar, and A.K. Mitra, *Drug delivery to the retina: challenges and opportunities.* Expert Opin Biol Ther, 2003. **3**(1): p. 45-56.

2. 2003, National Eye Institute.

3. Boubriak, O.A., J.P. Urban, S. Akhtar, K.M. Meek, A.J. Bron, *The effect of hydration and matrix composition on solute diffusion in rabbit sclera.* Exp Eye Res, 2000. **71**(5): p. 503-14.

4. Friedrich, S., Y.L. Cheng, and B. Saville, *Finite element modeling of drug distribution in the vitreous humor of the rabbit eye.* Ann Biomed Eng, 1997. **25**(2): p. 303-14.

5. Maurice, D.M., *Flow of water between aqueous and vitreous compartments in the rabbit eye.* Am J Physiol, 1987. **252**(1 Pt 2): p. F104-8.

6. Hughes, A., *A schematic eye for the rabbit.* Vision Res, 1972. **12**(1): p. 123-38.

7. Clark, A.F. and T. Yorio, *Ophthalmic drug discovery.* Nat Rev Drug Discov, 2003. **2**(6): p. 448-59.

8. Adamis, A.P., D.T. Shima , M.J. Tolentino, E.S. Gragoudas, N. Ferrara, J. Folkman, P.A. D'Amore, J.W. Miller, *Inhibition of vascular endothelial growth factor prevents retinal ischemia-associated iris neovascularization in a nonhuman primate.* Arch Ophthalmol, 1996. **114**(1): p. 66-71.

9. Danis, R.P., T.A. Ciulla, L.M. Pratt, W. Anliker, *Intravitreal triamcinolone acetonide in exudative age-related macular degeneration.* Retina, 2000. **20**(3): p. 244-50.

10. Jaffe, G.J., C.H. Yang, H. Guo, J.P. Denny, C. Lima, P. Ashton, *Safety and pharmacokinetics of an intraocular fluocinolone acetonide sustained delivery device.* Invest Ophthalmol Vis Sci, 2000. **41**(11): p. 3569-75.

11. Keam, S.J., L.J. Scott, and M.P. Curran, *Verteporfin : a review of its use in the management of subfoveal choroidal neovascularisation.* Drugs, 2003. **63**(22): p. 2521-54.

12. Miyamoto, H., Y. Ogura, M. Hashizoe, N. Kunou, Y. Honda, and Y. Ikada, *Biodegradable scleral implant for intravitreal controlled release of fluconazole.* Curr Eye Res, 1997. **16**(9): p. 930-5.

13. *Ganciclovir implants (Vitrasert).* Treat Rev, 1996(21): p. 10.

14. Hooper, C.Y. and R.H. Guymer, *New treatments in age-related macular degeneration.* Clin Experiment Ophthalmol, 2003. **31**(5): p. 376-91.

15. Bourlais, C.L., L. Acar, H. Zia, P.A. Sado, T. Needham, and R. Leverge, *Ophthalmic drug delivery systems--recent advances.* Prog Retin Eye Res, 1998. **17**(1): p. 33-58.

16. Geroski, D.H. and H.F. Edelhauser, *Drug delivery for posterior segment eye disease.* Invest Ophthalmol Vis Sci, 2000. **41**(5): p. 961-4.

17. *Anti-vascular endothelial growth factor therapy for subfoveal choroidal neovascularization secondary to age-related macular degeneration: phase II study results.* Ophthalmology, 2003. **110**(5): p. 979-86.

18. Gillies, M.C., J.M. Simpson, W. Luo, P. Penfold, A.B. Hunyor, W. Chua, P. Mitchell, and F. Billson, *A randomized clinical trial of a single dose of*

intravitreal triamcinolone acetonide for neovascular age-related macular degeneration: one-year results. Arch Ophthalmol, 2003. **121**(5): p. 667-73.

19. Jonas, J.B., I. Kreissig, A. Sofker, and R.F. Degenring, *Intravitreal injection of triamcinolone for diffuse diabetic macular edema.* Arch Ophthalmol, 2003. **121**(1): p. 57-61.

20. Anand, R., S.D. Nightingale, R.H. Fish, T.J. Smith, and P. Ashton, *Control of cytomegalovirus retinitis using sustained release of intraocular ganciclovir.* Arch Ophthalmol, 1993. **111**(2): p. 223-7.

21. Musch, D.C., D.F. Martin, J.F. Gordon, M.D. Davis, and B.D. Kuppermann, *Treatment of cytomegalovirus retinitis with a sustained-release ganciclovir implant. The Ganciclovir Implant Study Group.* N Engl J Med, 1997. **337**(2): p. 83-90.

22. Kurz, D. and T.A. Ciulla, *Novel approaches for retinal drug delivery.* Ophthalmol Clin North Am, 2002. **15**(3): p. 405-10.

23. Lim, J.I., R.A. Wolitz, A.H. Dowling, H.R. Bloom, A.R. Irvine, and D.M. Schwartz, *Visual and anatomic outcomes associated with posterior segment complications after ganciclovir implant procedures in patients with AIDS and cytomegalovirus retinitis.* Am J Ophthalmol, 1999. **127**(3): p. 288-93.

24. Shane, T.S. and D.F. Martin, *Endophthalmitis after ganciclovir implant in patients with AIDS and cytomegalovirus retinitis.* Am J Ophthalmol, 2003. **136**(4): p. 649-54.

25. Ambati, J., C.S. Canakis, J.W. Miller, E.S. Gragoudas, A. Edwards, D.J. Weissgold, I. Kim, F.C. Delori, and A.P. Adamis, *Diffusion of high molecular*

weight compounds through sclera. Invest Ophthalmol Vis Sci, 2000. **41**(5): p. 1181-5.

26. Prausnitz, M.R. and J.S. Noonan, *Permeability of cornea, sclera, and conjunctiva: a literature analysis for drug delivery to the eye.* J Pharm Sci, 1998. **87**(12): p. 1479-88.

27. Ambati, J., E.S. Gragoudas, J.W. Miller, T.T. You, K. Miyamoto, F.C. Delori, and A.P. Adamis, *Transscleral delivery of bioactive protein to the choroid and retina.* Invest Ophthalmol Vis Sci, 2000. **41**(5): p. 1186-91.

28. Weijtens, O., E.J. Feron, R.C. Schoemaker, A.F. Cohen, E.G. Lentjes, F.P. Romijn, and J.C. van Meurs, *High concentration of dexamethasone in aqueous and vitreous after subconjunctival injection.* Am J Ophthalmol, 1999. **128**(2): p. 192-7.

29. Simpson, A.E., J.A. Gilbert, D.E. Rudnick, D.H. Geroski, T.M Aaberg Jr, and H.F. Edelhauser, *Transscleral diffusion of carboplatin: an in vitro and in vivo study.* Arch Ophthalmol, 2002. **120**(8): p. 1069-74.

30. Yanagi, Y., Y. Tamaki, R. Obata, K. Muranaka, N. Homma, H. Matsuoka, and H. Mano, *Subconjunctival administration of bucillamine suppresses choroidal neovascularization in rat.* Invest Ophthalmol Vis Sci, 2002. **43**(11): p. 3495-9.

31. Gomori, J.M., R.I. Grossman, J.A. Shields, J.J. Augsburger, P.M. Joseph, and D. DeSimeone, *Ocular MR imaging and spectroscopy: an ex vivo study.* Radiology, 1986. **160**(1): p. 201-5.

32. Moseley, I., M. Brant-Zawadski, and C. Mills, *Nuclear magnetic resonance imaging of the orbit.* Br J Ophthalmol, 1983. **67**(6): p. 333-42.

33. Sassani, J.W. and M.D. Osbakken, *Anatomic features of the eye disclosed with nuclear magnetic resonance imaging.* Arch Ophthalmol, 1984. **102**(4): p. 541-6.

34. Cheng, H.M., K.K. Kwong, S. Dixon, G. Tanaka, J. Xiong, G. Moore, and D.A. Chesler, *Water movement in the rabbit eye.* Exp Eye Res, 1991. **52**(3): p. 337-9.

35. Cheng, H.M., K.K. Kwong, J. Xiong, and B.T. Woods, *Visualization of water movement in the living rabbit eye.* Graefes Arch Clin Exp Ophthalmol, 1992. **230**(1): p. 62-5.

36. Cheng, H.M., K.K. Kwong, J. Xiong, and C. Chang, *GdDTPA-enhanced magnetic resonance imaging of the aqueous flow in the rabbit eye.* Magn Reson Med, 1991. **17**(1): p. 237-43.

37. Berkowitz, B.A., Y. Sato, C.A. Wilson, and E. de Juan, *Blood-retinal barrier breakdown investigated by real-time magnetic resonance imaging after gadolinium-diethylenetriaminepentaacetic acid injection.* Invest Ophthalmol Vis Sci, 1991. **32**(11): p. 2854-60.

38. Wilson, C.A., J.L. Fleckenstein, B.A. Berkowitz, and M.E. Green, *Preretinal neovascularization in diabetic retinopathy: a preliminary investigation using contrast-enhanced magnetic resonance imaging.* J Diabetes Complications, 1992. **6**(4): p. 223-9.

39. Alikacem, N., T. Yoshizawa, K.D. Nelson, and C.A. Wilson, *Quantitative MR imaging study of intravitreal sustained release of VEGF in rabbits.* Invest Ophthalmol Vis Sci, 2000. **41**(6): p. 1561-9.

40. Worakul, N. and J.R. Robinson, *Review: Ocular pharmacokinetics/Pharmacodynamics.* Eur J Pharm Biopharm, 1997. **44**: p. 71 - 83.

41. Velez, G., P. Yuan, C. Sung, G. Tansey, G.F. Reed, C.C. Chan, R.B. Nussenblatt, and M.R. Robinson, *Pharmacokinetics and Toxicity of Intravitreal Chemotherapy for Primary Intraocular Lymphoma.* Arch Ophthalmol, 2001. **119**: p. 1518 - 1524.

42. Macha, S. and A.K. Mitra, *Ocular Pharmacokinetics in Rabbits using a Novel Dual Probe Microdyalysis Technique.* Exp Eye Res, 2001. **72**: p. 289 - 299.

43. A.J. Atkinson, Jr., C.E. Daniels, R.L. Dedrick, C.V. Grudzinskas, S.P. Markey, *Principles of Clinical Pharmacology*. 2001, London: Academic Press.

44. Tojo, K. and A. Isowaki, *Pharmacokinetic model for in vivo/in vitro correlation of intravitreal drug delivery.* Adv Drug Deliv Rev, 2001. **52**(1): p. 17-24.

45. Tojo, K., K. Nakagawa, Y. Morita, and A. Ohtori, *A pharmacokinetic model of intravitreal delivery of ganciclovir.* Eur J Pharm Biopharm, 1999. **47**(2): p. 99-104.

46. Tojo, K.J. and A. Ohtori, *Pharmacokinetic model of intravitreal drug injection.* Math Biosci, 1994. **123**(1): p. 59-75.

47. Friedrich, S., B. Saville, and Y.L. Cheng, *Drug distribution in the vitreous humor of the human eye: the effects of aphakia and changes in retinal permeability and vitreous diffusivity.* J Ocul Pharmacol Ther, 1997. **13**(5): p. 445-59.

48. Missel, P.J., *Hydraulic flow and vascular clearance influences on intravitreal drug delivery.* Pharm Res, 2002. **19**(11): p. 1636-47.

49. Missel, P.J., *Finite and infinitesimal representations of the vasculature: ocular drug clearance by vascular and hydraulic effects.* Ann Biomed Eng, 2002. **30**(9): p. 1128-39.

50. Wheeler, G.D., *Ruboxistaurin (Eli Lilly).* IDrugs, 2003. **6**(2): p. 159-63.

51. Saishin, Y., Y. Saishin, K. Takahashi, M.S. Seo, M. Melia, and P.A. Campochiaro, *The kinase inhibitor PKC412 suppresses epiretinal membrane formation and retinal detachment in mice with proliferative retinopathies.* Invest Ophthalmol Vis Sci, 2003. **44**(8): p. 3656-62.

52. *Preclinical and phase 1A clinical evaluation of an anti-VEGF pegylated aptamer (EYE001) for the treatment of exudative age-related macular degeneration.* Retina, 2002. **22**(2): p. 143-52.

53. *Anecortave acetate as monotherapy for treatment of subfoveal neovascularization in age-related macular degeneration: twelve-month clinical outcomes.* Ophthalmology, 2003. **110**(12): p. 2372-2383.

54. Jaffe, G.J., J. Ben-Nun, H. Guo, J.P. Dunn, and P. Ashton, *Fluocinolone acetonide sustained drug delivery device to treat severe uveitis.* Ophthalmology, 2000. **107**(11): p. 2024-33.

55. Bernatchez, S.F., A. Merkli, T.L. Minh, C. Tabatabay, J.M. Anderson, and R. Gurny., *Biocompatibility of a new semisolid bioerodible poly(ortho ester) intended for the ocular delivery of 5-fluorouracil.* J Biomed Mater Res, 1994. **28**(9): p. 1037-46.

56. Kim, H., R.J. D'Amato, R.J. Lutz, P. Yuan, J. Baffi, J.D. Wolfe, G. Byrnes, M.R. Robinson, and K.G. Csaky, *A subconjunctival Implant for Delivery of Cytochalasin E in a Model of Choroidal Neovascularization: A pilot study.* Invest Ophthalmol Vis Sci, 2003. **44**: p. E-Abstract 4429.

57. Kunou, N., Y. Ogura, T. Yasukawa, H. Kimura, H. Miyamoto, Y. Honda, and Y. Ikada, *Long-term sustained release of ganciclovir from biodegradable scleral implant for the treatment of cytomegalovirus retinitis.* J Control Release, 2000. **68**(2): p. 263-71.

58. Kunou, N., Y. Ogura, Y. Honda, S.H. Hyon, and Y. Ikada, *Biodegradable scleral implant for controlled intraocular delivery of betamethasone phosphate.* J Biomed Mater Res, 2000. **51**(4): p. 635-41.

59. Avitabile, T., F. Marano, F. Castiglione, C. Bucolo, M. Cro, L. Ambrosio, C. Ferrauto, and A. Reibaldi, *Biocompatibility and biodegradation of intravitreal hyaluronan implants in rabbits.* Biomaterials, 2001. **22**(3): p. 195-200.

60. Kompella, U.B., N. Bandi, and S.P. Ayalasomayajula, *Subconjunctival nano- and microparticles sustain retinal delivery of budesonide, a corticosteroid capable of inhibiting VEGF expression.* Invest Ophthalmol Vis Sci, 2003. **44**(3): p. 1192-201.

61. Zhou, T., H. Lewis, R.E. Foster, and S.P. Schwendeman, *Development of a multiple-drug delivery implant for intraocular management of proliferative vitreoretinopathy.* J Control Release, 1998. **55**(2-3): p. 281-95.

62. Araie, M. and D.M. Maurice, *The loss of fluorescein, fluorescein glucuronide and fluorescein isothiocyanate dextran from the vitreous by the anterior and retinal pathways.* Exp Eye Res, 1991. **52**(1): p. 27-39.

63. Kim, T.W., J.D. Lindsey, M. Aihara, T.L. Anthony, and R.N. Weinreb, *Intraocular distribution of 70-kDa dextran after subconjunctival injection in mice.* Invest Ophthalmol Vis Sci, 2002. **43**(6): p. 1809-16.

64. Lindsey, J.D. and R.N. Weinreb, *Identification of the mouse uveoscleral outflow pathway using fluorescent dextran.* Invest Ophthalmol Vis Sci, 2002. **43**(7): p. 2201-5.

65. Robinson, M.R., J. Baffi, P. Yuan, C. Sung, G. Byrnes, T.A. Cox, and K.G. Csaky, *Safety and pharmacokinetics of intravitreal 2-methoxyestradiol implants in normal rabbit and pharmacodynamics in a rat model of choroidal neovascularization.* Exp Eye Res, 2002. **74**(2): p. 309-17.

66. Ciulla, T.A., M.H. Criswell, R.P. Danis, M. Fronheiser, P. Yuan, T.A. Cox, K.G. Csaky, and M.R. Robinson, *Choroidal neovascular membrane inhibition in a laser treated rat model with intraocular sustained release triamcinolone acetonide microimplants.* Br J Ophthalmol, 2003. **87**(8): p. 1032-7.

67. Penfold, P.L., J.F. Gyory, A.B. Hunyor, and F.A. Billson, *Exudative macular degeneration and intravitreal triamcinolone. A pilot study.* Aust N Z J Ophthalmol, 1995. **23**(4): p. 293-8.

68. Challa, J.K., M.C. Gillies, P.L. Penfold, J.F. Gyory, A.B. Hunyor, and F.A. Billson, *Exudative macular degeneration and intravitreal triamcinolone: 18 month follow up.* Aust N Z J Ophthalmol, 1998. **26**(4): p. 277-81.

69. Ranson, N.T., R.P. Danis, T.A. Ciulla, and L. Pratt, *Intravitreal triamcinolone in subfoveal recurrence of choroidal neovascularisation after laser treatment in macular degeneration.* Br J Ophthalmol, 2002. **86**(5): p. 527-9.

70. Martidis, A., J.S. Duker, P.B. Greenberg, A.H. Rogers, C.A. Puliafito, E. Reichel, and C. Baumal, *Intravitreal triamcinolone for refractory diabetic macular edema.* Ophthalmology, 2002. **109**(5): p. 920-7.

71. Jonas, J.B., I. Kreissig, and R.F. Degenring, *Intravitreal triamcinolone acetonide as treatment of macular edema in central retinal vein occlusion.* Graefes Arch Clin Exp Ophthalmol, 2002. **240**(9): p. 782-3.

72. Ip, M.S. and K.S. Kumar, *Intravitreous triamcinolone acetonide as treatment for macular edema from central retinal vein occlusion.* Arch Ophthalmol, 2002. **120**(9): p. 1217-9.

73. Greenberg, P.B., A. Martidis, A.H. Rogers, J.S. Duker, and E. Reichel, *Intravitreal triamcinolone acetonide for macular oedema due to central retinal vein occlusion.* Br J Ophthalmol, 2002. **86**(2): p. 247-8.

74. Huang, X. and C.S. Brazel, *On the importance and mechanisms of burst release in matrix-controlled drug delivery systems.* J Control Release, 2001. **73**(2-3): p. 121-36.

75. Cunha-Vaz, J.G. and D.M. Maurice, *The active transport of fluorescein by the retinal vessels and the retina.* J Physiol, 1967. **191**(3): p. 467-86.

76. Maurice, D.M., *The use of fluorescein in ophthalmological research.* Invest Ophthalmol, 1967. **6**(5): p. 464-77.

77. Lutz, R.J., H. Kim, M. Lizak, and M.R. Robinson, *Magnetic Resonance Imaging of the eye with Gd-DTPA implants*. in *Controlled Release Society 30th Annual Conference*. 2003. Glasgow, Scotland.

78. Peiffer, R., L. Pohm-Thorsen, and K. Corcoran, *Models in Ophthalmology and Vision Research*, in *The biology of the Laboratory Rabbit*, P. Manning, D. Ringler, and C. Newcomer, Editors. 1994, Academic Press: San Diego. p. 409 - 433.

79. Baker, R.W., *Controlled Release of Biologically Active Agents*. 1987, New York: John Wiley and Sons.

80. Reisfeld, B., S. Blackband, V. Calhoun, S. Grossman, S. Eller, and K. Leong, *The use of magnetic resonance imaging to track controlled drug release and transport in the brain.* Magn Reson Imaging, 1993. **11**(2): p. 247-52.

81. Sugar, H.S., A. Riazi, and R. Schaffner, *The bulbar conjunctival lymphatics and their clinical significance.* Trans Am Acad Ophthalmol Otolaryngol, 1957. **61**(2): p. 212-23.

82. Bill, A., G. Sperber, and K. Ujiie, *Physiology of the choroidal vascular bed.* Int Ophthalmol, 1983. **6**(2): p. 101-7.

83. Stay, M.S., J. Xu, T.W. Randolph, V.H, Barocas, *Computer simulation of convective and diffusive transport of controlled-release drugs in the vitreous humor.* Pharm Res, 2003. **20**(1): p. 96-102.

84. Popesko, P., V. Rajtova, and J. Horak, *A Colour Atlas of Anatomy of Small laboratory animals*. Vol. 1. 1990, London, England: Wolfe Publishing Ltd.

85. Bill, A., *Movement of Albumin and Dextran through the Sclera.* Arch Ophthalmol, 1965. **74**: p. 248-52.

86. Bill, A., *Blood circulation and fluid dynamics in the eye.* Physiol Rev, 1975. **55**(3): p. 383-417.

87. O'Day, D.M., M.B. Fish, S.B. Aronson, A. Coon, and M. Pollycove, *Ocular blood flow measurement by nuclide labeled microspheres.* Arch Ophthalmol, 1971. **86**(2): p. 205-9.

88. Bill, A., *The routes for bulk drainage of aqueous humour in rabbits with and without cyclodialysis.* Doc Ophthalmol, 1966. **20**: p. 157-69.

89. Bill, A., *The role of ciliary blood flow and ultrafiltration in aqueous humor formation.* Exp Eye Res, 1973. **16**(4): p. 287-98.

90. Smith, R.S. and L.A. Rudt, *Ultrastructural studies of the blood-aqueous barrier. 2. The barrier to horseradish peroxidase in primates.* Am J Ophthalmol, 1973. **76**(6): p. 937-47.

91. Xu, J., J.J. Heys, V.H. Barocas, and T.W. Randolph, *Permeability and diffusion in vitreous humor: implications for drug delivery.* Pharm Res, 2000. **17**(6): p. 664-9.

92. Marmor, M.F., A.S. Abdul-Rahim, and D.S. Cohen, *The effect of metabolic inhibitors on retinal adhesion and subretinal fluid resorption.* Invest Ophthalmol Vis Sci, 1980. **19**(8): p. 893-903.

93. Tsukahara, Y. and D.M. Maurice, *Local pressure effects on vitreous kinetics.* Exp Eye Res, 1995. **60**(5): p. 563-73.

94. Marmor, M.F., A. Negi, and D.M. Maurice, *Kinetics of macromolecules injected into the subretinal space.* Exp Eye Res, 1985. **40**(5): p. 687-96.

95. Bill, A., *Aqueous humor dynamics in monkeys (Macaca irus and Cercopithecus ethiops).* Exp Eye Res, 1971. **11**(2): p. 195-206.

96. Gordon, M.J., K.C. Chu, A. Margaritis, A.J. Martin, C.R. Ethier, and B.K. Rutt, *Measurement of Gd-DTPA diffusion through PVA hydrogel using a novel magnetic resonance imaging method.* Biotechnol Bioeng, 1999. **65**(4): p. 459-67.

97. Balazs, E.A., T.C. Laurent, and U.B. Laurent, *Studies on the structure of the vitreous body. VI. Biochemical changes during development.* J Biol Chem, 1959. **234**(2): p. 422-30.

98. Algvere, P. and A. Bill, *Effects of vitrectomy and phakectomy on the drainage of the vitreous compartment.* Albrecht Von Graefes Arch Klin Exp Ophthalmol, 1981. **216**(3): p. 253-60.

99. Bill, A., *Some aspects of aqueous humour drainage.* Eye, 1993. **7**(Pt 1): p. 14-9.

100. Olsen, T.W., H.F. Edelhauser, J.I. Lim, and D.H. Geroski, *Human scleral permeability. Effects of age, cryotherapy, transscleral diode laser, and surgical thinning.* Invest Ophthalmol Vis Sci, 1995. **36**(9): p. 1893-903.

101. Bill, A., *The Albumin Exchange in the Rabbit Eye.* Acta Physiol Scand, 1964. **60**: p. 18-29.

102. Radius, R.L. and D.R. Anderson, *Distribution of albumin in the normal monkey eye as revealed by Evans blue fluorescence microscopy.* Invest Ophthalmol Vis Sci, 1980. **19**(3): p. 238-43.

103. Alm, A., A. Bill, and F.A. Young, *The effects of pilocarpine and neostigmine on the blood flow through the anterior uvea in monkeys. A study with radioactively labelled microspheres.* Exp Eye Res, 1973. **15**(1): p. 31-6.

104. Bill, A. and J. Stjernschantz, *Cholinergic vasoconstrictor effects in the rabbit eye: vasomotor effects of pentobarbital anesthesia.* Acta Physiol Scand, 1980. **108**(4): p. 419-24.

105. Alm, A. and A. Bill, *Ocular and optic nerve blood flow at normal and increased intraocular pressures in monkeys (Macaca irus): a study with radioactively labelled microspheres including flow determinations in brain and some other tissues.* Exp Eye Res, 1973. **15**(1): p. 15-29.

106. Bill, A., *Some aspects of the ocular circulation. Friedenwald lecture.* Invest Ophthalmol Vis Sci, 1985. **26**(4): p. 410-24.

107. Koyano, S., M. Araie, and S. Eguchi, *Movement of fluorescein and its glucuronide across retinal pigment epithelium-choroid.* Invest Ophthalmol Vis Sci, 1993. **34**(3): p. 531-8.

108. Zhang, J., Z. Tan, and N.D. Tran, *Chemical hypoxia-ischemia induces apoptosis in cerebromicrovascular endothelial cells.* Brain Res, 2000. **877**(2): p. 134-40.

109. Gupta, H. and R. Weissleder, *Targeted contrast agents in MR imaging.* Magn Reson Imaging Clin N Am, 1996. **4**(1): p. 171-84.

110. Rudin, M. and R. Weissleder, *Molecular imaging in drug discovery and development.* Nat Rev Drug Discov, 2003. **2**(2): p. 123-31.

111. Kolodny, N.H., S.T. Goode, W. Ryan, and T.F. Freddo, *Evaluation of therapeutic effectiveness using MR imaging in a rabbit model of anterior uveitis.* Exp Eye Res, 2002. **74**(4): p. 483-91.

112. Funk, R.H., J. Gehr, and J.W. Rohen, *Short-term hemodynamic changes in episcleral arteriovenous anastomoses correlate with venous pressure and IOP changes in the albino rabbit.* Curr Eye Res, 1996. **15**(1): p. 87-93.

113. Lizak, M.J., M.B. Datiles, A.H. Aletras, P.F. Kador, and R.S. Balaban, *MRI of the human eye using magnetization transfer contrast enhancement.* Invest Ophthalmol Vis Sci, 2000. **41**(12): p. 3878-81.

114. Thelwall, P.E., A.A. Neves, and K.M. Brindle, *Measurement of bioreactor perfusion using dynamic contrast agent-enhanced magnetic resonance imaging.* Biotechnol Bioeng, 2001. **75**(6): p. 682-90.

115. Kolodny, N.H., T.F. Freddo, B.A. Lawrence, C. Suarez, and S.P. Bartels, *Contrast-enhanced magnetic resonance imaging confirmation of an anterior protein pathway in normal rabbit eyes.* Invest Ophthalmol Vis Sci, 1996. **37**(8): p. 1602-7.

116. Berkowitz, B.A., P.S. Tofts, H.A. Sen, N. Ando, E. de Juan Jr, *Accurate and precise measurement of blood-retinal barrier breakdown using dynamic Gd-DTPA MRI.* Invest Ophthalmol Vis Sci, 1992. **33**(13): p. 3500-6.

117. Sen, H.A., B.A. Berkowitz, N. Ando, E. de Juan Jr, *In vivo imaging of breakdown of the inner and outer blood-retinal barriers.* Invest Ophthalmol Vis Sci, 1992. **33**(13): p. 3507-12.

118. Cussler, E.L., *Diffusion : mass transfer in fluid systems*. 2nd ed ed. 1997, New York: Cambridge University Press.

119. Fatt, I., *Flow and diffusion in the vitreous body of the eye.* Bull Math Biol, 1975. **37**(1): p. 85-90.

120. Ohtori, A. and K. Tojo, *In vivo/in vitro correlation of intravitreal delivery of drugs with the help of computer simulation.* Biol Pharm Bull, 1994. **17**(2): p. 283-90.

121. Bogdanov, A.A., Jr., R. Weissleder, H.W. Frank, A.V. Bogdanova, N. Nossif, B.K. Schaffer, E. Tasi, and M.I. Papisov, *A new macromolecule as a contrast agent for MR angiography: preparation, properties, and animal studies.* Radiology, 1993. **187**(3): p. 701-6.

122. Zeimer, R.C., N.P. Blair, and J.G. Cunha-Vaz, *Pharmacokinetic interpretation of vitreous fluorophotometry.* Invest Ophthalmol Vis Sci, 1983. **24**(10): p. 1374-81.

123. Velez, G., P. Yuan, C. Sung, G. Tansey, G.F. Reed, C.C. Chan, R.B. Nussenblatt, and M.R. Robinson, *Pharmacokinetics and toxicity of intravitreal chemotherapy for primary intraocular lymphoma.* Arch Ophthalmol, 2001. **119**(10): p. 1518-24.

124. Lee, T.W. and J.R. Robinson, *Drug delivery to the posterior segment of the eye: some insights on the penetration pathways after subconjunctival injection.* J Ocul Pharmacol Ther, 2001. **17**(6): p. 565-72.

125. Gaul, G.R. and R.F. Brubaker, *Measurement of aqueous flow in rabbits with corneal and vitreous depots of fluorescent dye.* Invest Ophthalmol Vis Sci, 1986. **27**(9): p. 1331-5.

126. Antcliff, R.J., D.J. Spalton, M.R. Stanford, E.M. Graham, T.J. Ffytche, and J. Marshall, *Intravitreal triamcinolone for uveitic cystoid macular edema: an optical coherence tomography study.* Ophthalmology, 2001. **108**(4): p. 765-72.

127. Benitez Del Castillo Sanchez, J.M. and J. Garcia Sanchez, *[Intravitreal injection of triamcinolone acetonide in non infectious uveitis].* Arch Soc Esp Oftalmol, 2001. **76**(11): p. 661-4.

128. Martidis, A., J.S. Duker, and C.A. Puliafito, *Intravitreal triamcinolone for refractory cystoid macular edema secondary to birdshot retinochoroidopathy.* Arch Ophthalmol, 2001. **119**(9): p. 1380-3.

129. Young, S., G. Larkin, M. Branley, and S. Lightman, *Safety and efficacy of intravitreal triamcinolone for cystoid macular oedema in uveitis.* Clin Experiment Ophthalmol, 2001. **29**(1): p. 2-6.

130. Conway, M.D., C. Canakis, C. Livir-Rallatos, and G.A. Peyman, *Intravitreal triamcinolone acetonide for refractory chronic pseudophakic cystoid macular edema.* J Cataract Refract Surg, 2003. **29**(1): p. 27-33.

131. Benhamou, N., P. Massin, B. Haouchine, F. Audern, R. Tadayoni, and A. Gaudric, *Intravitreal triamcinolone for refractory pseudophakic macular edema.* Am J Ophthalmol, 2003. **135**(2): p. 246-9.

132. Schindler, R.H., D. Chandler, R. Thresher, and R. Machemeber, *The clearance of intravitreal triamcinolone acetonide.* Am J Ophthalmol, 1982. **93**(4): p. 415-7.

133. Scholes, G.N., W.J. O'Brien, G.W. Abrams, and M.F. Kubicek, *Clearance of triamcinolone from vitreous.* Arch Ophthalmol, 1985. **103**(10): p. 1567-9.

134. Beer, P.M., S.J. Bakri, R.J. Singh, W. Liu, G.B. Peters, and M. Miller, *Intraocular concentration and pharmacokinetics of triamcinolone acetonide after a single intravitreal injection.* Ophthalmology, 2003. **110**(4): p. 681-686.

135. Machemer, R., *Five cases in which a depot steroid (hydrocortisone acetate and methylprednisolone acetate) was injected into the eye.* Retina, 1996. **16**(2): p. 166-7.

136. Jonas, J.B., *Concentration of intravitreally injected triamcinolone acetonide in aqueous humour.* Br J Ophthalmol, 2002. **86**(9).

137. Foy, B.D. and J. Blake, *Diffusion of paramagnetically labeled proteins in cartilage: enhancement of the 1-D NMR imaging technique.* J Magn Reson, 2001. **148**(1): p. 126-34.

138. Lauffer, R.B. and T.J. Brady, *Preparation and water relaxation properties of proteins labeled with paramagnetic metal chelates.* Magn Reson Imaging, 1985. **3**(1): p. 11-6.

139. Bourges, J.L., S.E. Gautier, F. Delie, R.A. Bejjani, J.C. Jeanny, R. Gurny, D. BenEzra, and F.F. Behar-Cohan, *Ocular drug delivery targeting the retina and retinal pigment epithelium using polylactide nanoparticles.* Invest Ophthalmol Vis Sci, 2003. **44**(8): p. 3562-9.